8-9-2012 12:00 AM

Characterization of the Interaction between the Parkin Ubiquitin-like domain and Ataxin-3 Ubiquitin Interacting Domains

Jane J. Bai
The University of Western Ontario

Supervisor
Gary S Shaw
The University of Western Ontario

Graduate Program in Biochemistry
A thesis submitted in partial fulfillment of the requirements for the degree in Master of Science

Characterization of the Interaction between the Parkin Ubiquitin-like domain and Ataxin-3 Ubiquitin Interacting Domains

(Spine Title: Characterization of the Interaction between Parkin and Ataxin-3)

(Thesis Format: Intergrated Article)

by

Jane J. Bai

Graduate Program
in
Biochemistry

A thesis submitted in partial fulfillment for
the degree of Master of Science

Faculty of Graduate Studies
The University of Western Ontario
London, Ontario, Canada

THE UNIVERSITY OF WESTERN ONTARIO
School of Graduate and Postdoctoral Studies

CERTIFICATE OF EXAMINATION

Supervisor

Dr. Gary Shaw

Supervisory Committee

Dr. Caroline Schild-Poulter

Dr. James Choy

Examiners

Dr. James Choy

Dr. Graeme Hunter

Dr. Marco Prado

The thesis by

Jane Jing Bai

entitled:

Characterization of the Interaction between the Parkin Ubiquitin-like domain and Ataxin-3 Ubiquitin Interacting Domains

is accepted in partial fulfillment of the
requirements for the degree of
Master of Science

Date

Chair of the Thesis Examination Board

Abstract

The ubiquitin signaling pathway (USP) consists of hundreds of enzymes which are tightly regulated for proper maintenance of intracellular protein level homeostasis. The main goals of this thesis were to characterize the interaction of two proteins involved in the USP, the E3 ubiquitin ligase called parkin, and the Deubiquitinating (DUB) enzyme, ataxin-3. The effect of disease-state substitutions in the parkin ubiquitin-like domain (UbLD) on the interaction with ataxin-3 was investigated through NMR ^{1}H-^{15}N HSQC titration experiments and affinity binding assays. The three UIM regions in ataxin-3 bind the hydrophobic patch of parkin UbLD (K_D = 230 μM) and are proposed to use a multivalent binding mechanism. The disease-state UbLD proteins ($UbLD^{V15M}$, $UbLD^{R33Q}$, $UbLD^{K48A}$) retain their interaction with ataxin-3. Other DUB enzymes and E3 ligases have been reported to have regulatory interplay, which has triggered interest in studying protein pairings such as ataxin-3 and parkin.

Acknowledgements

I would like to thank all of those who helped me persevere throughout my graduate career at Western University. Specifically, I would like to thank Brian Dempsey for teaching me all the lab basics, for giving me guidance throughout my time in the lab, and for standing by my side numerous times while I was operating the French press. To Kathy Barber, thank you so much for all your help and advice when it came down to problem solving and experimental design. I appreciate all the times you went out of your way to help me make the most of my experiments and for picking up my late night phone calls from the lab. To all past and present lab members: Atoosa, Chee, Chantal, Julia, Ben, Don, Anne, Noah, Jake, Tara, Esma, Liliana, Jillian, Evan, Ventzi, Mariena, and Steven, thank you for making my time in the lab so enjoyable. I will cherish the many memories I have of the Shaw Lab: the uncontrollable laughing bouts, controversial relationship conversation, Euchre games and many more great moments involving quinoa baked goods and buffets with Chee. I would especially like to thank Sue Safadi, for motivating me, for making revisions to the thesis, and for taking me out on painful runs (that she called her 'easy runs'), which in turn made my thesis writing more enjoyable and efficient. She is a wonderful role model.

I would like to thank my Mom and Dad, for their love and support throughout this process; this work is dedicated to them. To Regan, thank you for all the hugs when I needed them the most and for keeping my spirits high. Thank you Mary, Mandy, Vanessa, Alyx and Yuan, for always being a phone call away to give me advice and listen to my experimental achievements and complications.

To my advisory committee Dr. James Choy and Dr. Caroline Schild-Poulter, thank you for all of your help and for providing me with valuable feedback along the way.

Lastly, I would like to thank my supervisor, Dr. Gary Shaw. I have learned so much in these short two years of the value of patience, perseverance, hard work, versatility and confidence

through his example. I am extremely grateful for this experience and I feel honored to have worked under his supervision.

Table of Contents

List of Figures

List of Tables

List of Abbreviations, Symbols and Nomenclature

ARJP	Autosomal recessive juvenile parkinson's disease
CUE	Coupling of ubiquitin conjugation to endoplasmic reticulum degradation
DUB	Deubiquitinating
DUIM	Double-sided ubiquitin interacting motif
E6,AP	Ubiquitin ligase E3A
ERAD	Endoplasmic reticulum associated degradation
HECT	Homologous to E6-AP C-terminal domain
HSQC	Heteronuclear single quantum coherence
IBR	In-between-RING
ITC	Isothermal titration calorimetry
JAMM	Jab1/MPN domain-associated metalloisopeptidase
MJD	Machado Joseph Disease
NMR	Nuclear magnetic resonance
OTU	Ovarian tumor domain
RBS	Ribosome binding site
RING	Really interesting new gene
PD	Parkinson's Disease
SPR	Surface plasmon resonance
TEV	Tobacco etch virus
Ub	Ubiquitin
UBA	Ubiquitin-associated
Ubld	ubiquitin-like domain
$Ubld^{R42P}$	R42P mutant Ubld protein
$Ubld^{K48A}$	K48A mutant Ubld protein

UBP	Ubiquitin-specific peptidases
UCH	Ubiquitin C-terminal hydrolases
UIM	Ubiquitin-interacting motif
UPD	unique parkin specific domain
USP	Ubiquitin signaling pathway
UTR	Untranslated region
VCP	Valosin-containing protein

Chapter 1
INTRODUCTION

1.1 The ubiquitin signaling pathway

Protein degradation is a tightly orchestrated process that is required to maintain protein level homeostasis, which is essential for biological pathways such as cellular division, DNA repair, and proteasomal degradation. The ubiquitination signaling pathway (USP) is most famously known for its role in eukaryotic protein degradation by sending specific proteins to the proteasomal degradation machinery at the right time. The ubiquitin (Ub) molecule is 8.6 kDa, globular in shape, very robust and highly conserved in all eukaryotes. A cascade of three enzymes, the ubiquitin-activating (E1), ubiquitin-conjugating (E2), and ubiquitin-ligase (E3) enzymes are utilized for attaching a mono-ubiquitin species or building a chain of ubiquitin moieties on a substrate (Figure 1.1). These enzymes were originally named in the order that they were eluted from an anion-exchange column (1). The covalent attachment of Ub moieties to substrates is an ATP driven process and is done so in a specific manner which is facilitated by the multiple combinations of E1, E2 and E3. Of the three classes of proteins involved in ubiquitination, the E3 ubiquitin ligase proteins has been an especially attractive target for macromolecular research due to the discovery of more than 1000 different homologues, suggesting that the E3 protein is heavily contributing to the substrate specificity in the pathway (2). To date there are ~1000 human E3 enzymes identified, ~40 E2 enzymes, and 2 E1 enzymes identified (3). An addition to the complexity of Ub attachment is the type of linkage that can be made between adjacent Ub moieties in a poly-Ub chain. There are 7 linkage possibilities, due to the presence of seven lysine residues within the Ub

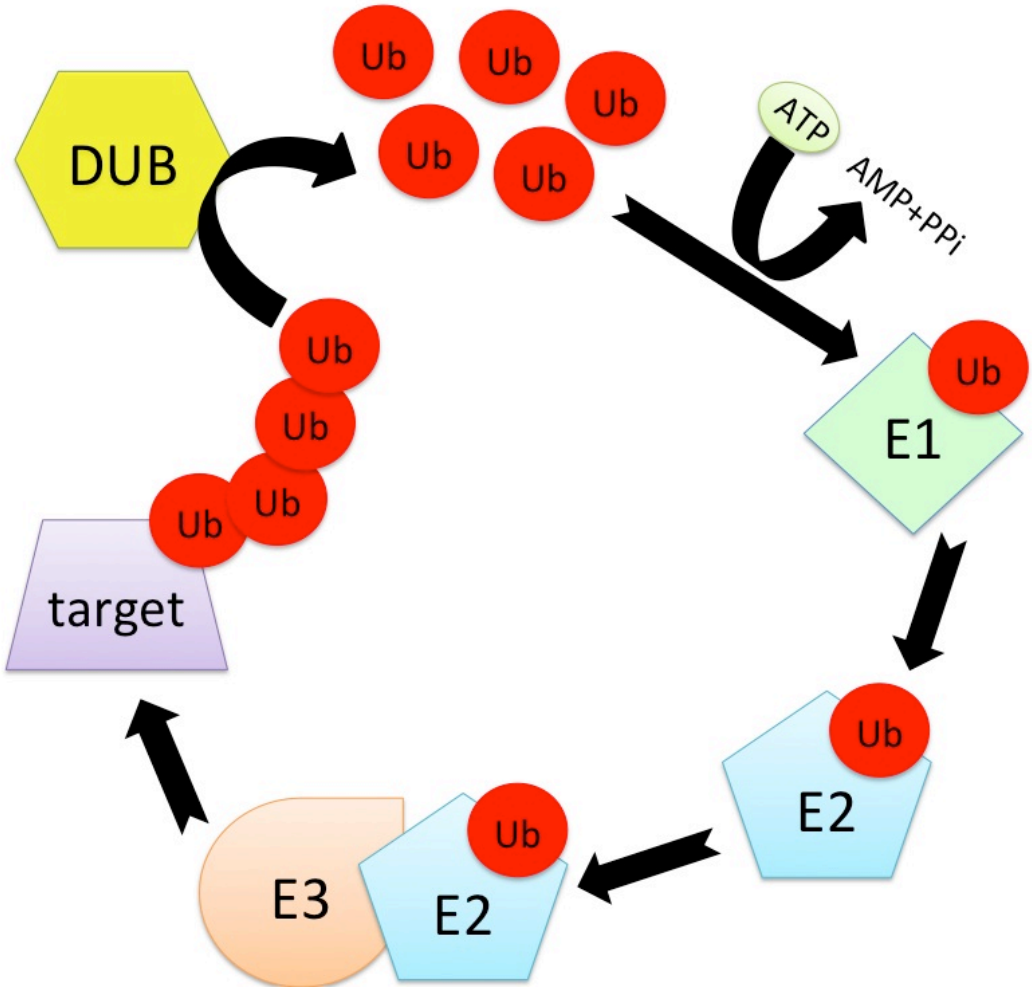

Figure 1.1 Schematic of the ubiquitin conjugation and recycling process in the ubiquitin signaling pathway. Ubiquitin (Ub) is a signaling molecule that is conjugated onto a target protein to signal for essential cellular processes such as a degradation signal, DNA repair, or endocytosis. The Ub is activated by the E1 activating enzyme, which requires an ATP molecule for the formation of a high energy thiolester bond to form between E1-Ub. The E1 then transfers the Ub moiety to the E2 enzyme, forming the Ub-E2 complex. Then the E3 acts as a scaffold protein to direct the Ub directly from the E2 to the target substrate, on the condition that it is a RING-type E3 enzyme. The target protein can have either a monoubiquitin attached or, after successive rounds of the E1-E2-E3 cascade, the target protein can have a poly-Ub chain attached. This process is reversible by deubiquitinating (DUB) enzymes, which act to detach Ub moieties to recycle Ub molecules, edit Ub conjugation errors, or for Ub processing.

molecule, and the arrangement of the linkages provide variety in the orientation of the Ub chain in three dimensional space. The type of linkage that is created in a poly-Ub chain, is a unique signal, which determines the fate of the substrate that its attached to. The most studied linkage pattern is the Lys^{48} Ub linkage which is known to signal for proteasomal degradation (4).

The multistep enzymatic reaction for attachment of a ubiquitin moiety to a substrate protein is also a reversible process. The group of enzymes that perform the reverse reaction are known as ubiquitin specific proteases or deubiquitinating (DUB) enzymes and in mammals there are 5 gene families of DUB enzymes: Ubiquitin C-terminal Hydrolases (UCHs), Ubiquitin-specific Peptidases (UBPs), Ovarian Tumor domain proteins (OTU), Josephin proteins and the Jab1/MPN domain-associated Metalloisopeptidase (JAMM) domain proteins (5). Most of these DUB enzymes are cysteine proteases, which utilize three residues, called the catalytic triad, including the cysteine that has the essential thiol group for catalyzing the Ub hydrolysis (6) (Figure 1.2).

Currently, there is interest in understanding how E3 enzymes are able to recognize specific substrates, and due to the large numbers of E2 and E3 enzymes available, many E2/E3 combinations are possible. Interestingly, certain E3 ligases have been found to interact with specific DUB enzymes, which seems counter-intuitive in the context of energetics used for Ub chain building. However, when considering the possibility of errors in attaching Ub to the correct substrate and using the correct linkage, and constant

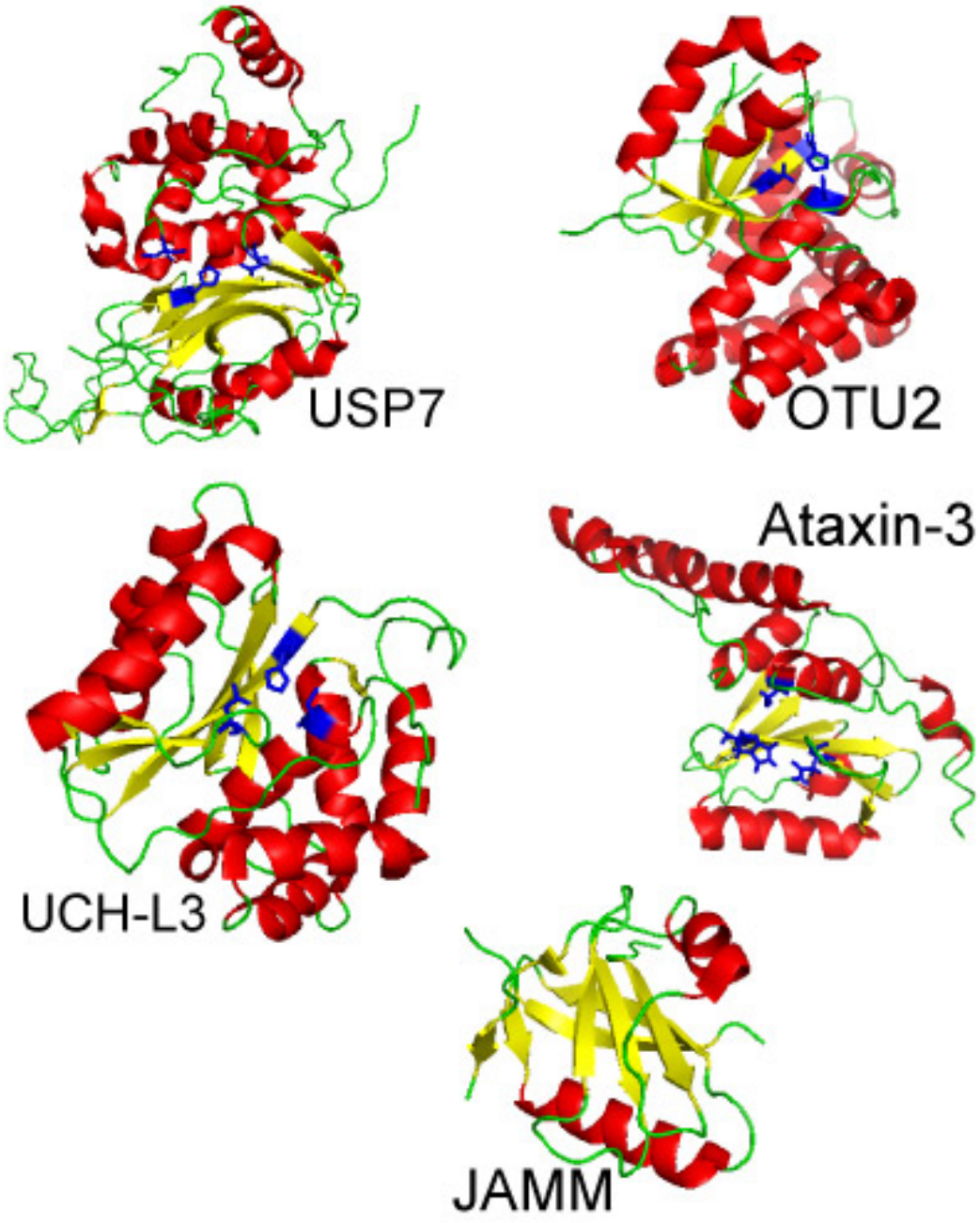

Figure 1.2 Ribbon representation of DUB enzymes, each enzyme belongs to one of the five families of DUB enzymes. The DUB enzyme belonging to the USP, UCH, OTU, and MJD domains all have a conserved catalytic triad consisting of a Cys, His and Asp residue. The catalytic triad is depicted in blue with the side chains portrayed. The JAMM domain is a metalloisopeptidase and does not utilize a catalytic triad. The name of the protein is indicated beside the catalytic domain ribbon representation. The ribbon depictions were created in PyMOL and the PDB for USP7 (1NBF), UCH-L3 (1XD3), OTU2 (1TFF), ataxin-3 (1YXB), and JAMM (1R5X).

reversibility requirements for cellular environment changes, there seems to be a need for DUB enzymes to rapidly edit these problems to adapt to a constantly changing cellular environment (7, 8). When the maintenance of protein homeostasis is abnormal in the cell, disease prone events like protein misfolding and aggregation can occur. Enzymes involved in the USP have been linked to neurodegenerative diseases, such as Parkinson's disease and Spinocerebellar ataxias (7).

1.2 E3 ubiquitin ligase

E3 Ub-ligases fall under two major groups, the HECT (Homologous to E6-AP C-terminal domain) or RING (Really Interesting New Gene) group (8). Apart from their unique structural features, they are also set apart from one another in their function as an E3 ligase protein. The HECT type E3 ligases form a thioester intermediate with Ub and further mediates the transfer to the substrate protein. RING type E3 enzymes are different and often described as more of a scaffold protein, which functions to interact with an E2-Ub conjugate and substrate to mediate the transfer of the Ub moiety directly from the E2 (8).

1.3 Parkin

1.3.1 PARK2 gene and domain architecture, expression of parkin, subcellular localization and function

PARK2 is the gene encoding the parkin protein and its location in the human genome, based on positional cloning, is on the long arm of chromosome 6 (6q25.2-27) (9). PARK2 is a large gene spanning 1.5 megabases containing 12 exons and is expressed

in many tissue types such as brain, skeletal muscle, and heart (10, 11). Interestingly, it is expressed in many areas of the brain including the substantia nigra (10).

Parkin is a RING-type E3 ligase composed of 465 residues and has a molecular weight of 52 kDa. Parkin consists of multiple domains; listed from the N-terminus to C-terminus, UbLD (Ubiquitin-Like Domain), UPD (Unique-Parkin Domain), RING0, RING1, IBR (In-Between-RING), followed by RING2 (12) (Figure 1.3). The RING domains and IBR domain contain two Zn^{2+} ions each that are coordinated by cysteine and histidine residues. Without the Zn^{2+} ions, two of the protein domains (IBR, RING2) become completely unfolded (12).

The discoveries that identified parkin as a USP protein came from evidence that it has E3 ligase activity and could interact with E2 enzymes, such as UbcH7 and UbcH8 (13). Originally, E3 ligases were thought to be constitutively active, however, after further investigation, parkin activity was proposed to be governed by autoregulation, post-translational modification, such as ubiquitination or/and phosphorylation (14). Many putative substrates have been identified for parkin such as synphillin-1 (15), Pael-R (16), cyclin E (17) and several others. A popular hypothesis for parkin function is that it is fundamentally important for regulating appropriate levels of its protein substrates, especially avoiding accumulations of aggregate-prone substrates such as alpha-synuclein, Aβ peptide and Huntington protein (13). These aggregate-prone substrates of parkin, such as synphillin-1 and alpha-synuclein, with Ub and parkin itself have all been identified immunopositive in nigral cell Lewy bodies (15). Recent studies show a role for parkin in mitochondrial regulation, and its importance in retaining the mitochondrial DNA integrity by

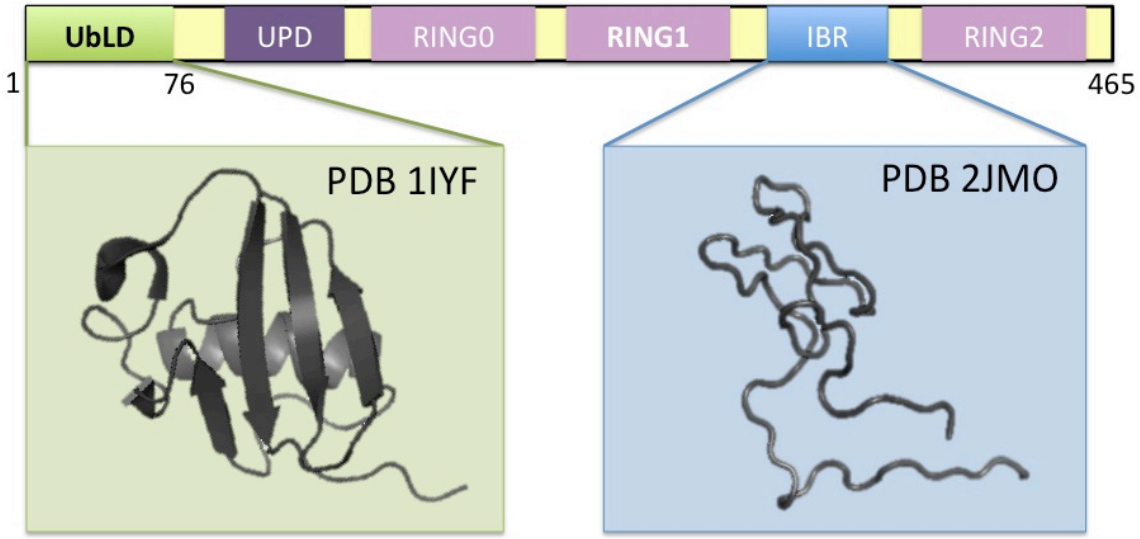

Figure 1.3 Domain topology of the E3 ligase parkin protein. Parkin is a 465 residue protein and is composed of six domains. It has an N-terminal Ubiquitin-like domain (UbLD), which was structurally solved by NMR. Following the UbLD, is the unique parkin domain (UPD). RING0 and RING1 (really interesting new gene) are next in the sequence, followed by an In-Between RING (IBR) domain, which was also structurally solved by NMR spectroscopy. The most C-terminal domain is the RING2 domain. Unlike the IBR and RING domains, the UbLD and the UPD domains do not coordinate two zinc ions. The ribbon diagrams of the UbLD and IBR were made using PyMOL and the PDB for parkin UbLD is 1IYF, and for parkin IBR is 2JMO.

promoting repair and by protection from reactive oxidative stress (18). Parkin has also been reported to bind tightly with microtubules for stabilization and quality control purposes, and interestingly, the microtubule network is crucial for another type of protein degradation mechanism known as aggregsomal degradation (19). The multiple roles of parkin in different cellular processes are still being investigated and this is an important aspect to appreciate especially when considering the outcome of pathogenic mutations on parkin.

1.3.2 N-terminal ubiquitin like domain of the parkin protein

UbLD proteins are often found within multidomain proteins and the function of each UbLD within the USP is still under investigation (20). Like Ub, they possess the β-grasp fold which has a hydrophobic face on the solvent exposed side of the β-sheets (Figure 1.4). What is unique to UbLD proteins, compared to the Ub molecule, is that they are unable to be conjugated to the lysine residue of a substrate protein because they lack the C-terminal glycine. Not to be confused with Ub-like domains, SUMO, ISG15, NEDD8 are examples of free Ub-like proteins that are covalently attached to substrates utilizing the same mechanism of Ub conjugation. The parkin N-terminal UbLD has 30% identity and 62% homology with the human Ub molecule (21) (Figure 1.4). The function of the UbLD is thought to be a recruitment domain for substrate recognition. It has been previously shown to interact with o-glycosylated alpha-synclein, an aggregation prone protein found in Lewy bodies; S5a, a proteasomal subunit; Eps15 an endocytosis involved protein; and ataxin-3, a DUB enzyme (2, 22, 23).

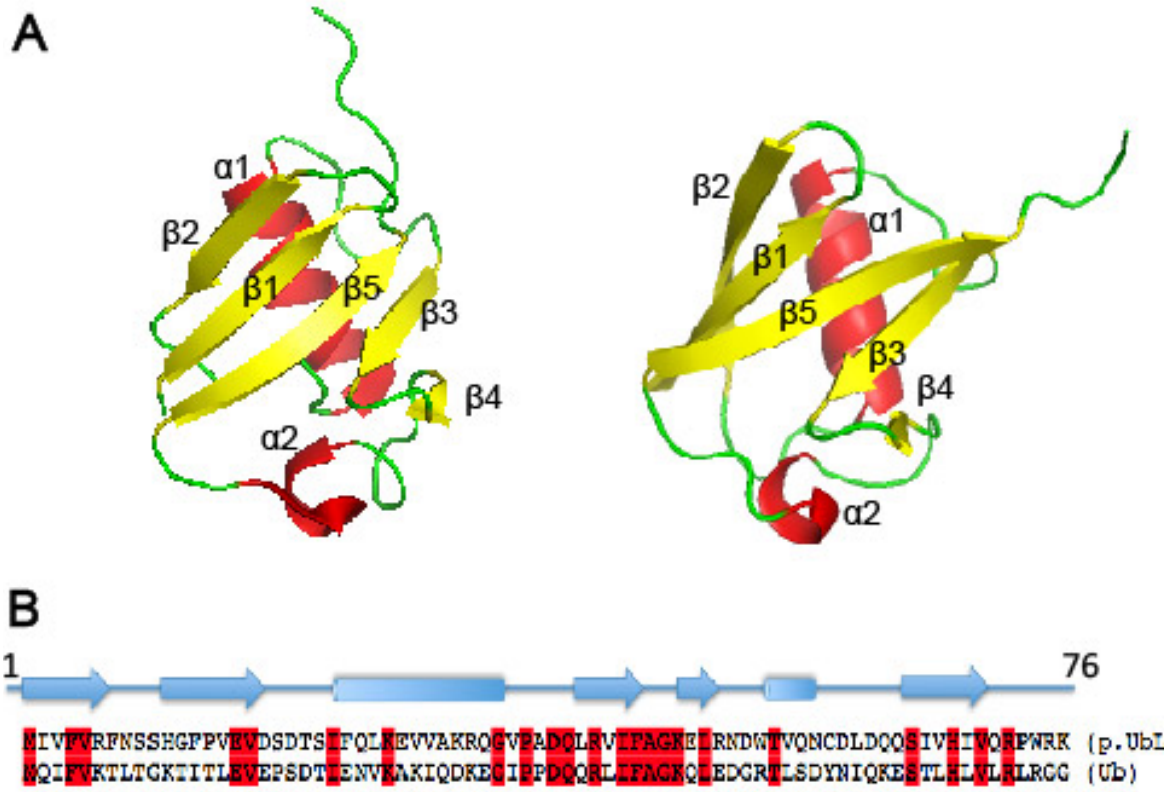

Figure 1.4 Structural and sequence comparison between the human Ub and parkin UbLD molecule. A) Both the parkin UbLD (left) and Ub (right) molecule share the beta-grasp fold which consists of 5 β-sheets and 2 α-helices. B) The parkin UbLD and human Ub sequence share 30% sequence identity, which is indicated with a red background. The ribbon diagram was created in PyMOL and the PDB for the parkin UbLD is 1IYF and human Ub is 1UBQ.

1.3.3 Autosomal recessive juvenile Parkinsonism is linked to the PARK2 gene

Parkinson's disease (PD) is the second most prevalent neurodegenerative disease next to Alzheimer's disease. The usual age of onset for PD is past the age of 50, however, there are approximately 5-10% of PD patients that have the misfortune of being diagnosed at a very early age. Acquiring the disease before the age of 40 is uncommon compared to the idiopathic late-onset form of the disease and is labeled as early-onset PD (10). Within this group of early-onset PD patients, a small group will have inherited it in an autosomal recessive fashion with complete penetrance. Autosomal Recessive Juvenile Parkinsonism (ARJP) affects men and women equally and its prevalence across various regions seems to be similar. The pathogenic characteristic of many idiopathically contracted patients include cytoplasmic insoluble protein aggregate, known as Lewy bodies (13). However, Lewy bodies are infrequently presented in parkin linked ARJP patients (24, 25).

ARJP exhibits locus heterogeneity; there are five known monogenic mutants that are linked to the same disease phenotype and same inheritance pattern. The most common form of ARJP arises from PARK2 gene mutations, which codes for the parkin protein, and accounts for 50% of early-onset PD (26). Initial ARJP disease cases were characterized in Japanese families and were mostly caused by large exon deletions, but as the search for parkin-linked ARJP patients progressed, more single amino acid substitutions were characterized as disease mutations (21). These mutations were found throughout the PARK2 gene with a concentration of missense type mutations occurring in the RING1-IBR-RING2 C-terminus region (14, 27) (Figure 1.5).

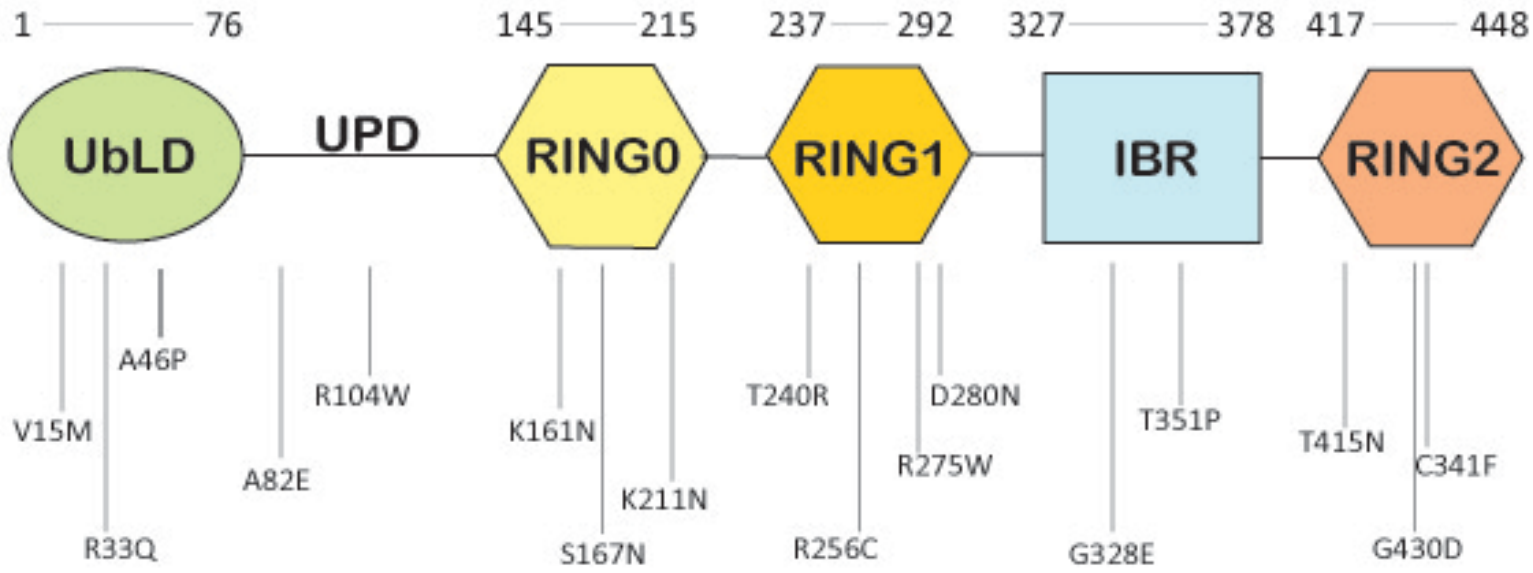

Figure 1.5 Schematic representation of parkin and the ARJP substitutions identified within the parkin sequence. The sites of the disease state mutations that cause an early-onset Parkinson's disease, by an autosomal recessive inheritance pattern, are indicated below the domain representation of parkin. ARJP single amino acid substitutions are found throughout the parkin protein with the majority of them identified in the RING1-IBR-RING2 regions. Not all of the substitutions are shown in this figure. The residue numbers that are indicated above the domain schematic represent the boundaries of each domain within the parkin protein.

1.4 Ataxin-3

1.4.1 ATXN3 gene topology

The gene that encodes for the ataxin-3 protein is called ATXN3 and is located on chromosome 14 (14q24.3-q32) (28). The human ATXN3 gene is approximately 48 Kb and is composed of 11 exons (29). There is a CAG trinucleotide repeat located within exon 10 that is prone to unstable expansions which cause neurodegeneration when the repeat number passes a threshold of >45 (29). Meanwhile, wild-type alleles can range from 11 to 44 CAG trinucleotide repeats (30).

1.4.2 Ataxin-3 domain architecture

The ataxin-3 protein has often been described as having unique domain topology due to the arrangement and number of Ubiquitin Interacting Motif (UIM) regions it possesses. Ataxin-3 is composed of an N-terminal catalytic Josephin domain, spanning residues 1-170 (Figure 1.6). The Josephin domain contains the catalytic cysteine (Cys^{14}) that is required for its DUB activity. Following the folded Josephin domain are two tandem UIM regions, (UIM1, UIM2). UIM1 spans residues 224-243 and UIM2 spans residues 244-263. Following UIM2, there is a variable glutamine tract that can vary from 11 to 44 repeats, which are non-disease causing lengths (30). At the C-terminus of ataxin-3, following the poly-glutamine tract, there is a third UIM that spans residues 331-348, (UIM3) (Figure 1.6).

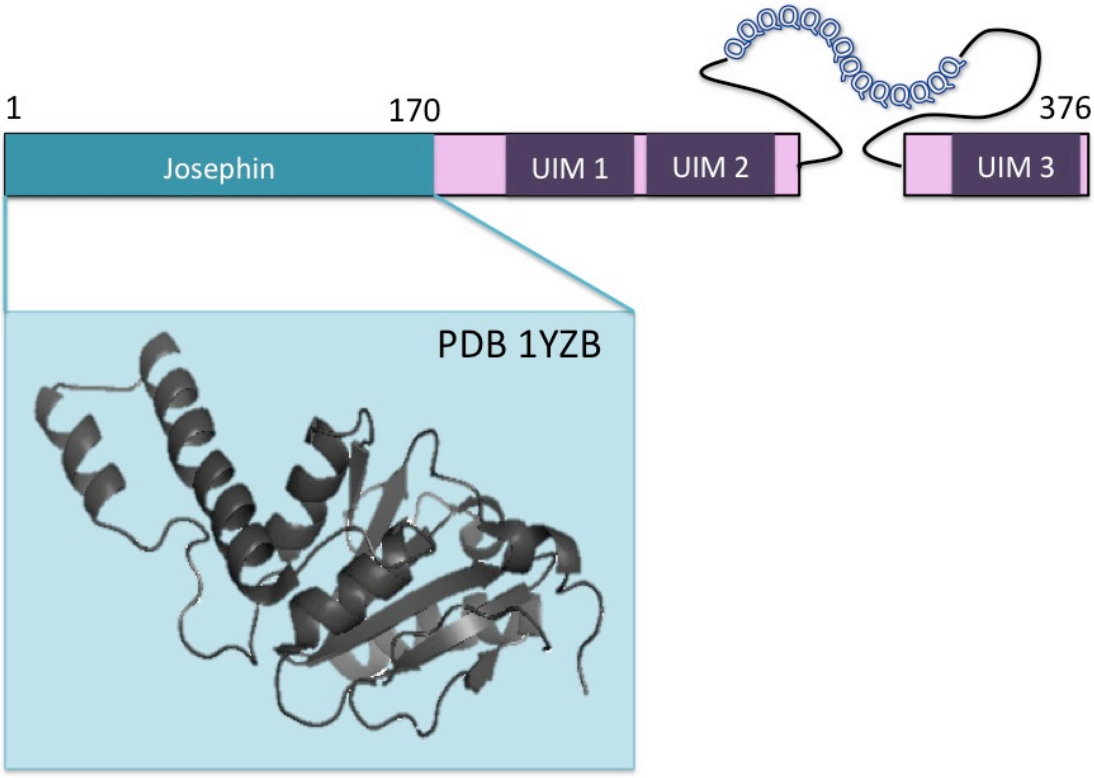

Figure 1.6 Schematic of the domain topology within the ataxin-3 DUB enzyme. Ataxin-3 consists of 5 distinct regions: the N-terminal catalytic Josephin domain (residues 1-170); two UIM regions (residues 224-243 and 244-263); a variable poly-glutamine expansion that can consist of 11-44 residues for a non-disease state; and a C-terminal UIM region (residues 331-348). The N-terminal Josephin domain was structurally determined by both NMR spectroscopy and X-ray crystallography. The ribbon diagram was made using PyMOL and the PDB for ataxin-3 Josephin domain is 1YZB.

1.4.3 Ataxin-3 expression, splice isoforms, subcellular localization and function

The normal non-expanded form of human ataxin-3 is approximately 42 kDa, depending on the glutamine tract variability, and is expressed ubiquitously in many tissues including neuronal tissue. Ataxin-3 is predominantly a cytoplasmic protein based on immunohistochemical studies in various human neuronal cells (31). The mechanisms to regulate the expression of the ATXN3 gene are unclear, due to the variation at the 3' untranslated region (UTR) and the lack of study in the 5' UTR (29).

Ataxin-3 functions as a deubiquitinating (DUB) enzyme, and falls under the Josephin gene family of DUB proteases because of its sequence homology with other Josephin genes (6). It has a preference to detach Lys^{63} linked poly-Ub chains, *in vitro* (32-34). The ataxin-3 protein participates in the ubiquitin-signalling pathway based on three pieces of evidence; (a) it is composed of a catalytic Josephin domain which has a DUB function, (b) it has three UIM sites involved in poly-Ub and UbLD interactions, and (c) it has many binding partners involved in the proteasomal pathway such as VCP (valosin-containing protein) (35), E6,AP (Ubiquitin ligase E3A) (36), and parkin (37). However, ataxin-3 is not restricted in participating with just the USP, it has also been found to play a role in DNA repair and ERAD (endoplasmic reticulum associated degradation) (38, 39).

Ataxin-3 has been shown to have over 50 splice variants but only two have been extensively characterized and found to be expressed in a tissue specific manner. One of the splice variants encodes the full-length sequence which includes all three UIM sites. The other splice variant lacks the C-terminal third UIM site but includes the

polyglutamine stretch of ataxin-3 (40, 41). In human and murine brain, the splice variant encoding three UIM sites is the predominant isoform (40).

1.4.4 Ubiquitin interaction motif

Poly-Ub binding assays involving the human proteasomal subunit, S5a, were used to identify the UIM, though at the time it was originally known as the pUB motif (42). The UIM is one of fifteen identified protein groups dedicated to Ub or/and UbLD recognition. Interestingly, the Ub-recruitment domains vary in size and their three-dimensional fold suggesting that Ub can accommodate an interaction for many domains, such as the UBA (Ubiquitin-Associated), DUIM (Double-sided Ubiquitin Interacting Motif), and CUE (Coupling of Ubiquitin conjugation to Endoplasmic reticulum degradation) (43). All of the Ub recruitment domains have weak binding affinities to mono Ub, in the 100 μM to 2 mM range, determined by either NMR, ITC (Isothermal Titration Calorimetry) or SPR (Surface Plasmon Resonance) methods (43).

One of the first reviews that provided analysis of the identified UIM containing proteins reported that the UIM is composed of twenty residues and contain a conserved acidic stretch of approximately four residues prior to a series of highly conserved alanine and serine residues (44) (Figure 1.7). The same group also noticed that many proteins containing the UIM regions often have more than one UIM site and can present itself in a wide variety of proteins with roles in endocytosis, proteasomal substrate recruitment, and DUB function (44). Further investigation of the UIM sequences sparked notice of an interesting trend of alternating large-small-large-small-large residues in between the two

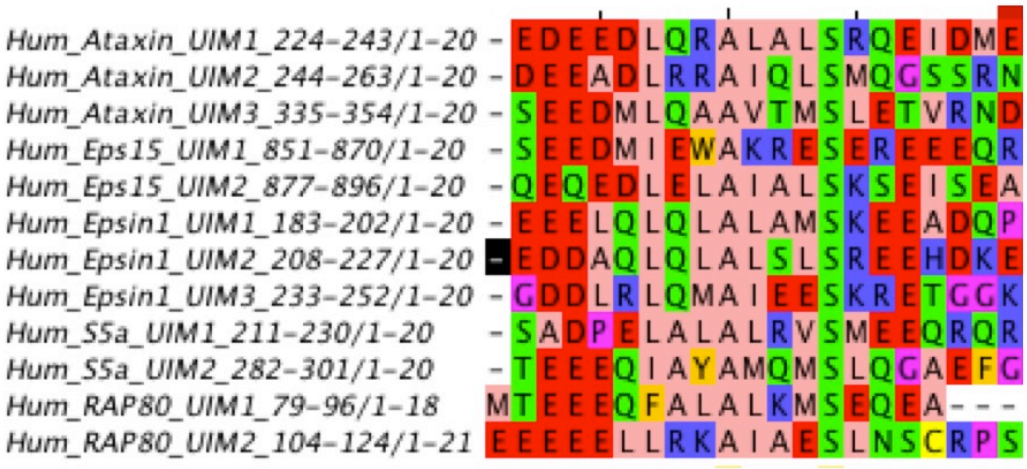

Figure 1.7 Sequence alignment of the ubiquitin interacting motif of human proteins. Selected human proteins (ataxin-3, Eps15, Epsin1 S5a, Rap80) containing ubiquitin-interacting motifs (UIM) have their UIM sequences aligned. The protein name, UIM position, residue position, and the number of residues within the identified UIM is indicated on the left of the sequence. The motif consists of approximately 20 residues, starting with an N-terminal acidic stretch (red) of 3 to 5 residues followed by a hydrophobic stretch (pink). There is a conserved alanine and serine residue that borders the hydrophobic stretch within each UIM. This sequence alignment was created in JalView.

acidic patches of the UIM sequences (45) (Figure 1.7). Although the UIM sites of most proteins have high sequence similarities between one another, it cannot be assumed that all UIM sites will interact to Ub or UbLD proteins (2).

The UIM region containing UIM1 and UIM2 of ataxin-3, spanning residues 194-261, has been reported to possess α-helical structures separated by a flexible linker by NMR studies (46). The structure of the two UIM site in Vps27, a yeast protein involved in vacuolar protein sorting, was also characterized to have a helical conformation by X-ray crystallography, NMR spectroscopy and circular dichroism (45, 47, 48). These are just two examples of structurally determined UIM domains that are helical. Although structures of other UIM domains have yet to be determined they are also thought to be α-helical in structure (43). It has been reported that the helical-type of Ub binding domain, such as the UIM, DUIM and CUE are all thought to bind to the same site on Ub on its Ile^{44} hydrophobic patch (43).

1.4.5 Polyglutamine expansion in ataxin-3 causes Machado Joseph Disease

Polyglutamine diseases are characterized by protein misfolding leading to intracellular or intranuclear aggregate formation, caused by long repeats of CAG trinucleotides encoding for a poly-glutamine expansion, which eventually lead to neurodegeneration. The ataxin-3 protein is one of ten identified polyglutamine diseases which causes Machado Joseph Disease (MJD) (49) when its polyglutamine stretch is expressed passed a threshold of >45 residues. MJD is the most common dominantly inherited ataxia. Its name ‘Machado-Joseph’ originates from observations of two Azorian families that presented the disease in the 1970s (50). Interestingly, MJD patients exhibit a

wide variation of clinical presentations of parkinsonism characteristics, progressive external ophthalmoplegia, difficulty talking and difficulty swallowing (49). The affected brain areas based on MRI and neuroimaging studies indicates that the pons, midbrain, fourth ventricle, and basal ganglia are all affected in addition to the cerebellum and brainstem (51-55). The polyglutamine tract lies between the second and third UIM site of the ataxin-3 protein. The study of polyglutamine disease causing proteins are often focused on understanding the protein conformation of the wildtype and disease state proteins to understand how it relates to protein misfolding and aggregation. The difficulty in performing biophysical and biochemical analyses comes from issues in purifying great yields of the disease state proteins that are soluble in solution (56).

1.5 Scope of Thesis

Parkin and ataxin-3 are both multidomain proteins that play a role in the USP. The aim of this work was to characterize the interaction between the recruitment domains of these proteins. Investigation of their interaction will improve the overall understanding of the biological roles these proteins contribute to the USP. There has been evidence to support the direct interaction between ataxin-3 and parkin through affinity binding assays, however, a detailed analysis of the residues that are involved, the mechanism and the affinity of the interaction have not been deduced (23).

The goals of this thesis were:

1) Determine the binding surface on parkin UbLD when ataxin-3 is bound to it.

2) Determine which combination of UIM region(s) in ataxin-3 are crucial for the interaction with the parkin UbLD.
3) Propose a biologically relevant binding model for parkin and ataxin-3.
4) Address the biological consequence of structurally benign ARJP substitutions and the interactions of these proteins with ataxin-3.

To address the goals, ^{1}H-^{15}N HSQC titrations and chemical shift perturbation analyses were carried out using NMR spectroscopy to reveal residues that participate in the binding interface, identify which UIM sequences participate in the interaction with the UbLD and determine the binding affinity of these interactions. Analysis of the binding affinities between the UbLD and various ataxin-3 UIM constructs, with either C-terminal UIM deletions or 'functional knockouts' of the UIM sites, assisted in proposing a type of binding mechanism that could explain the parkin ataxin-3 interaction. The same ^{1}H-^{15}N HSQC titration experiments were utilized for the interaction study between ARJP substituted UbLD proteins and ataxin-$3^{194-361}$, to determine how their structures are affected by the substitution, and determine whether the ARJP substitution perturbed the affinity of the interaction. A four-part hypothesis was proposed; a) the parkin UbLD has a unique ataxin-3 binding site, b) all three UIMs in ataxin-3 are important for parkin binding, c) parkin uses a multivalent binding mechanism to recruit ataxin-3, d) structurally benign ARJP mutations in the parkin UbLD will decrease the binding affinity to ataxin-3.

There is growing evidence to support that ataxin-3 and parkin interact with each other to regulate both of their catalytic function (23, 37). This body of work highlights the

interaction mechanism, binding sites, and ARJP substitutions in the interaction studies between parkin and ataxin-3.

1.6 References

1. Hershko, A., Heller, H., Elias, S., and Ciechanover, A. (1983) Components of ubiquitin-protein ligase system. Resolution, affinity purification, and role in protein breakdown. *J.Biol.Chem.* **258,** 8206-8214

2. Safadi, S.S., and Shaw, G.S. (2010) Differential interaction of the E3 ligase parkin with the proteasomal subunit S5a and the endocytic protein Eps15. *J.Biol.Chem.* **285,** 1424-1434

3. Ye, Y., and Rape, M. (2009) Building ubiquitin chains: E2 enzymes at work. *Nat.Rev.Mol.Cell Biol.* **10,** 755-764

4. Wilkinson, K.D. (2005) The discovery of ubiquitin-dependent proteolysis. *Proc.Natl.Acad.Sci.U.S.A.* **102,** 15280-15282

5. Singhal, S., Taylor, M.C., and Baker, R.T. (2008) Deubiquitylating enzymes and disease. *BMC Biochem.* **9 Suppl 1,** S3

6. Nijman, S.M., Luna-Vargas, M.P., Velds, A., Brummelkamp, T.R., Dirac, A.M., Sixma, T.K., and Bernards, R. (2005) A genomic and functional inventory of deubiquitinating enzymes. *Cell.* **123,** 773-786

7. Upadhya, S.C., and Hegde, A.N. (2005) Ubiquitin-proteasome pathway components as therapeutic targets for CNS maladies. *Curr.Pharm.Des.* **11,** 3807-3828

8. Hegde, A.N., and Upadhya, S.C. (2011) Role of ubiquitin-proteasome-mediated proteolysis in nervous system disease. *Biochim.Biophys.Acta.* **1809,** 128-140

9. Matsumine, H., Saito, M., Shimoda-Matsubayashi, S., Tanaka, H., Ishikawa, A., Nakagawa-Hattori, Y., Yokochi, M., Kobayashi, T., Igarashi, S., Takano, H., Sanpei, K., Koike, R., Mori, H., Kondo, T., Mizutani, Y., Schaffer, A.A., Yamamura, Y., Nakamura, S., Kuzuhara, S., Tsuji, S., and Mizuno, Y. (1997) Localization of a gene for an

autosomal recessive form of juvenile Parkinsonism to chromosome 6q25.2-27. *Am.J.Hum.Genet.* **60,** 588-596

10. Kitada, T., Asakawa, S., Hattori, N., Matsumine, H., Yamamura, Y., Minoshima, S., Yokochi, M., Mizuno, Y., and Shimizu, N. (1998) Mutations in the parkin gene cause autosomal recessive juvenile parkinsonism. *Nature.* **392,** 605-608

11. Lucking, C.B., Durr, A., Bonifati, V., Vaughan, J., De Michele, G., Gasser, T., Harhangi, B.S., Meco, G., Denefle, P., Wood, N.W., Agid, Y., Brice, A., French Parkinson's Disease Genetics Study Group, and European Consortium on Genetic Susceptibility in Parkinson's Disease (2000) Association between early-onset Parkinson's disease and mutations in the parkin gene. *N.Engl.J.Med.* **342,** 1560-1567

12. Hristova, V.A., Beasley, S.A., Rylett, R.J., and Shaw, G.S. (2009) Identification of a novel Zn2+-binding domain in the autosomal recessive juvenile Parkinson-related E3 ligase parkin. *J.Biol.Chem.* **284,** 14978-14986

13. Marin, I., Lucas, J.I., Gradilla, A.C., and Ferrus, A. (2004) Parkin and relatives: the RBR family of ubiquitin ligases. *Physiol.Genomics.* **17,** 253-263

14. Chaugule, V.K., Burchell, L., Barber, K.R., Sidhu, A., Leslie, S.J., Shaw, G.S., and Walden, H. (2011) Autoregulation of Parkin activity through its ubiquitin-like domain. *EMBO J.* **30,** 2853-2867

15. Chung, K.K., Zhang, Y., Lim, K.L., Tanaka, Y., Huang, H., Gao, J., Ross, C.A., Dawson, V.L., and Dawson, T.M. (2001) Parkin ubiquitinates the alpha-synuclein-interacting protein, synphilin-1: implications for Lewy-body formation in Parkinson disease. *Nat.Med.* **7,** 1144-1150

16. Imai, Y., Soda, M., Hatakeyama, S., Akagi, T., Hashikawa, T., Nakayama, K.I., and Takahashi, R. (2002) CHIP is associated with Parkin, a gene responsible for familial Parkinson's disease, and enhances its ubiquitin ligase activity. *Mol.Cell.* **10,** 55-67

17. Staropoli, J.F., McDermott, C., Martinat, C., Schulman, B., Demireva, E., and Abeliovich, A. (2003) Parkin is a component of an SCF-like ubiquitin ligase complex and protects postmitotic neurons from kainate excitotoxicity. *Neuron.* **37,** 735-749

18. Rothfuss, O., Fischer, H., Hasegawa, T., Maisel, M., Leitner, P., Miesel, F., Sharma, M., Bornemann, A., Berg, D., Gasser, T., and Patenge, N. (2009) Parkin protects

mitochondrial genome integrity and supports mitochondrial DNA repair. *Hum.Mol.Genet.* **18,** 3832-3850

19. Rankin, C.A., Roy, A., Zhang, Y., and Richter, M. (2011) Parkin, A Top Level Manager in the Cell's Sanitation Department. *Open Biochem.J.* **5,** 9-26

20. Grabbe, C., and Dikic, I. (2009) Functional roles of ubiquitin-like domain (ULD) and ubiquitin-binding domain (UBD) containing proteins. *Chem.Rev.* **109,** 1481-1494

21. Fishman, P.S., and Oyler, G.A. (2002) Significance of the parkin gene and protein in understanding Parkinson's disease. *Curr.Neurol.Neurosci.Rep.* **2,** 296-302

22. Shimura, H., Schlossmacher, M.G., Hattori, N., Frosch, M.P., Trockenbacher, A., Schneider, R., Mizuno, Y., Kosik, K.S., and Selkoe, D.J. (2001) Ubiquitination of a new form of alpha-synuclein by parkin from human brain: implications for Parkinson's disease. *Science.* **293,** 263-269

23. Durcan, T.M., and Fon, E.A. (2011) Mutant ataxin-3 promotes the autophagic degradation of parkin. *Autophagy.* **7,** 233-234

24. Mori, H., Kondo, T., Yokochi, M., Matsumine, H., Nakagawa-Hattori, Y., Miyake, T., Suda, K., and Mizuno, Y. (1998) Pathologic and biochemical studies of juvenile parkinsonism linked to chromosome 6q. *Neurology.* **51,** 890-892

25. Takahashi, H., Ohama, E., Suzuki, S., Horikawa, Y., Ishikawa, A., Morita, T., Tsuji, S., and Ikuta, F. (1994) Familial juvenile parkinsonism: clinical and pathologic study in a family. *Neurology.* **44,** 437-441

26. Safadi, S.S., and Shaw, G.S. (2007) A disease state mutation unfolds the parkin ubiquitin-like domain. *Biochemistry.* **46,** 14162-14169

27. Hedrich, K., Eskelson, C., Wilmot, B., Marder, K., Harris, J., Garrels, J., Meija-Santana, H., Vieregge, P., Jacobs, H., Bressman, S.B., Lang, A.E., Kann, M., Abbruzzese, G., Martinelli, P., Schwinger, E., Ozelius, L.J., Pramstaller, P.P., Klein, C., and Kramer, P. (2004) Distribution, type, and origin of Parkin mutations: review and case studies. *Mov.Disord.* **19,** 1146-1157

28. Takiyama, Y., Nishizawa, M., Tanaka, H., Kawashima, S., Sakamoto, H., Karube, Y., Shimazaki, H., Soutome, M., Endo, K., and Ohta, S. (1993) The gene for Machado-Joseph disease maps to human chromosome 14q. *Nat.Genet.* **4,** 300-304

29. Ichikawa, Y., Goto, J., Hattori, M., Toyoda, A., Ishii, K., Jeong, S.Y., Hashida, H., Masuda, N., Ogata, K., Kasai, F., Hirai, M., Maciel, P., Rouleau, G.A., Sakaki, Y., and Kanazawa, I. (2001) The genomic structure and expression of MJD, the Machado-Joseph disease gene. *J.Hum.Genet.* **46,** 413-422

30. Maciel, P., Costa, M.C., Ferro, A., Rousseau, M., Santos, C.S., Gaspar, C., Barros, J., Rouleau, G.A., Coutinho, P., and Sequeiros, J. (2001) Improvement in the molecular diagnosis of Machado-Joseph disease. *Arch.Neurol.* **58,** 1821-1827

31. Paulson, H.L., Perez, M.K., Trottier, Y., Trojanowski, J.Q., Subramony, S.H., Das, S.S., Vig, P., Mandel, J.L., Fischbeck, K.H., and Pittman, R.N. (1997) Intranuclear inclusions of expanded polyglutamine protein in spinocerebellar ataxia type 3. *Neuron.* **19,** 333-344

32. Burnett, B., Li, F., and Pittman, R.N. (2003) The polyglutamine neurodegenerative protein ataxin-3 binds polyubiquitylated proteins and has ubiquitin protease activity. *Hum.Mol.Genet.* **12,** 3195-3205

33. Chai, Y., Berke, S.S., Cohen, R.E., and Paulson, H.L. (2004) Poly-ubiquitin binding by the polyglutamine disease protein ataxin-3 links its normal function to protein surveillance pathways. *J.Biol.Chem.* **279,** 3605-3611

34. Winborn, B.J., Travis, S.M., Todi, S.V., Scaglione, K.M., Xu, P., Williams, A.J., Cohen, R.E., Peng, J., and Paulson, H.L. (2008) The deubiquitinating enzyme ataxin-3, a polyglutamine disease protein, edits Lys63 linkages in mixed linkage ubiquitin chains. *J.Biol.Chem.* **283,** 26436-26443

35. Kobayashi, T., Tanaka, K., Inoue, K., and Kakizuka, A. (2002) Functional ATPase activity of p97/valosin-containing protein (VCP) is required for the quality control of endoplasmic reticulum in neuronally differentiated mammalian PC12 cells. *J.Biol.Chem.* **277,** 47358-47365

36. Mishra, A., Dikshit, P., Purkayastha, S., Sharma, J., Nukina, N., and Jana, N.R. (2008) E6-AP promotes misfolded polyglutamine proteins for proteasomal degradation and suppresses polyglutamine protein aggregation and toxicity. *J.Biol.Chem.* **283,** 7648-7656

37. Durcan, T.M., Kontogiannea, M., Thorarinsdottir, T., Fallon, L., Williams, A.J., Djarmati, A., Fantaneanu, T., Paulson, H.L., and Fon, E.A. (2011) The Machado-Joseph disease-associated mutant form of ataxin-3 regulates parkin ubiquitination and stability. *Hum.Mol.Genet.* **20,** 141-154

38. Wang, G., Sawai, N., Kotliarova, S., Kanazawa, I., and Nukina, N. (2000) Ataxin-3, the MJD1 gene product, interacts with the two human homologs of yeast DNA repair protein RAD23, HHR23A and HHR23B. *Hum.Mol.Genet.* **9,** 1795-1803

39. Zhong, X., and Pittman, R.N. (2006) Ataxin-3 binds VCP/p97 and regulates retrotranslocation of ERAD substrates. *Hum.Mol.Genet.* **15,** 2409-2420

40. Harris, G.M., Dodelzon, K., Gong, L., Gonzalez-Alegre, P., and Paulson, H.L. (2010) Splice isoforms of the polyglutamine disease protein ataxin-3 exhibit similar enzymatic yet different aggregation properties. *PLoS One.* **5,** e13695

41. Bettencourt, C., Santos, C., Montiel, R., Costa Mdo, C., Cruz-Morales, P., Santos, L.R., Simoes, N., Kay, T., Vasconcelos, J., Maciel, P., and Lima, M. (2010) Increased transcript diversity: novel splicing variants of Machado-Joseph disease gene (ATXN3). *Neurogenetics.* **11,** 193-202

42. Deveraux, Q., Ustrell, V., Pickart, C., and Rechsteiner, M. (1994) A 26 S protease subunit that binds ubiquitin conjugates. *J.Biol.Chem.* **269,** 7059-7061

43. Hurley, J.H., Lee, S., and Prag, G. (2006) Ubiquitin-binding domains. *Biochem.J.* **399,** 361-372

44. Hofmann, K., and Falquet, L. (2001) A ubiquitin-interacting motif conserved in components of the proteasomal and lysosomal protein degradation systems. *Trends Biochem.Sci.* **26,** 347-350

45. Fisher, R.D., Wang, B., Alam, S.L., Higginson, D.S., Robinson, H., Sundquist, W.I., and Hill, C.P. (2003) Structure and ubiquitin binding of the ubiquitin-interacting motif. *J.Biol.Chem.* **278,** 28976-28984

46. Song, A.X., Zhou, C.J., Peng, Y., Gao, X.C., Zhou, Z.R., Fu, Q.S., Hong, J., Lin, D.H., and Hu, H.Y. (2010) Structural transformation of the tandem ubiquitin-interacting motifs in ataxin-3 and their cooperative interactions with ubiquitin chains. *PLoS One.* **5,** e13202

47. Swanson, K.A., Kang, R.S., Stamenova, S.D., Hicke, L., and Radhakrishnan, I. (2003) Solution structure of Vps27 UIM-ubiquitin complex important for endosomal sorting and receptor downregulation. *EMBO J.* **22,** 4597-4606

48. Patel, M.M., Sgourakis, N.G., Garcia, A.E., and Makhatadze, G.I. (2010) Experimental test of the thermodynamic model of protein cooperativity using temperature-induced unfolding of a Ubq-UIM fusion protein. *Biochemistry.* **49,** 8455-8467

49. Costa Mdo, C., and Paulson, H.L. (2012) Toward understanding Machado-Joseph disease. *Prog.Neurobiol.* **97,** 239-257

50. Nakano, K.K., Dawson, D.M., and Spence, A. (1972) Machado disease. A hereditary ataxia in Portuguese emigrants to Massachusetts. *Neurology.* **22,** 49-55

51. Etchebehere, E.C., Cendes, F., Lopes-Cendes, I., Pereira, J.A., Lima, M.C., Sansana, C.R., Silva, C.A., Camargo, M.F., Santos, A.O., Ramos, C.D., and Camargo, E.E. (2001) Brain single-photon emission computed tomography and magnetic resonance imaging in Machado-Joseph disease. *Arch.Neurol.* **58,** 1257-1263

52. Klockgether, T., Skalej, M., Wedekind, D., Luft, A.R., Welte, D., Schulz, J.B., Abele, M., Burk, K., Laccone, F., Brice, A., and Dichgans, J. (1998) Autosomal dominant cerebellar ataxia type I. MRI-based volumetry of posterior fossa structures and basal ganglia in spinocerebellar ataxia types 1, 2 and 3. *Brain.* **121 (Pt 9),** 1687-1693

53. Murata, Y., Yamaguchi, S., Kawakami, H., Imon, Y., Maruyama, H., Sakai, T., Kazuta, T., Ohtake, T., Nishimura, M., Saida, T., Chiba, S., Oh-i, T., and Nakamura, S. (1998) Characteristic magnetic resonance imaging findings in Machado-Joseph disease. *Arch.Neurol.* **55,** 33-37

54. Taniwaki, T., Sakai, T., Kobayashi, T., Kuwabara, Y., Otsuka, M., Ichiya, Y., Masuda, K., and Goto, I. (1997) Positron emission tomography (PET) in Machado-Joseph disease. *J.Neurol.Sci.* **145,** 63-67

55. Yoshizawa, T., Watanabe, M., Frusho, K., and Shoji, S. (2003) Magnetic resonance imaging demonstrates differential atrophy of pontine base and tegmentum in Machado-Joseph disease. *J.Neurol.Sci.* **215,** 45-50

56. Chow, M.K., Ellisdon, A.M., Cabrita, L.D., and Bottomley, S.P. (2006) Purification of polyglutamine proteins. *Methods Enzymol.* **413,** 1-19

Chapter 2

CHARACTERIZATION OF THE INTERACTION BETWEEN THE PARKIN UBLD AND THE UIM REGION OF ATAXIN-3

2.1 Introduction

Parkin and ataxin-3 are both multi-domain proteins that function in the ubiquitin signaling pathway (USP). The roles of the proteins are opposing. Parkin is an E3 ubiquitin ligase that is responsible in attaching ubiquitin (Ub) on a specific set of substrates, whereas, ataxin-3 is a deubiquitinating (DUB) enzyme which acts to remove Ub moieties from poly-ubiquitin chains (1). There is growing interest in the USP as protein misfolding diseases are linked to these pathways. The concern is that when disease mutations or malfunctions in the regulators of the USP ensue, the protein homeostasis in the cell becomes disrupted to seed cellular aggregation and cell death. Recently, it has been shown that the direct interaction of these two proteins can regulate their catalytic function and turnover via autophagy (1). Interaction studies between parkin and ataxin-3 have been previously investigated by GST binding assays and co-immunoprecipitations, however, the binding interface and mechanism for the interaction remains unknown (1). Some difficulties in interpreting this interaction result from purification problems of the unstable full-length parkin, and the lack of solved structures of the full-length parkin and ataxin-3 proteins, which limits the prediction of docking sites of the interaction. The strategy employed to overcome this obstacle was to identify the specific region(s) of interaction and purify only these critical domains required for the interaction. By isolating the regions of recruitment from parkin and ataxin-3, the ^{1}H-^{15}N HSQC spectra will be easier to analyze and resonances can be unambiguously followed

in an NMR titration, which was the main source of data collection. Based on deubiquitination assays with a C-terminal deletion of the three Ubiquitin Interacting Motifs (UIM) within ataxin-3 (Δ194-361), the C-terminus of ataxin-3 was found not to be important for its DUB activity. It was then postulated the UIM region functions as a recruitment domain for ubiquitin chains on substrate proteins and may be important for positioning the ubiquitin chain for cleavage by the DUB catalytic portion of ataxin-3. The parkin UbLD has 30% sequence identity with ubiquitin and possesses a similar 3D structure, which made it a potential candidate for interactions with the UIM region of ataxin-3 (3). The UIM regions of Eps15, an endocytic protein, and S5a, a regulatory 19s subunit, have been shown to bind to the hydrophobic patch of the UbLD by NMR chemical shift perturbation studies. However, a docking site has not been determined for the ataxin-3 UIM region (2). Unlike the Eps15 and S5a protein, which only have two UIMs, the ataxin-3 gene encodes a unique arrangement of three UIM regions spanning ataxin-3 residues 224-243, 244-263, 331-348 for UIM1, UIM2, and UIM3, respectively. Currently, there is controversial evidence whether all three UIMs are important (3, 4, 5) for the proper functioning of ataxin-3.

In this work, the aims were to identify the binding site on the parkin UbLD for the UIM region of ataxin-$3^{194-361}$, to calculate the binding affinities, to determine which UIM from the C-terminus of ataxin-3 interacts with parkin, and use this data to predict what type of binding mechanism is employed for their interaction. The characterization of the binding interaction between ataxin-3 and parkin will be utilized for predicting how Autosomal Recessive Juvenile Parkinsonism (ARJP) substitutions might influence binding.

2.2 Materials and Methods

2.2.1 Parkin ubiquitin-like domain

The DNA encoding human parkin ubiquitin-like domain (1-77) was previously inserted into the NdeI and BamHI sites of the pET44a vector (Novagen) (2). The parkin UbLD constructs were verified by DNA sequencing (Robarts Sequencing Facility).

2.2.2 Ataxin-3 ubiquitin interacting motifs

The cDNA encoding full-length human ataxin-3 construct was a generous gift from Dr. Edward Fon (McGill, Montreal, Quebec). The ataxin-3 cDNA contained a 14 residue polyglutamine tract as well as an N-terminal hexa-histidine tag. Site-directed mutagenesis was previously used to incorporate a TEV cleavage site to allow for removal of a 6-residue N-terminal histidine tag from ataxin-3 constructs. The His-tagged ataxin-$3^{194\text{-}361}$ construct, containing all three UIM regions, was inserted into the BamHI and XhoI sites of the pET21a vector (Novagen). Site-directed mutagenesis was also used to generate a C-terminal deletion construct, consisting of residues 194-261, by encoding a stop site prior to the poly-glutamine stretch of ataxin-3. To create a single UIM construct of just the N-terminal $UIM^{194\text{-}244}$, the same approach was executed by using site directed mutagenesis to make a stop site prior to the DNA sequence encoding the second UIM.

The individually intact UIM genes were synthesized by DNA2.0 in their house pJexpress414 vector and cloned into the NdeI and XhoI sites (Fig. 2.1). The conserved serine, (residues 236, 256 and 347 within UIM1, 2, and 3) and hydrophobic stretch in the core UIM sequence (residues 229-243, 249-253, 340-344) were substituted to alanine

residues and designed in the computer program Gene Designer 2.0. All genetic elements were identical to the wild-type ataxin-3 constructs mentioned above. Three vectors were ordered to experiment with individual functional UIMs; functional knockout of UIM I/II, functional knockout of UIM II/III, and functional knockout of UIM I/III. DNA sequencing was carried out to ensure the correct sequence of the ataxin-3 UIM genes (Robarts Research Institute).

2.2.3 Expression and purification of the parkin ubiquitin-like domain

The human parkin UbLD was overexpressed in BL21(DE3) Codon PlusRIL *Escherichia coli* strain and was cloned without an affinity tag. The bacterial culture was diluted 1:100 volume ratio in LB media, and grown at 37°C until an A_{600} of 0.6-0.7 was reached. The culture was grown with constant shaking overnight at 16°C after induction of expression by the addition of 1 mM isopropyl 1-thio-β-D-galactopyranoside. The starter culture and large bacterial cultures contained the antibiotic ampicillin (50 μg/mL). Cells were lysed with either an EmulsiFlex-05 homogenizer (AVESTIN) or French press and centrifuged at 132380 g for one hour. The cell homogenate was filtered through a MILLEX HV 0.45 μm filter unit (MILLIPORE) before loading onto a HiTrap Q XL column, using a AKTA FPLC system (GE Healthcare). The binding buffer contained 25

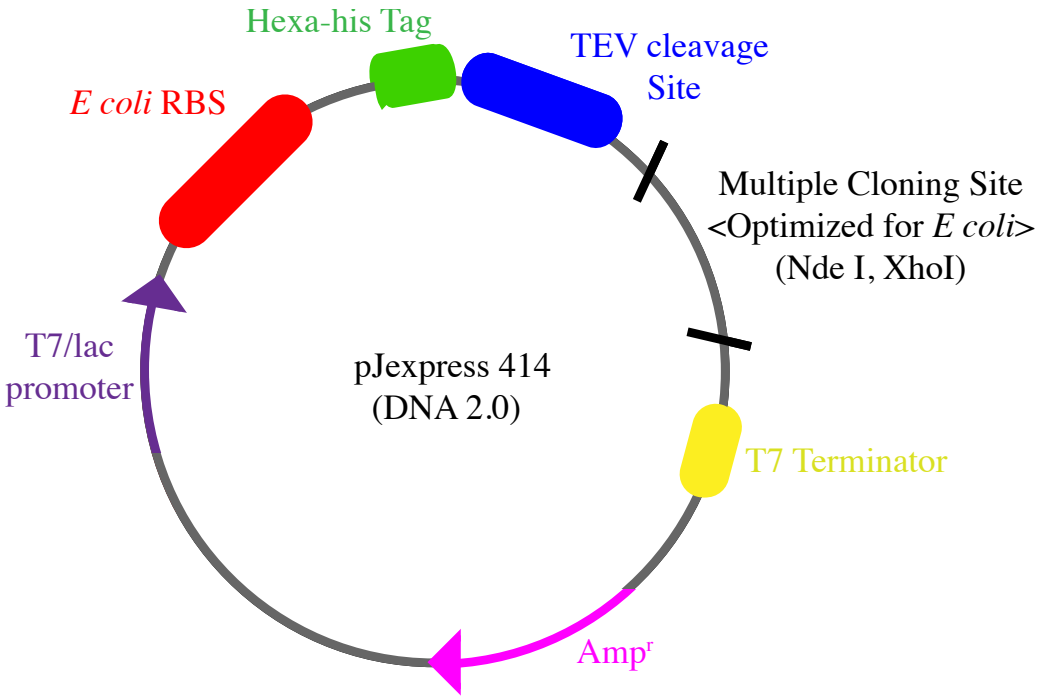

Figure 2.1 Diagrammatic representation of the DNA 2.0 pJexpress414 vector. The individually intact UIM genes were inserted into the NdeI and XhoI sites of the pJexpress 414 vector. The genetic elements such as the hexa-His tag and the TEV cleavage site matches the genetic elements for all the previously mentioned ataxin-3 protein constructs. The multiple cloning site was optimized for *E. coli* expression. All of the genetic elements and multiple cloning site sequence were designed in the computer program Gene Designer 2.0.

mM Tris and 1 mM EDTA at pH 9.0, and the elution buffer contained 25 mM Tris, 1 mM EDTA and 1 M NaCl at pH 9.0. The protein eluted in the flowthrough fractions and was further purified on a size exclusion column (G75) at 4°C in 50 mM Na_2HPO_4, 150 mM NaCl, 1 mM EDTA, 1 mM DTT, at pH 8.0 with a flowrate of 6ml/hour. The integrities of all ARJP substituted proteins were confirmed previously using electrospray ionization mass spectrometry (UWO Biological Mass Spectrometry Laboratory) (2).

2.2.4 Expression and purification of ataxin-3 ubiquitin interacting motifs

All six human ataxin-3 UIM constructs were overexpressed in a BL21(DE3) Codon PlusRIL *Escherichia coli* strain. The bacterial culture was diluted 1:100 volume ratio in LB media, and grown at 37°C until an A_{600} of 0.6-0.7 was reached. The culture was grown with constant shaking overnight at 16°C after induction of expression by the addition of 1 mM isopropyl 1-thio-β-D-galactopyranoside. The starter culture and large bacterial cultures contained the antibiotic ampicillin (50 μg/mL). Cells were lysed with either an EmulsiFlex-05 homogenizer (AVESTIN) or French press and ultracentrifuged at 132380 g. The cell homogenate was filtered through a MILLEX HV 0.45 μm filter unit (MILLIPORE) before loading onto a Ni-NTA fast protein liquid chromatography affinity column (GE healthcare). The loading buffer contained 50mM Na_2HPO_4, 500nM NaCl, 10mM imidazole at pH8, and the elution buffer was identical except with the addition of 500mM imidazole. The protein samples were dialyzed overnight at 4°C in the loading buffer with an addition of TEV protease (1.2mg/1L bacterial preparation) for cleavage, and reloaded onto the Ni-NTA column. Cleaved UIM proteins came off in the

flowthrough. All six of the ataxin-3 UIM constructs were purified using the same protocol.

2.2.5 NMR Spectroscopy titration experiments

All ^{1}H-^{15}N Heteronuclear Single Quantum Coherence (HSQC) NMR experiments were performed on a 600 MHz Varian Inova spectrometer (BioNMR Facility, UWO). All protein samples were extensively dialyzed into 11 mM KH_2PO_4, 150 mM NaCl, 1 mM EDTA, 1 mM dithiothreitol, at pH 7. Imidazole (100 μM) was added in the final NMR sample to serve as a pH indicator. All spectra were recorded at 25°C. Chemical shift perturbation upon binding between protein samples were monitored and fit with either a non-linear regression global fit for a 1:1 binding model or a 3:1 multivalent global fit with equivalent affinities.

Consider,

$$P + L \rightleftharpoons PL$$

P - protein

L - ligand

PL - protein-ligand complex

The equation that was used for non-linear regression global fitting for a 1:1 binding site was,

$$PL = \frac{(Pt + X + K_D) - \sqrt{(Pt + X + K_D)^2 - (4 + X + Pt)}}{2}$$

$$Y = n \cdot B \cdot ({}^{PL}/_{Pt})$$

PL - Protein-Ligand Complex

Pt - Total Protein

X - Added Ligand Concentration

K_D - Dissociation Constant (same units as Pt)

n - number of identical sites

B - Normalization Factor

The normalization factor is required for the global fit of the binding curves. Since the chemical shift differences of different resonances that change upon addition of ligand are not identical.

For a 3:1 multivalent model, consider,

$$P + L \rightleftharpoons PL_1 \qquad K_1$$
$$P + L \rightleftharpoons PL_2 \qquad K_2$$
$$P + L \rightleftharpoons PL_3 \qquad K_3$$

Where PL_1, PL_2, PL_3 are three different sites on the ligand (ataxin-3) that the protein can bind.

P - protein

L - ligand

PL_x - protein-ligand complex

Assuming the ligand binds to each site with equal affinity (ie. $K_1 = K_2 = K_3 = K_D$), then the equation used to globally fit a three multi-site binding model is,

$$PL = \frac{(n \cdot Pt + n \cdot X + K_D) - \sqrt{(n \cdot Pt + n \cdot X + K_D)^2 - (4 \cdot n^2 \cdot x \cdot Pt)}}{2 \cdot n^2}$$

$$Y = n \cdot B \cdot ({}^{PL}/_{Pt})$$

The computer programs used to fit data were Prism 4 and NMRViewJ version 8.0.rc4. Titration experiments that were performed are listed (Table 2.1). Protein samples were sent to the Amino Acid Analysis facility (Sick Kids Hospital, Toronto, ON) for acquiring accurate protein concentration values. Details regarding the concentrations of ^{15}N-labeled proteins as well as titrant proteins can be found in the results section.

Table 2.1 The protein combinations used in the ^{1}H-^{15}N HSQC titration experiments

^{15}N Isotopically Labeled	**Unlabeled Protein (Titrant)**
Parkin UbLD	Ataxin-3 UIM123 $^{194-361}$
Parkin UbLD	Ataxin-3 UIM12 $^{194-261}$
Parkin UbLD	Ataxin-3 UIM1 $^{194-244}$
Parkin UbLD	Ataxin-3 UIM3*$^{194-361}$
Parkin UbLD	Ataxin-3 UIM2*$^{194-361}$
Parkin UbLD	Ataxin-3 UIM1*$^{194-361}$
Ataxin-3 UIM123$^{194-361}$	Parkin UbLD
Ataxin-3 UIM12$^{194-264}$	Parkin UbLD
Ataxin-3 UIM123$^{194-361}$	Ubiquitin

* - indicates the ataxin-3 UIM constructs that are full-length (including residues 194-361) but with only one functional UIM with the other two UIMs are 'functionally knocked out' by alanine substitutions. In this context, functional is defined as being able to retain interaction with the UbLD. In contrast, 'functionally knocked out' means that conserved residues in the UIM sequence have been substituted by alanine residues and can no longer interact with the UbLD.

2.3 Results

2.3.1 Molecular biology, expression and purification of parkin ubiquitin like domain

The human parkin UbLD gene had previously been inserted into the NdeI and BamHI sites of the pET44a vector (Novagen) (3). The overexpression of the UbLD in BL21(DE3) Codon PlusRIL *Escherichia coli* strain was induced with 1mM IPTG and the overexpressed protein band can be seen just below the 10 kDa molecular weight ladder, as expected since the molecular weight of the UbLD is 8824 Da (Figure 2.2). The rate of protein separation of the sizing column was 6ml/hr and the fractions containing pure UbLD protein elutes from the column between hours 65-75 or shown as lanes 7-10 in Figure 2.2B. Purified proteins were checked on an SDS-PAGE gel for purity.

2.3.2 Molecular biology, expression, and purification of ataxin-3 UIM123$^{194-361}$ and other ataxin-3 constructs

The ataxin-3 UIM123$^{194-361}$ construct with three intact UIM regions was successfully inserted into the BamHI and XhoI sites of the pET21a vector (Novagen), previously done. Site-directed mutagenesis was then used to incorporate a TEV cleavage site to allow for the removal of a 6-residue N-terminal histidine tag from ataxin-3 construct.

All of the ataxin-3 protein constructs were overexpressed in a BL21(DE3) Codon PlusRIL *Escherichia coli* strain. All ataxin-3 protein constructs have the same genetic elements, an N-terminal six histidine-tag followed by a TEV cleavage site upstream of the ataxin-3 UIM gene. Two Ni^{2+}-NTA FPLC column steps were completed to obtain a tag free protein that just includes pure fractions of ataxin-3 UIMs (Figure 2.3). In

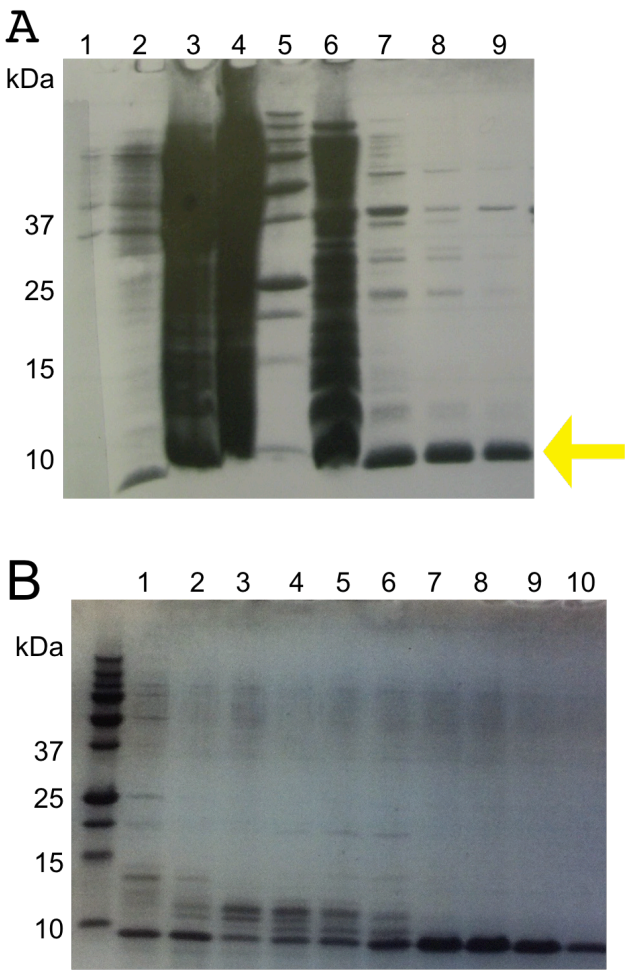

Figure 2.2 SDS-PAGE of parkin ubiquitin-like domain expression and purification. A) Lanes 1 and 2 are the pre-induction and post IPTG induction expression test for the UbLD. Lane 3 is the lysate, prior to loading onto the HiTrap Q XL column and lane 4 is the flow through off the column. Lane 5 is the molecular weight ladder. Lane 6 is the elution fraction off the Q XL column. Lanes 7-9 show fractions collected from the G75 sizing column. B) The SDS-PAGE of protein fractions collected off of the G75 sizing column. The UbLD, which has a calculated molecular weight of 8824 kDa, migrates just below the 10kDa molecular ladder band. Both gels were stained in Coomassie brilliant blue.

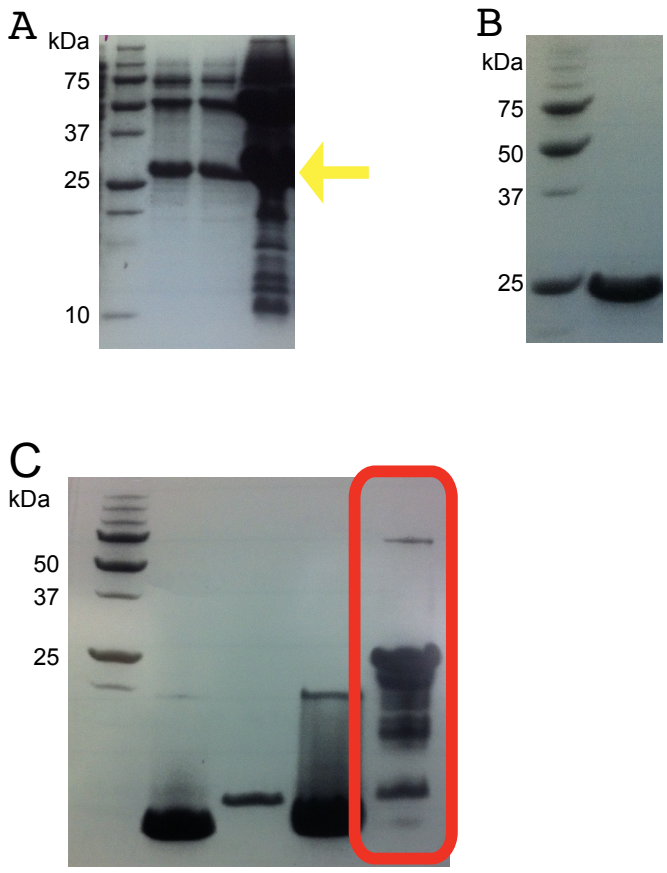

Figure 2.3 Purification of ataxin-3 UIM123$^{194-361}$. A) The three lanes are showing the first elution fractions off of the Ni^{2+}-NTA column of the ataxin-3 purification, prior to TEV cleavage of the hexa-histidine tag. The yellow arrow indicates the overexpressed His-tagged ataxin-3 UIM123$^{194-361}$ protein. B) SDS-PAGE showing the elution fraction of the second part of the ataxin-3 purification. This fraction was eluted from the second Ni^{2+}-NTA column pass through, following TEV cleavage overnight. C) The lane highlighted in the red box is showing the degradation of ataxin-3 UIM123$^{194-361}$ construct over two weeks time at 4°C.

between the two Ni^{2+}-column steps, the protein was extensively dialyzed in a low imidazole buffer with TEV specific protease to cleave the N-terminal six histidine tag from the ataxin-3 protein construct. His-tagged ataxin-3 $UIM123^{194-361}$ migrates to greater than 25 kDa, but after the TEV cleavage step, the ataxin-3 $UIM123^{194-361}$ protein migrates just short of 25 kDa (Figure 2.3). After purification of the ataxin-3 UIM region, it was observed that this region was prone to degradation (Figure 2.3).

2.3.3 Ataxin-3 $UIM123^{194-361}$ confers a docking site on the hydrophobic patch of the parkin UbLD

Titration experiments monitored by ^{1}H-^{15}N HSQC spectra were performed with ^{15}N-labelled parkin UbLD and unlabeled ataxin-3, to identify the binding site of ataxin-3 on the UbLD. The ^{1}H-^{15}N HSQC spectrum of ^{15}N UbLD in the absence of binding partner displays disperse peaks in the proton dimension, indicative of a well-folded protein. Each peak represents the amide proton correlated to its amide nitrogen, thus, each amino acid in the sequence, except proline residues, will have a corresponding resonance. Resonances that shift upon titrations of a binding partner are indicative of nuclei experiencing a local environmental change, which are the residues involved in the interaction. The binding site on parkin was determined by measuring the absolute change in chemical shift (in ppm) of the UbLD resonances with titrations of up to 6 equivalents of ataxin-3 $UIM123^{194-361}$ construct (Figure 2.4). The resonances that shifted greater than 0.5 standard deviation above the average chemical shift were mapped on the surface of the UbLD (Figure 2.5). The backbone assignments of both parkin UbLD and most residues of the ataxin-3 UIMs construct were previously determined, and all of the resonances were

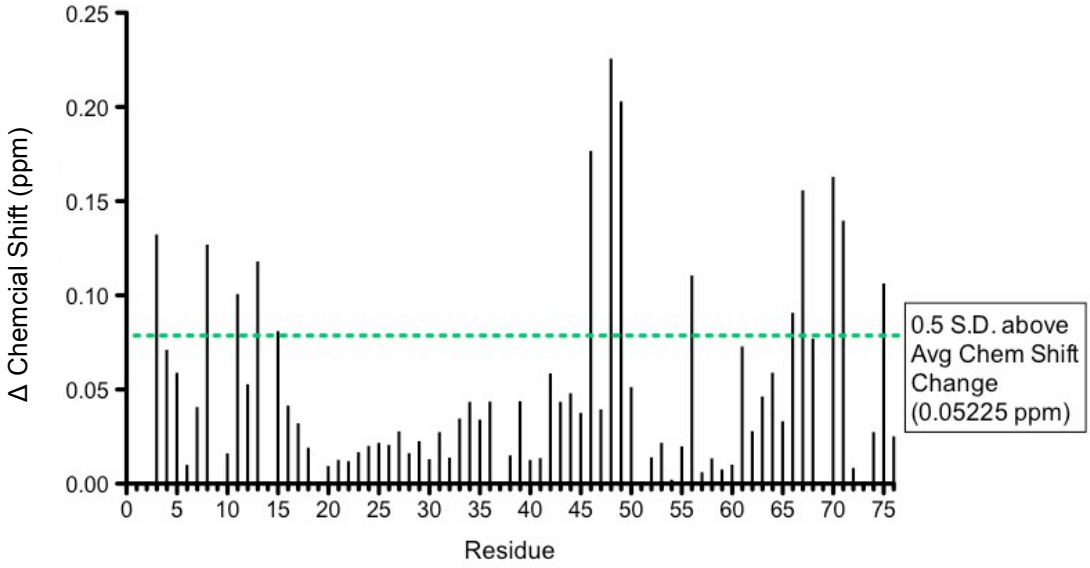

Figure 2.4 NMR chemical shift perturbation data of parkin UbLD upon ataxin-3 UIMs$^{194\text{-}361}$ binding. Chemical shift perturbation map of UbLD by measuring the absolute change in magnitude of the peak shifts that occurs after addition of 6 eq. of ataxin-3. The concentration of the UbLD protein sample was 105 μM. The absolute change in magnitude of the resonance shifts were calculated using the equation, $((0.2 \times \Delta\delta N^2) + \Delta\delta H^2)^{1/2}$. The dotted green line indicates 0.5 S.D. above the average chemical shift perturbation value. The residues on parkin that display more than 0.5 standard deviation above the average chemical shift are V3, N8, H11, F13, V15, A46, K48, E49, V56, I66, V67, H68, V70, Q71, and R75.

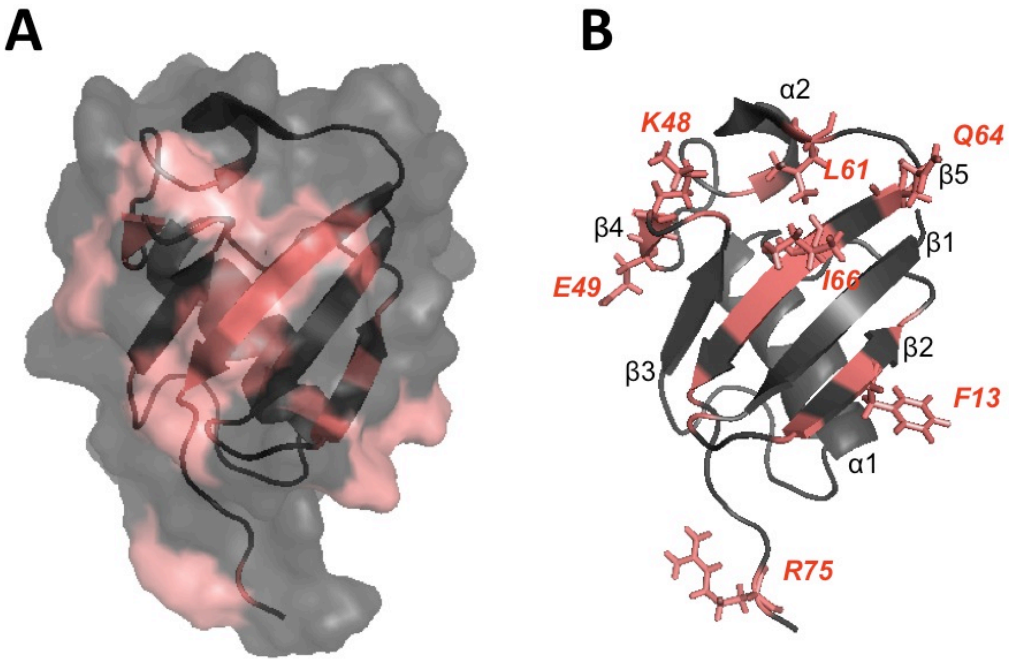

Figure 2.5 Surface and ribbon representation of the binding surface for ataxin-3$^{194-361}$ on the parkin ubiquitin like domain. A) A surface representation, coloured in pink, of where ataxin-3$^{194-361}$ binds on the UbLD. The residues that displayed more than 0.5 standard deviation above the average chemical shift were mapped on the surface of the UbLD which is highlighted in pink. B) The seven amino acid side chains that displayed the greatest chemical shift perturbations upon addition of 6 equivalents of the full UIMs ataxin-3 construct are shown. The individual beta strands and alpha helices from the beta-grasp fold blanketing over the alpha helix are labeled.

accounted for when a standard ^{1}H-^{15}N HSQC spectra of the UbLD$^{1-77}$ and ataxin-3 UIM123$^{194-364}$ construct were collected (3). The residues on parkin that display greater than 0.5 standard deviation above the average chemical shift were Val^{3}, Asn^{8}, His^{11}, Phe^{13}, Val^{15}, Ala^{46}, Lys^{48}, Glu^{49}, Val^{56}, Ile^{66}, Val^{67}, His^{68}, Val^{70}, Gln^{71}, and Arg^{75} (Figure 2.4). Most of these residues are found on the solvent exposed hydrophobic patch of the UbLD, as highlighted in pink (Figure 2.5). Ala^{46} and Ile^{66} are two of the hydrophobic residues on the hydrophobic patch of parkin that are influenced by ataxin-3 UIM123$^{194-361}$ binding. From the perspective of the parkin protein, residues participating in the interaction are dominated by hydrophobic amino acid residues (Leu^{61}, Ile^{66}, Phe^{13}), followed by basic amino acid residues (Lys^{48}). The binding site on the UbLD is composed of residues from multiple secondary structures, suggesting that the three-dimensional fold of this domain must be intact to expose the docking site for ataxin-3.

2.3.4 Parkin UbLD interacts with all three ubiquitin interacting motifs from ataxin-3

^{1}H-^{15}N HSQC titration experiments were utilized to investigate which UIM from ataxin-3 participates in the interaction with the UbLD. For each NMR titration experiment, 6-8 titration points were collected by incrementally adding unlabeled UbLD to ^{15}N-labeled ataxin-3 UIM123$^{194-361}$. At each titration point, a standard ^{1}H-^{15}N HSQC experiment was collected. By overlaying the spectra taken from each titration point, the resonances that were 'shifting' on the ataxin-3 could be identified. Many NMR titration experiments were utilized to systematically identify whether UIM1, UIM2 and/or UIM3 participate in the interaction with parkin. However, the experiment involving ^{15}N-labeled ataxin-3 UIM123$^{194-361}$ titrated with unlabeled UbLD$^{1-77}$ was the only experiment that

revealed whether any or all of the three UIM regions of ataxin-3 were interacting with the UbLD.

The backbone assignments of the ataxin-3 UIMs construct were previously assigned, by previous graduate student Dr. Safadi, and all of the resonances were accounted for when collecting a standard ^{1}H-^{15}N HSQC spectra of the ataxin-3 UIM123$^{194-361}$ construct. The dissociation constant from the perspective of each UIM were globally fitted to a 1:1 non-linear regression fit, $K_{D,\ UIM1}$= 2092±654 μM, $K_{D,\ UIM2}$= 1071±263 μM, $K_{D,\ UIM3}$= 1975±368 μM (Figure 2.6). The dissociation constant for UIM1 is in the same range within error for both KDs of the other two UIMs. Meanwhile, the K_D between UIM2 and UIM3 are not in the same range within error, with UIM2 having a slightly tighter binding to the UbLD than UIM3. The K_D values were calculated solely based on the amide proton shifts, due to the greater magnitude of perturbation in the proton dimension as compared with nitrogen dimension (Figure 2.7). However, there was difficulty finding appropriate resonances from each UIM to measure chemical shifts from, due to the collapse of many resonances in the proton dimension of the ^{1}H-^{15}N HSQC spectrum of ataxin-3 UIM123$^{194-361}$ protein alone, which is indicative of random coils in protein fold (Figure 2.7). From UIM1, residues A232, A234, D241 were followed, while in UIM2 only one residue (D248) could be unambiguously followed. In UIM3, amino acid residues S335, V344, and T345 were followed to obtain the K_D (Figures 2.6, 2.7). Despite the collapse in the proton dimension of the spectrum, there are still other resonances from each UIM that are clearly identified to be shifting in response to additions of UbLD protein (Figure 2.7). The individual binding affinities of the UIM

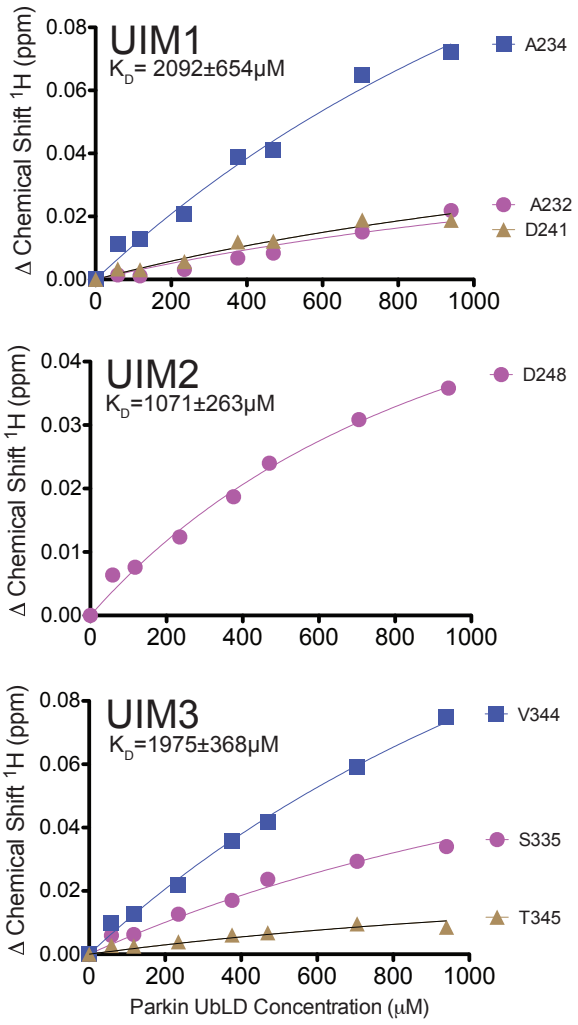

Figure 2.6 Binding curves of the change in proton chemical shift of resonances from UIM1, UIM2, and UIM3 of ataxin-3 with titrations of parkin UbLD. Measurements were taken from NMR ^{1}H-^{15}N HSQC titration experiments with samples containing ^{15}N ataxin-3 UIM123$^{194\text{-}361}$ (73μM) and additions of unlabeled UbLD (0, 58.7, 117.5, 235, 376, 470, 705, 940μM). The K_D values are $K_{D,UIMI}$ = 2092±654 μM, $K_{D,UIM2}$ = 1071±263 μM, and $K_{D,UIM3}$ = 1975±368 μM based on a global fit of non-linear regression analysis for 1:1 binding. The corresponding amino acid residue of which the chemical shifts were measured are indicated to the right side of the binding curve.

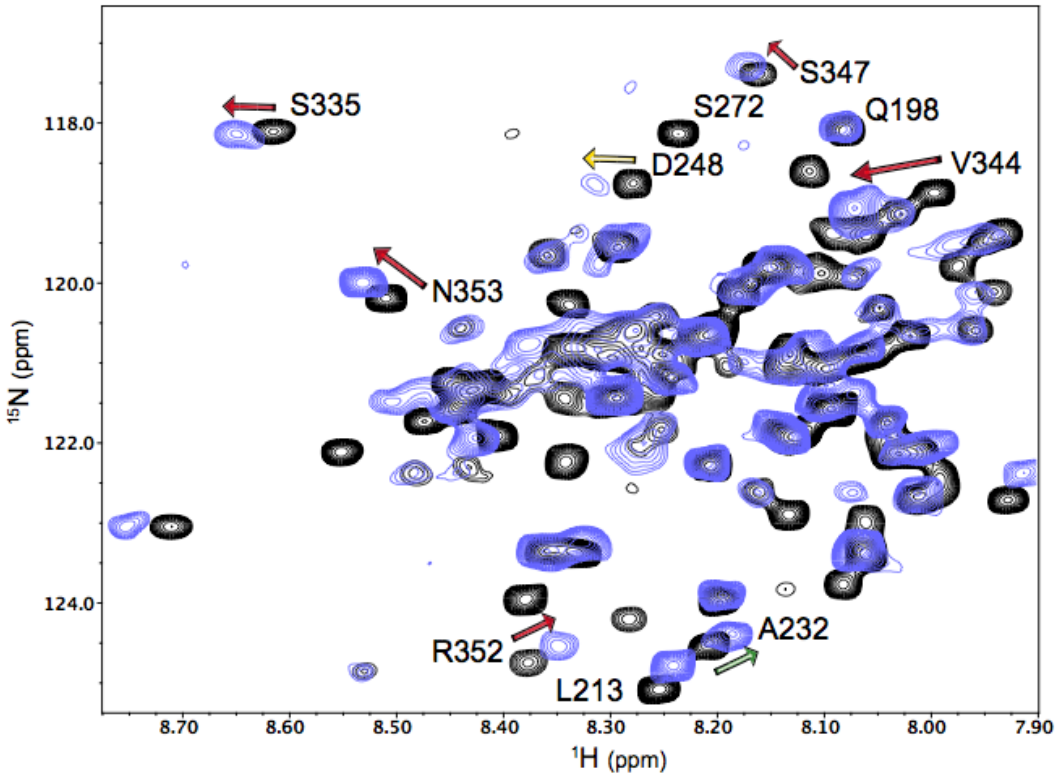

Figure 2.7 Region of the ^{1}H-^{15}N HSQC spectrum of ataxin-3 UIM123$^{194-361}$ overlaid with a ^{1}H-^{15}N HSQC spectra of ataxin-3 UIM123$^{194-361}$ with 12 equivalents of parkin UbLD (blue). NMR data was collected with Varian INOVA 600 MHz NMR spectrometer with samples in a buffer containing 10 mM KH_2PO_4, 1 mM EDTA, 1 mM DTT pH 7.0 at 25°C (pH indicator, Imidazole). The starting concentration of ^{15}N labeled ataxin-3 UIM123$^{194-361}$ was 73µM and was titrated with up to 12 equivalents of UbLD. The red arrows indicate the direction of chemical shift changes upon UbLD additions for residues in UIM3. The yellow and green arrows indicate chemical shifting directions for UIM2 and UIM1, respectively.

regions are all in the millimolar range suggesting that UIM1, UIM2 and UIM3 are all able to make weak interactions with the UbLD.

The same experiments were repeated except with a ^{15}N-labelled species of the ataxin-3 UIM12$^{194\text{-}261}$ construct (containing only UIM1 and UIM2) with incremental titrations of the UbLD to greater than 10 equivalents. The fitting of the binding curve was poor due to not reaching saturation in binding of the isotopically labeled protein. The binding affinity for both UIM1 and UIM2 were in the same range within error of all three UIMs in the ^{15}N ataxin-3 UIM123$^{194\text{-}361}$ experiment, mentioned above. The dissociation constants were derived from considering chemical shift changes only in the proton dimension, amino acid residues from UIM1 used to obtain a $K_{D,\ UIM1}$ = 3075±563 μM, were A232, A234, D241, residues from UIM2 to obtain a $K_{D,\ UIM2}$ = ~15400±20000 μM, were solely based on residue D248. The deletion of the most C-terminal UIM and poly-glutamine tract (14Q) clears up some of the congestion of resonances in the proton dimension of the ^{1}H-^{15}N HSQC spectrum. When comparing the ataxin-3 UIM12$^{194\text{-}261}$ spectrum with the ataxin-3 UIM123$^{194\text{-}361}$ spectrum, many of the residues belonging to the third UIM or closely surrounding the motif, which are resonances that can only be found in the ataxin-3$^{194\text{-}361}$ ^{1}H-^{15}N HSQC spectrum, can be observed to experience chemical shift perturbations upon addition of the UbLD. Thus, the third UIM is participating in the interaction with the UbLD, along with UIM1 and UIM2.

2.3.5 ^{1}H-^{15}N HSQC experiments of ^{15}N parkin UbLD with titrations of individually intact ataxin-3 support that all three UIM regions are able to interact with the UbLD

To support the findings from the titration experiments involving ^{15}N-labelled ataxin-3$^{194\text{-}361}$ and UbLD additions, which showed that all three UIM regions were

participating in the interaction with the parkin UbLD, the complementary experiments were carried out. This involved overexpressing the individual functional UIM regions, and titration of these proteins into ^{15}N-labelled UbLD. The conserved serine and 5 hydrophobic core residues, both within the UIM region, were substituted for alanine residues to ensure that the UIM was no longer able to bind to the parkin UbLD. Comparisons of the UbLD ^{1}H-^{15}N HSQC spectrum alone overlaid with a ^{1}H-^{15}N HSQC spectrum of the UbLD with an addition of the most concentrated addition of ataxin-3$^{194-361}$ intact UIM1, UIM2 and UIM3 shows that there were many similarities between the resonances that experience a change in its chemical shift (Figures 2.8, 2.9, 2.10). Lys^{48}, Glu^{49}, and Ile^{66} displayed the greatest chemical shift change upon binding to the ataxin-3, and the corresponding resonances were consistently shifting in the same direction for each separate titration experiment for additions of either intact UIM1, UIM2, or UIM3 constructs (Figure 2.9ADG, Figure 2.10). There were only local changes to the UbLD upon binding each UIM, as only a few residues shift upon titrations of UIM1, 2 or 3. Most of the resonances from the UbLD did not change upon titration of any of the UIM regions (Figure 2.8). One such resonance was Val^{29}, which is buried beneath the beta-grasp fold, was not perturbed by complex formation. It is proximal to Val^{17}, another residue that was not perturbed greatly by complex formation with the UbLD (Figure 2.9CFI). Although most of the residues of the UbLD behaved similarly upon UIM1, 2 or 3 titrations, not all of the peaks shifted in identical magnitudes or direction (Figures 2.8, 2.10). The absolute chemical shift perturbations were measured to derive the dissociation constant for each titration experiment. The dissociation constants were $K_{D,\ intact\ UIM1}$ = 840

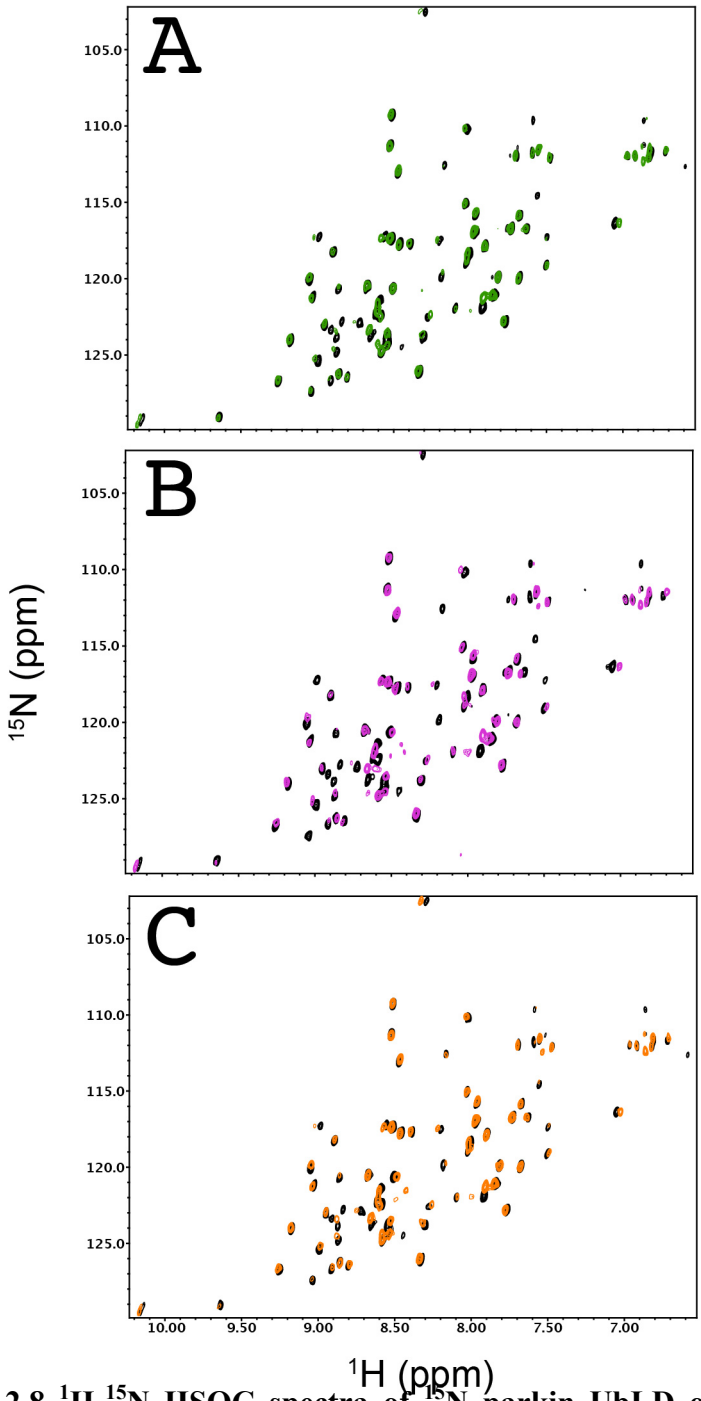

Figure 2.8 ^{1}H-^{15}N HSQC spectra of ^{15}N parkin UbLD overlaid with spectra following additions of functionally intact ataxin-3 UIM1*$^{194-361}$ (A), UIM2*$^{194-361}$ (B), and UIM3*$^{194-361}$ (C). NMR data was collected with Varian INOVA 600 MHz NMR spectrometer with samples in a buffer containing 10 mM KH_2PO_4, 1 mM EDTA, 1 mM DTT pH 7.0 at 25°C (pH indicator, Imidazole). The starting concentration of ^{15}N labeled parkin UbLD was 100µM (for all three titrations) and was titrated with up to (A) 6.5, (B) 8, (C) 7.9 equivalents ataxin-3, respectively.

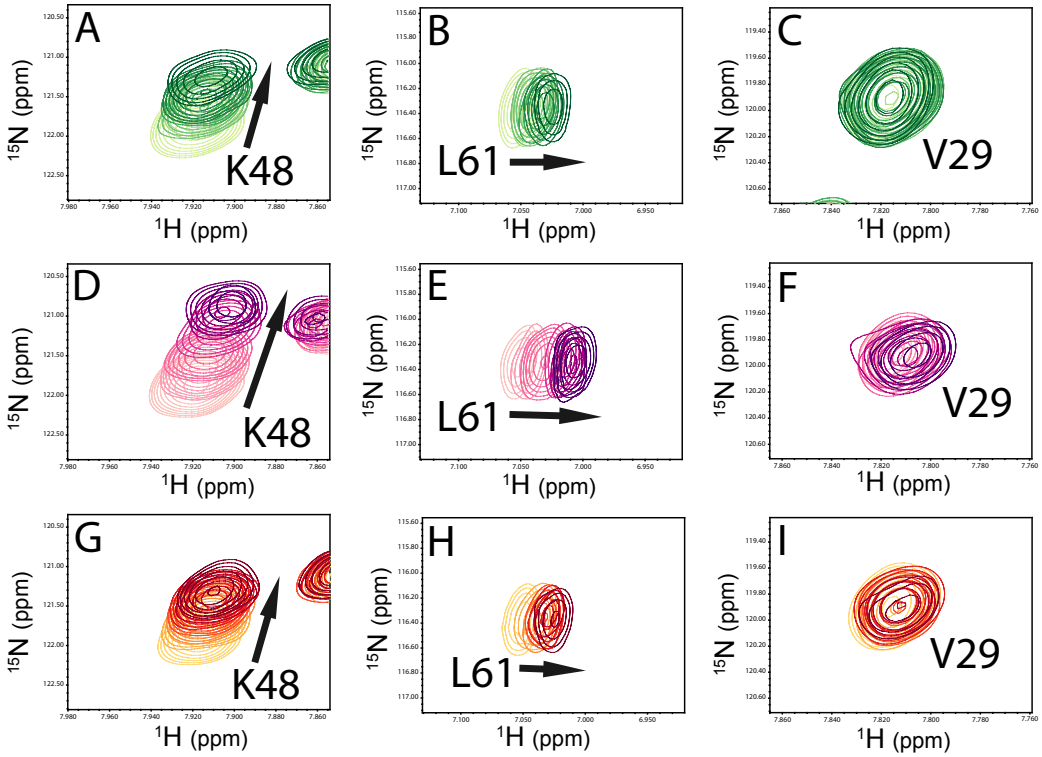

Figure 2.9 Selected region of ^{1}H-^{15}N HSQC spectra of ^{15}N parkin UbLD overlaid with HSQC spectra with incremental additions of functionally intact ataxin-3 UIM1*$^{194-361}$ (A-C), UIM2*$^{194-361}$ (D-F), and UIM3*$^{194-361}$ (G-I). Spectra were collected on a Varian INOVA 600 MHz NMR spectrometer with samples in a buffer containing 10 mM KH_2PO_4, 150 mM NaCl, 1 mM EDTA, 1 mM DTT pH 7.0 at 25°C (pH indicator, Imidazole). The starting concentration of ^{15}N labeled parkin UbLD was 100 μM (for all three titrations) and was titrated with up to (A) 6.5, (B) 8, (C) 7.9 equivalents ataxin-3, respectively. The similar behaviour for resonances of amino acid residues Lys^{48}, Leu^{61} and Val^{29} for all three sets of titration experiments is shown.

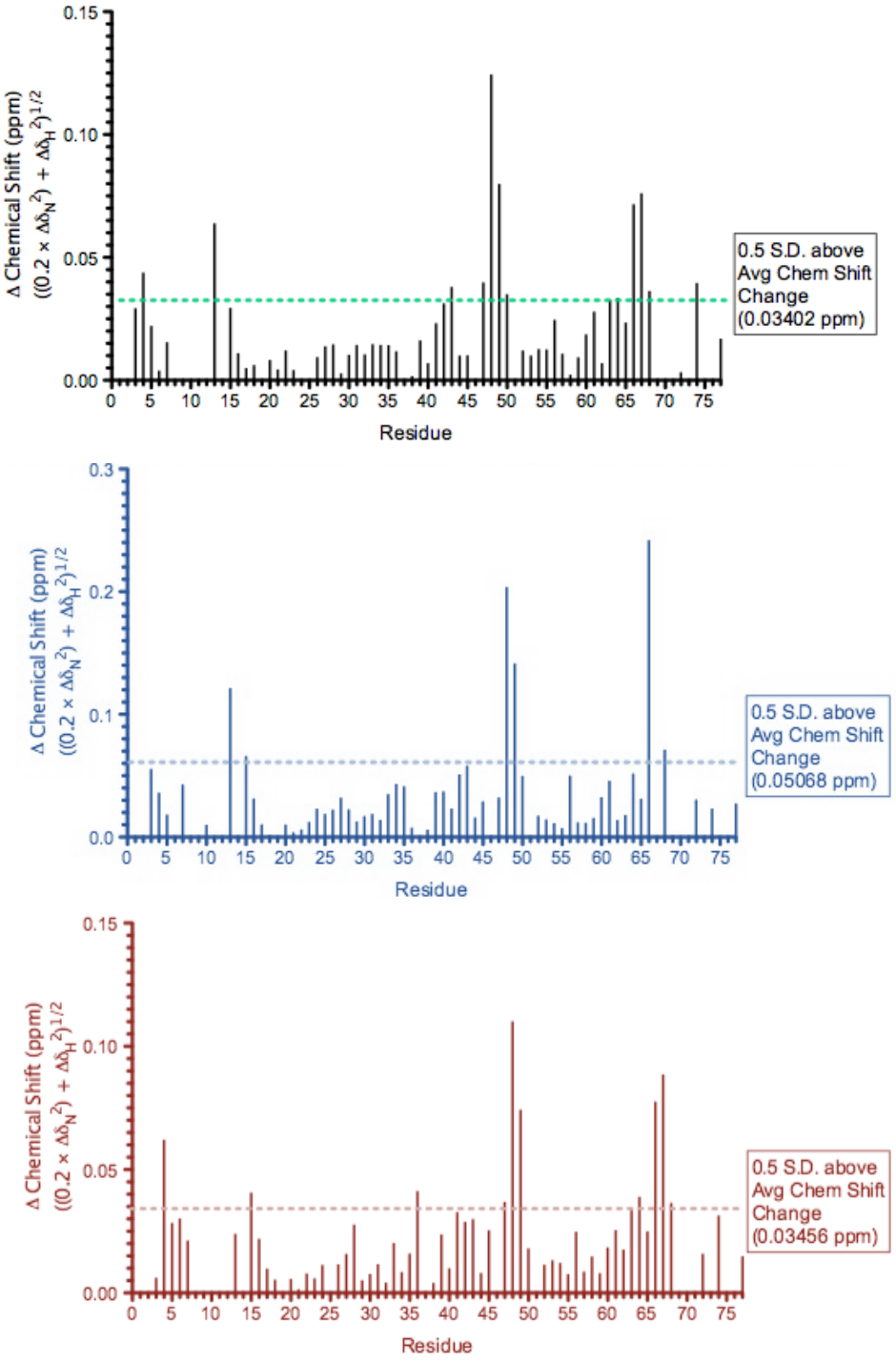

Figure 2.10 NMR chemical shift perturbation data comparison of the parkin UbLD interaction with individual functional ataxin-3 UIM1*$^{194-361}$ (black), UIM2*$^{194-361}$ (blue), and UIM3*$^{194-361}$ (red). Chemical shift perturbation data of the UbLD was determined by measuring the absolute change in magnitude of peak shifts that occurred after addition of 6 eq. of ataxin-3. The absolute change in magnitude of the resonance shifts were calculated using the equation, $((0.2 \times \Delta\delta N^2) + \Delta\delta H^2)^{1/2}$. The dotted line indicates 0.5 S.D. above the average chemical shift perturbation value. The residues on parkin that display more than 0.5 standard deviation above the average chemical shift were K48, E49, I66, and H68.

± 189 μM, $K_{D,\ intact\ UIM2}$ = 502 ± 41 μM, $K_{D,\ intact\ UIM3}$ = 921 ± 165 μM (Figure 2.11). The absolute chemical shifts were measured following residues Lys^{48}, Glu^{49} and Leu^{61} for each titration experiment in order to generate binding curves. Other residues observed to shift were Val^{43}, Glu^{64}, and His^{68}; corresponding experiment for which these residues were measured are found on Figure 2.11. The data collected from these three titration experiments support the finding that all three UIM regions of ataxin-3 are participating in the interaction with the UbLD.

2.3.6 ^{1}H-^{15}N HSQC experiments of UbLD with titrations of C-terminal deletions of UIM regions display an increase in binding affinity when all three UIM regions are present

Resonances of the ^{15}N UbLD displaying the greatest chemical shifts in the ^{1}H-^{15}N HSQC spectrum were measured (Figure 2.12, 2.13). After plotting the changes in chemical shift in response to increased concentrations of C-terminal deletion ataxin-3 constructs, the dissociation constants were determined by a global fitting of the non-linear regression analysis for a 1:1 binding curve.

The dissociation constants obtained for the full UIM construct to ^{15}N UbLD were 235.7 ± 14.0 μM, and 221.7 ± 17.6 μM, in the nitrogen and amide proton dimension, respectively (Figure 2.13A). The interaction appears to be weaker when the third UIM is deleted, the K_D values obtained for the ataxin-3 $UIM12^{194\text{-}261}$ construct titrated into the ^{15}N UbLD were 422.5±25.8 μM, and 433.7±37.3 μM, in the nitrogen and amide proton dimension, respectively (Figure 2.13B). When only the most N-terminal UIM is available to interact

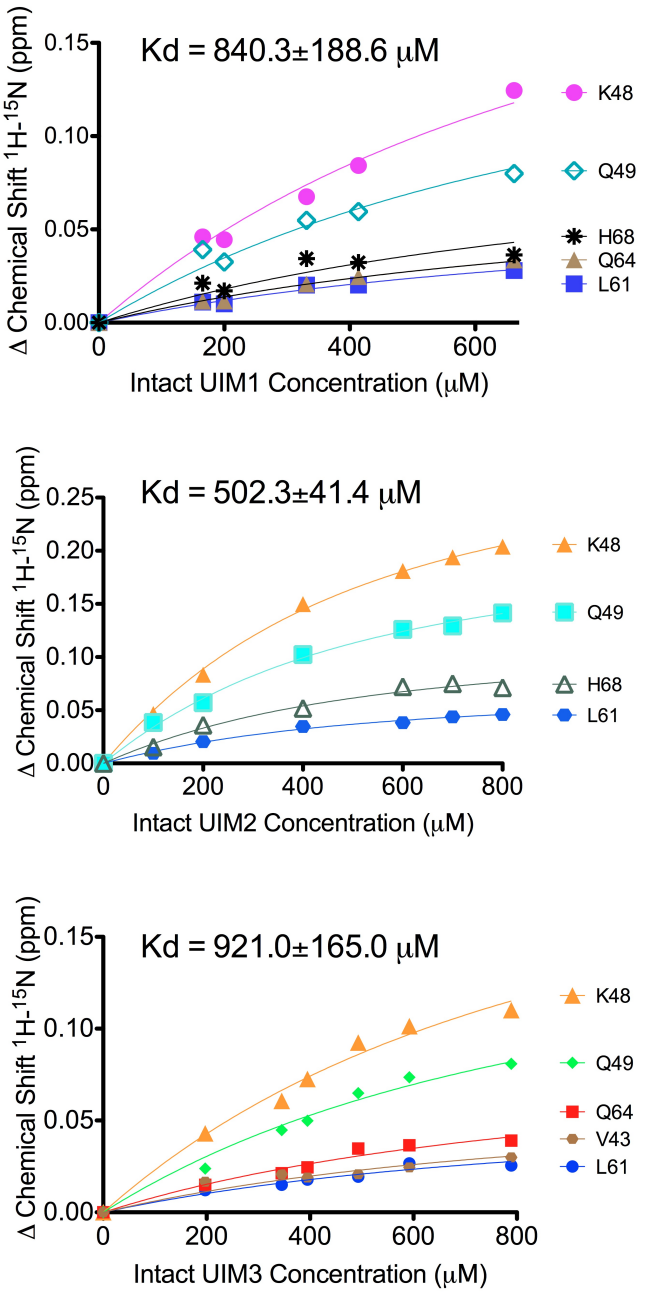

Figure 2.11 Binding curves of the absolute change in chemical shift of ^{15}N UbLD with titrations of ataxin-3 UIM1$^{*194-361}$, UIM2$^{*194-361}$, and UIM3$^{*194-361}$. The absolute chemical shifts take into consideration both the proton and nitrogen chemical shifts. The K_D values are K_{DUIMI} = 840.3±188.6 μM, K_{DUIM2} = 502.3±41.4 μM, and K_{DUIM3} = 921.0±165.0 μM based on a global fit of non-linear regression analysis for 1:1 binding. The corresponding amino acid residue of which the chemical shifts were measured are indicated to the right side of the binding curve.

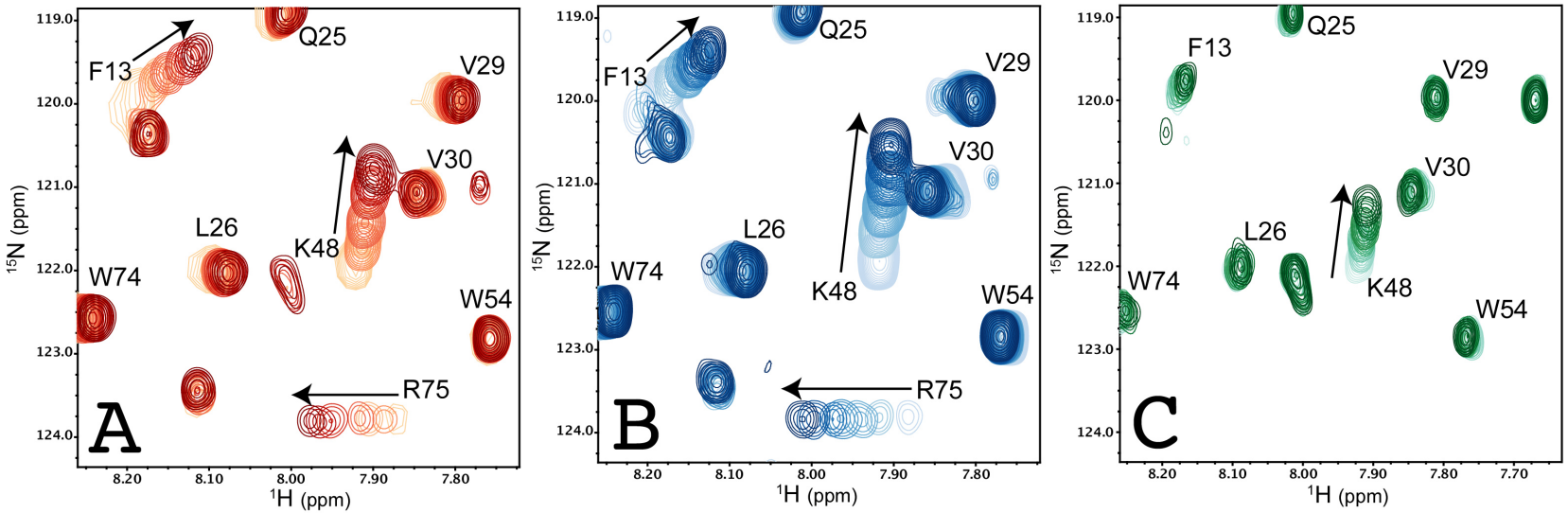

Figure 2.12 Close-up view of overlaid HSQC spectra of ^{15}N UbLD titrated with ataxin-3 (A) UIM123$^{194\text{-}361}$, (B) UIM12$^{194\text{-}261}$ and (C) UIM1$^{194\text{-}244}$. NMR data was collected with Varian INOVA 600 MHz NMR spectrometer with samples in a buffer containing 10 mM KH_2PO_4, 1 mM EDTA, 1 mM DTT pH 7.0 at 25°C (pH indicator, Imidazole). The starting concentration of ^{15}N labeled parkin UbLD was 105μM, 100μM, 40μM and was titrated with up to 6, 5, 10 equivalents ataxin-3, respectively. The arrows indicate the direction of peak shifts upon increasing the ataxin-3 concentration.

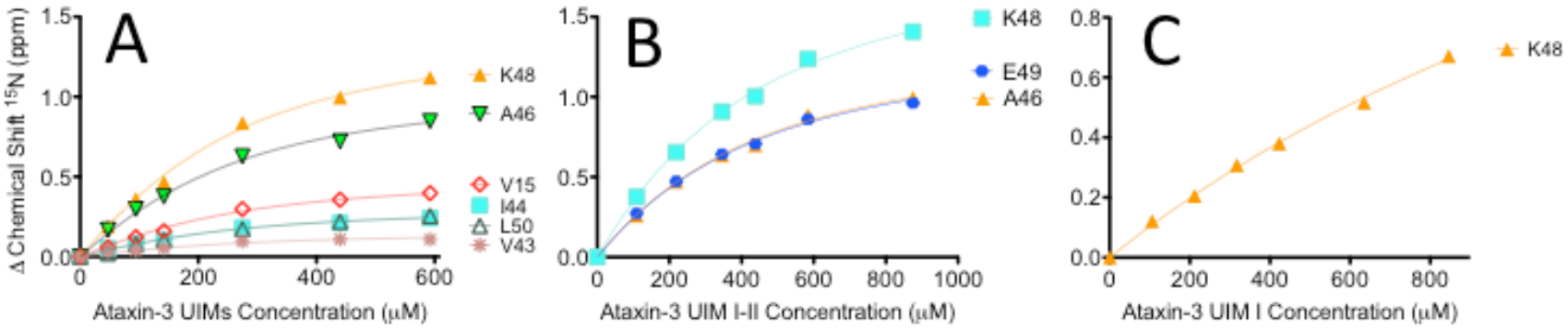

Figure 2.13 Binding curves determined by the change in chemical shift of the nitrogen dimension only, for ^{15}N UbLD with incremental titrations of (A) UIM123, (B) UIM12, and (C) UIM1. The K_D values are $K_{DUIM123}$ = 235.7±14.0 μM, K_{DUIM12} = 422.5±28.5 μM, and K_{DUIM1} = >2000±400 μM based on a global fit of non-linear regression analysis for 1:1 binding. The corresponding amino acid residues of which the chemical shifts were measured are indicated to the right side of the binding curve.

with the UbLD, the K_D was greater than 2 mM with a standard error of 400 μM (Figure 2.7C). The poor fit of the binding curve can be attributed from not being able to saturate the UbLD with enough substrate. Another difficulty that arose was due to resonance behaviour, such as peak intensity changes, which made it difficult to distinguish the peak above noise of the HSQC. Therefore, some peaks could not be unambiguously assigned in order to track the changes in chemical shift. An example of this behaviour was seen by Arg^{75} (Figure 2.13C). The only residue that could be unambiguously followed for UIM1 construct and gave the best fit was Lys^{48} (Figure 2.13C).

Most of the residues that displayed large chemical shift changes are located on the fourth and fifth β-strand, such as Lys^{48} and Glu^{49} on the fourth β-strand, and Gln^{64}, Ile^{66} on the fifth β-strand. Other residues outside this region that shifted include residues Phe^{13}, which resides at the N-terminus (2^{nd} β-strand), and Arg^{75} located at the C-terminus tail of the UbLD. While these residues are not clustered in exactly the same regions, they all fall on the beta-grasp face of the UbLD (Figure 2.5).

2.3.7 Modelling the binding mechanism of the ataxin-3 UIM123$^{194-361}$ with UbLD using a multivalent binding mechanism

The observations that all three UIM regions were participating in the interaction with parkin and that the greater the number of intact UIM regions correlates with strengthening the interaction led to the prediction that a multivalent binding mechanism could be employed by the UIM domains in ataxin-3. A new model was designed to fit the binding curves and accomodate for a three-site binding mechanism, under the assumption that all the binding sites have equal affinities to the UbLD. The resulting K_D was

calculated to be 669±62 μM and 725±43 μM in the proton and nitrogen dimension, respectively (Figure 2.14).

2.4 Discussion

^{1}H-^{15}N HSQC titration experiments were used to determine the binding site of the ataxin-3 UIM123$^{194-361}$ protein construct on the UbLD. To ensure that the chemical shift perturbations were due to protein interactions and not residues that are susceptible to pH changes, imidazole was added as a pH indicator to all of the NMR samples. Confidence in the reliability of the data can be based on four observable traits in the HSQC spectra; linear peak shifting, no systematic peak shifting is occurring, the peak shifts of different residues are in different directions, and the center of each peak is easily measurable and able to be followed (Figures 2.9, 2.12).

2.4.1 The UIM regions of ataxin-3 interacts with the hydrophobic patch of the UbLD

^{1}H-^{15}N HSQC titration experiments of ^{15}N UbLD with up to a 6 equivalent addition of ataxin-3 UIM123$^{194-361}$ revealed that most of the interacting residues reside on the solvent exposed surface of the beta-grasp fold of the UbLD, highlighted in pink (Figure 2.5). This region of interaction is similar to the interaction shown between the ataxin-3 UIM123$^{194-361}$ bound to ubiquitin molecules (7). Like the UbLD interaction, the UIM region confers a docking site on the hydrophobic patch of Ub, centered on Leu^{8}, Ile^{44}, Lys^{48} and Val^{70} (7). When comparing the chemical shift perturbation map of ^{15}N Ub vs. ^{15}N UbLD

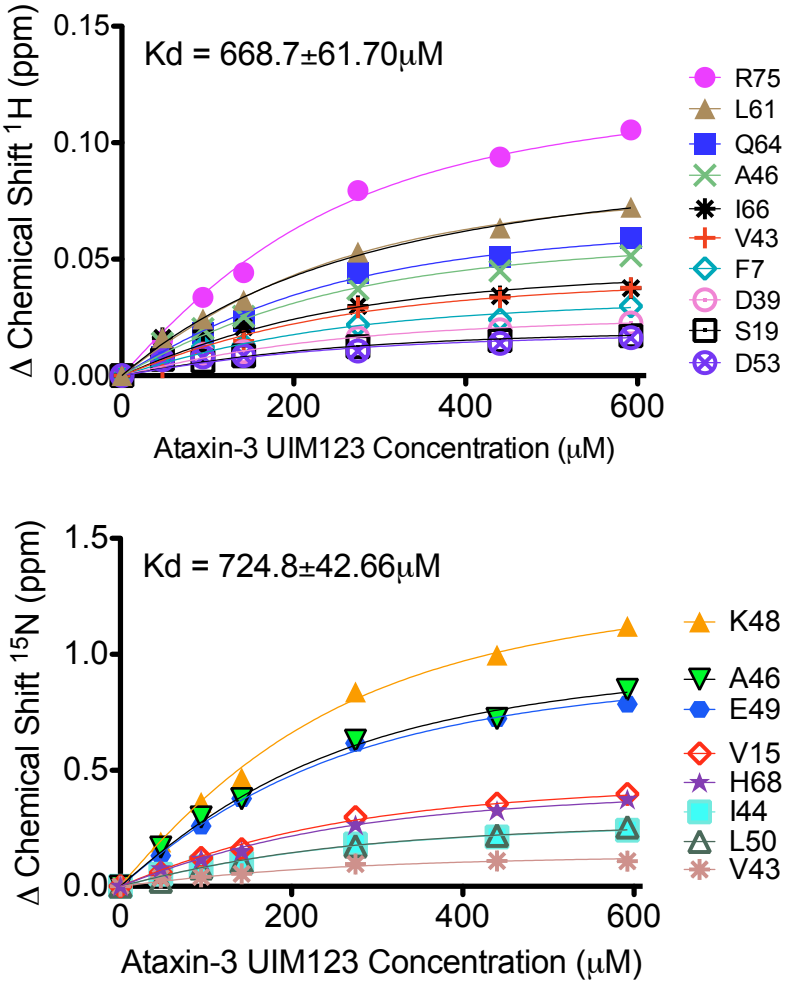

Figure 2.14 Binding curves of proton and nitrogen changes in chemical shift of ^{15}N UbLD with titrations of ataxin-3$^{194-361}$. The K_D values are 668.7±61.70 μM and 724.8±42.66 μM in the proton and nitrogen dimension, respectively. The fitting is based on a multisite non-linear regression analysis for 3:1 binding, with three equivalent affinity sites. The corresponding amino acid residues of which the chemical shifts were measured are indicated to the right side of the binding curve.

upon ataxin-3 binding, plotting the magnitude of chemical shift as a function of the residue position, the overall trends in which residues shift the greatest are almost identical (for example positions 8-13, 46-49, and residues at the C-terminus of both proteins) (7). The binding site on the UbLD and Ub is complementary to the UIM region of ataxin-3, which is composed of an acidic stretch of 3-4 residues followed by a hydrophobic core of typically 5 amino acid residues. Based on affinity binding assays the third UIM was found to not participate in the interaction to Ub and the K_D of the Ub to ataxin-3 $UIM12^{194-261}$ interaction is just below 100 μM, which is relatively tight binding in the scope of UIM to UbLD binding interactions (7). The interaction between ataxin-3 and Ub is important for surveillance of its substrate proteins. Since ataxin-3 is a DUB enzyme, it is able to edit ubiquitin chains, preferably Lys^{63} Ub linkages important in DNA repair pathways, or specific substrates that require its surveillance (8). The biological importance of the interaction between ataxin-3 and the parkin UbLD is not well estabilished. Recently, ataxin-3 has been found to divert E2-Ub from parkin ubiquitylation by forming a stable complex between the E2, parkin, and ataxin-3, causing the ataxin-3 protein to become ubiquitylated (9). This is not the conventional de-ubiquitylating mechanism, and ataxin-3 was originally thought to detach distal Ub moieties from a Ub-chain, though it is interesting that this mechanism is specific to parkin and could potentially rely on the UIM UbLD interaction (9). Despite the differences of biological importance in the interactions between Ub or UbLD to the UIMs of ataxin-3, the same hydrophobic and basic face of the Ub or UbLD is utilized to contact the UIM region.

2.4.2 Parkin UbLD makes weak and direct interactions with the three UIM regions of ataxin-3

The arrangement of UIM sites within ataxin-3 are unique because no other UIM-containing protein has three motifs in the same topology as ataxin-3, which are all located within the flexible C-terminal tail (10). A variable poly-glutamine tract separates the second and third UIM, that when expanded to greater than 45 residues, causes the most common dominantly inherited spinocerebellar ataxia. Meanwhile, UIM regions 1 and 2 are much closer with one another in the protein sequence. The ataxin-$3^{194\text{-}361}$ protein bound to the UbLD with a K_D of ~230 μM, when the binding curves were globally fit with a 1:1 non-linear regression curve (Figure 2.13). This relatively weak interaction was expected, considering that other UIM-containing proteins such as Eps15 and S5a both bind to the UbLD with K_Ds in the range of 100-200 μM (2). With the interaction of ataxin-3 with UbLD proteins being transient in nature, these weak K_D values are biologically significant.

2.4.3 All three UIM regions of ataxin-3 participate in the interaction with parkin

The most compelling results to show that all three UIMs are participating in the interaction to the UbLD were the NMR titrations of ^{15}N ataxin-3 UIM$123^{194\text{-}361}$ with UbLD additions and the reverse experiments of ^{15}N UbLD with individually intact UIM regions. Previous evidence has shown that the conserved serine, which is present amongst all UIM sequences, is absolutely essential for the interaction with the UbLD and Ub (1, 12). To ensure that the UIM region has been 'knocked down' in its ability to interact to

the UbLD, we substituted five core hydrophobic residues to alanine residues to abolish interaction with the hydrophobic patch of the UbLD, and for preservation of the helical nature of the UIMs (2). Alanine substitutions of two conserved regions, the serine and five residue hydrophobic core both within the UIM sequence, provide confidence that the interaction between the UIM and UbLD is abolished.

NMR titration experiments of ^{15}N UbLD with the C-terminal deletion ataxin-3 construct of UIM1$^{194-244}$, as well as the titration experiments with ataxin-3 UIM1*$^{194-361}$ provide evidence that supports that UIM1 is able to weakly bind to the UbLD (Figures 2.11, 2.12C). The binding affinity was in agreement for both titration experiments with a K_D value in the millimolar range. The observation that the binding affinities are in agreement, provides confidence that the alanine substitutions of the conserved serine and hydrophobic core of the UIM has lost its ability to interact with the UbLD.

Based on the NMR titration experiments of ^{15}N UbLD with ataxin-3 UIM2*$^{194-361}$, the second UIM has the tightest affinity to the UbLD compared with ataxin-3 UIM1*$^{194-361}$ and ataxin-3 UIM3*$^{194-361}$ (Figure 2.10). It is not clear why the second UIM has the tightest binding affinity. Interestingly, previous evidence has shown that the opposite trend occurs for interaction with a single ubiquitin moiety. The ataxin-3 UIM1 binds tighter (K_D = 215 μM) than UIM2 (K_D = 309 μM), and UIM3 has the weakest affinity (K_D > 3000 μM) (7). The explanation for why one UIM has a higher preference to bind the UbLD versus Ub or vice versa needs further investigation, however, in the scope of binding affinities, these are all within the same relatively weak binding range.

The NMR titration experiments of the ^{15}N UbLD with ataxin-3 UIM3*$^{194-361}$ additions, as well as the complementary experiment with ^{15}N ataxin-3 UIM123$^{194-361}$ both

provide compelling evidence to support that the third UIM is participating in the interaction. The ^{1}H-^{15}N HSQC spectra of ^{15}N ataxin-3 UIM123$^{194-361}$ was difficult to analyze due the overlap of peaks found in the proton dimension (7.7-8.8 ppm) which is indicative of a random coil protein (13). Some of the residues that are nearby or within the third UIM, S335, V344, and T345, could be tracked in the ^{1}H-^{15}N HSQC spectrum, and showed clear chemical shift perturbation upon additions of up to 10 equivalents of the UbLD (Figure 2.7). These same conserved residues are present within the third UIM, so one may predict that it is also involved in the interaction based on sequence identity to the N-terminal UIM regions. However, UIM interactions cannot be predicted based solely on sequence similarity as seen for UIM containing protein S5a which only utilizes its N-terminal UIM for interactions with parkin (1, 2).

2.4.4 Differential interactions of the parkin UbLD with UIM-containing proteins Eps15, S5a and ataxin-3

In 2001, there were approximately 30 reported proteins containing the ubiquitin interacting motif, and most of them contained more than one UIM (10). Since all UIMs have conserved elements within their ~20 amino acid motif, there is likely a lot of overlap in terms of which UIMs are able to bind to the UbLDs. The question then becomes, how can the parkin UbLD recognize which protein it is interacting with if many of its binding partners have UIMs? Two of the thirty identified UIM-containing proteins, Eps15 and S5a, have been extensively studied for their differential interaction with the parkin UbLD (2). K48, A46, and I66 are the hydrophobic residues on parkin that are occupied by the UIM(s) of Eps15, S5a and ataxin-3. Residues V56 and V15 in parkin

display large absolute chemical shift changes when ataxin-3 is added, whereas, in both Eps15 and S5a's docking site, these two particular residues do not display a peak shift above the average shift (Figure 2.4) (2). Although, Eps15, S5a and ataxin-3 all contain more than one UIM in the C-terminal tail of their respective full-length proteins, the Eps15, S5a and ataxin-3 proteins behave very differently in their binding mechanisms to the UbLD.

Eps15 utilizes two UIM regions to bind to the UbLD of parkin, meanwhile, S5a only uses one UIM and there is a clear distinction that the amount of surface area that is able to bind one UIM is less (9). Simply due to the number of surface residues displaying large chemical shifts upon addition of the ataxin-3 UIM123$^{194\text{-}361}$, there seems to be a surface area that can accommodate one or two UIM regions simultaneously, but not three simultaneously. Further investigation of the binding between the proteins suggests that the third UIM is not a bystander in the interaction with parkin. The work presented here has shown that although the ataxin-3 UIM123$^{194\text{-}361}$ confers a docking site that is in the same region where other UIM-containing proteins, such as Eps15 and S5a, bind to the parkin UbLD, the mechanism of interaction for ataxin-3 may be unique compared to Eps15 and S5a.

2.4.5 The UIM region of ataxin-3 employs a multivalent binding mechanism to interact with the UbLD

The multivalent binding mechanism is characterized by multiple weak binding sites that have fast off-rates, such that when the number of binding moieties increases, the affinity of binding becomes tighter (16). There are many pieces of evidence to suggest

that a multivalent binding interaction could be employed by the UIM region of ataxin-3, one of which were the initial K_D calculations between parkin and ataxin-3, which were carried out with a simple 1:1 binding model, referred to as the macroscopic dissociation constant. The preliminary analysis, from the ataxin-3 C-terminal deletion titration experiments, showed that increasing the number of UIM regions also increases the binding affinity to parkin. There was a tenfold increase in having the three UIM regions present versus one (Figure 2.13). Rap80, a DNA repair protein reported to use multivalent binding mechanisms to interact with ubiquitin chains, was found to have an increased affinity with increasing poly-ubiquitin chain length (16). Interestingly, Rap80 has two tandem UIM regions and the discovery of how it binds to ubiquitin chains, preferentially Lys^{63} Ub linkages, was through ^{1}H-^{15}N NMR titration experiments as well as molecular dynamic simulations.

After close inspection of the data collected from the ^{1}H-^{15}N HSQC titration experiments with the UbLD and various UIM constructs, a new multivalent binding equation was derived. The model assumes that only a single UbLD can bind to a single UIM site at one time point with equal binding affinities, which was validated from considering the chance that two UbLD moieties could simultaneous bind was very unlikely, that the affinities of each UIM interacting with the UbLD were similarily weak, and that the docking site on the UbLD could accommodate one to two UIM sites. The K_Ds derived from the multivalent 3:1 binding model were 668.7±62 μM and 724.8±43 μM in the proton and nitrogen dimension, respectively. Importantly, these K_D values were similar to the K_D values derived from the experiments involving ataxin-3 UIM1*$^{194-361}$, UIM2*$^{194-361}$, and UIM3*$^{194-361}$, which were 840.3±188.6 μM, 502.3±41.4 μM, and

921.0±165.0 μM, respectively (Figure 2.11). The similarity between the two derived K_D values, fit with the appropriate 1:1 or multivalent 3:1 binding model, provides support that the multivalent type of fit is appropriate for the chemical shift perturbation data when the ataxin-3 UIM123$^{194\text{-}361}$ construct is titrated into ^{15}N UbLD.

2.4.6 Biological importance of the DUB enzyme and E3 ligase interaction

In 2010, the Fon group proposed that self-ubiquitinating E3 ligases have a 'relationship' with DUB enzyme(s) to prevent their own rapid turnover via the proteasome. This has been seen for other E3:DUB pairs, such as MDM2:HAUSP, and ITCH:FAM/USP9X (1,14). Recently, there has been evidence to supporting the importance of the interaction of parkin and ataxin-3. Interestingly, ataxin-3 can be ubiquitylated, preferentially at Lys^{117}, which enhances its DUB catalytic activity *in vitro* and in cells (15). Ataxin-3 was shown to preferentially deubiquitinate FLAG-parkin ubiquitin chains versus free ubiquitin chains or ubiquitin chains on other RING E3 ligases such as SIAH and CIAP2 (1). As well, there is evidence to show that ataxin-3 has a unique mechanism to prevent parkin from being ubiquitylated by sequestering an E2 (Ubc7) in complex with parkin and diverting the Ub moiety onto ataxin-3 itself (9). This suggests that there is specificity in the DUB function of ataxin-3 for parkin. In addition, cyclohexamide pulse-chase experiments, when the ataxin-3 polyglutamine tract is at a disease relevant length (82Qs), causes parkin levels to drop in the cell due to increased turnover by autophagy (1). All of these examples provide growing evidence to support that ataxin-3 has a 'partnership' with parkin for interplay in regulating each other's function.

In this work, NMR titration experiments were used to identify the binding site that the UIMs of ataxin-3 confer on parkin UbLD, as well as, investigate the binding mechanism and importance of the third C-terminal UIM. In identifying the site of interaction on the UbLD, prediction of ARJP mutations that may be relevant for disrupting the interaction to ataxin-3 is possible. Further, this work provides evidence that the binding interface on parkin where the three UIMs of ataxin-3 interacts, lies on the hydrophobic patch of parkin but provides unique contacts that have not been present in Eps15 or S5a UIM to UbLD protein interactions (2). Individually, each UIM has a very weak affinity for the UbLD, in the one millimolar range. The binding affinity is the greatest when all three UIMs are intact and are available to interact with the UbLD. Collectively, the results led to the prediction that there may be a multivalent binding mechanism between the UIM region of ataxin-3 and the parkin UbLD.

2.5 References

1. Durcan, T.M., Kontogiannea, M., Thorarinsdottir, T., Fallon, L., Williams, A.J., Djarmati, A., Fantaneanu, T., Paulson, H.L., and Fon, E.A. (2011). The Machado-Joseph disease-associated mutant form of ataxin-3 regulates parkin ubiquitination and stability. Hum. Mol. Genet. *20,* 141-154.
2. Safadi, S.S., and Shaw, G.S. (2010). Differential interaction of the E3 ligase parkin with the proteasomal subunit S5a and the endocytic protein Eps15. J. Biol. Chem. *285,* 1424-1434.
3. Safadi, S.S., and Shaw, G.S. (2007). A disease state mutation unfolds the parkin ubiquitin-like domain. Biochemistry *46,* 14162-14169.
4. Harris, G.M., Dodelzon, K., Gong, L., Gonzalez-Alegre, P., and Paulson, H.L.

(2010). Splice isoforms of the polyglutamine disease protein ataxin-3 exhibit similar enzymatic yet different aggregation properties. PLoS One *5,* e13695.

5. Berke, S.J., Chai, Y., Marrs, G.L., Wen, H., and Paulson, H.L. (2005). Defining the role of ubiquitin-interacting motifs in the polyglutamine disease protein, ataxin-3. J. Biol. Chem. *280,* 32026-32034.
6. Mao, Y., Senic-Matuglia, F., Di Fiore, P.P., Polo, S., Hodsdon, M.E., and De Camilli, P. (2005). Deubiquitinating function of ataxin-3: insights from the solution structure of the Josephin domain. Proc. Natl. Acad. Sci. U. S. A. *102,* 12700-12705.
7. Song, A.X., Zhou, C.J., Peng, Y., Gao, X.C., Zhou, Z.R., Fu, Q.S., Hong, J., Lin, D.H., and Hu, H.Y. (2010). Structural transformation of the tandem ubiquitin-interacting motifs in ataxin-3 and their cooperative interactions with ubiquitin chains. PLoS One *5,* e13202.
8. Winborn, B.J., Travis, S.M., Todi, S.V., Scaglione, K.M., Xu, P., Williams, A.J., Cohen, R.E., Peng, J., and Paulson, H.L. (2008). The deubiquitinating enzyme ataxin-3, a polyglutamine disease protein, edits Lys63 linkages in mixed linkage ubiquitin chains. J. Biol. Chem. *283,* 26436-26443.
9. Durcan, T.M., Kontogiannea, M., Bedard, N., Wing, S.S., and Fon, E.A. (2012). Ataxin-3 deubiquitination is coupled to Parkin ubiquitination via E2 ubiquitin-conjugating enzyme. J. Biol. Chem. *287,* 531-541.
10. Hofmann, K., and Falquet, L. (2001). A ubiquitin-interacting motif conserved in components of the proteasomal and lysosomal protein degradation systems. Trends Biochem. Sci. *26,* 347-350.
11. Safadi, S. S., & Shaw G. S. (2009). Structure, Stability and Interactions of the Parkin Ubiquitin-like domain.
12. Fischer, J.A. (2003). Deubiquitinating enzymes: their roles in development, differentiation, and disease. Int. Rev. Cytol. *229,* 43-72.
13. Wishart, D.S., Sykes, B.D., and Richards, F.M. (1992). The chemical shift index: a fast and simple method for the assignment of protein secondary structure through NMR spectroscopy. Biochemistry *31,* 1647-1651.
14. Kon, N., Kobayashi, Y., Li, M., Brooks, C.L., Ludwig, T., and Gu, W. (2010).

Inactivation of HAUSP in vivo modulates p53 function. Oncogene *29,* 1270-1279.

15. Todi, S.V., Scaglione, K.M., Blount, J.R., Basrur, V., Conlon, K.P., Pastore, A., Elenitoba-Johnson, K., and Paulson, H.L. (2010). Activity and cellular functions of the deubiquitinating enzyme and polyglutamine disease protein ataxin-3 are regulated by ubiquitination at lysine 117. J. Biol. Chem. *285,* 39303-39313.
16. Markin, C.J., Xiao, W., and Spyracopoulos, L. (2010). Mechanism for recognition of polyubiquitin chains: balancing affinity through interplay between multivalent binding and dynamics. J. Am. Chem. Soc. *132,* 11247-11258.

Chapter 3

STRUCTURALLY INTACT DISEASE STATE MUTATIONS WITHIN PARKIN UBLD RETAIN INTERACTION WITH THE ATAXIN-3 UIM REGION

3.1 Introduction

Greater than 50% of Autosomal Recessive Juvenile Parkinsonism (ARJP) patients have mutations attributed to the parkin gene (1). In the parkin Ubiquitin-Like Domain (UbLD) alone, there have been 20 ARJP substitutions identified in 16 different amino acid residue positions (2). This chapter provides analysis on a selection of these ARJP single amino acid substitutions within the UbLD and interaction studies with ataxin-3. Certain ARJP substitutions on the UbLD can compromise the interaction with the UIM regions, as seen previously, with the UIM-containing protein S5a, which is a component of the 19S regulatory subunit involved in proteasomal degradation (1). The loss of the parkin-S5a interaction is proposed to result in impaired delivery of parkin ubiquitylated substrates to the proteasome. This could be a source of pathogenesis to seed protein misfolding diseases. This work aimed to determine what effect certain ARJP substitutions would have on the interaction of the UbLD with the UIM containing region of ataxin-3. However, the biological outcome of the disruption of the parkin UbLD interaction with ataxin-3 is unknown. Currently, binding assays provide evidence to suggest that the interaction between ataxin-3 and parkin is bimodal, with a second interaction site located in the Josephin domain of ataxin-3 to the IBR-RING2 of parkin (3). It may be possible that if the interaction between an ARJP mutant containing UbLD and ataxin-3 UIM

region is compromised, the interaction between parkin and ataxin-3 may still exist through the 2nd interaction site, the parkin IBR-RING2 and the Josephin domain.

The following ARJP substitutions were selected for study, $UbLD^{V15M}$ (4), $UbLD^{R33Q}$ (5), $UbLD^{A46P}$ (6), and $UbLD^{K48A}$ (7). The ARJP substitutions were selected because they have minimal affect on the three dimensional structure of the UbLD based on extensive structural characterization by NMR spectroscopy and circular dichroism spectropolarimetry (2). The only exception is $UbLD^{A46P}$, which has been previously shown to be unfolded (4). Secondly, these ARJP substitutions have been shown to participate in the interaction or are nearby the interaction site between the UIM region of ataxin-3 and the UbLD. Understanding the underlying mechanisms for the wildtype interaction of parkin and ataxin-3, discussed in Chapter 2, are highlighted here by showing how these disease relevant substitutions on parkin may compromise the interaction to the UIM regions.

In this work, the aim was to investigate ARJP substituted UbLD proteins that are structurally unaffected, to determine whether these mutations specifically alter the interaction with ataxin-3. To address this objective the structures of several ARJP substituted UbLD proteins ($UbLD^{V15M}$ and $UbLD^{K48A}$) were assessed by NMR ^{1}H-^{15}N HSQC titration experiments, and the interaction between ataxin-3 $UIM123^{194-361}$ and substituted UbLD proteins were investigated by an affinity binding assay and NMR titrations. Lastly, the binding affinities were quantified by NMR titrations.

3.2 Materials and Methods

3.2.1 Parkin ARJP substitutions within the UbLD

Parkin UbLD molecular biology details are described in Chapter 2. The ARJP relevant mutants used for the interaction studies (V15M, R33Q, A46P, K48A) were generated previously through using QuikChange Site-Directed Mutagenesis Kit (Stratagene, La Jolla, CA) (2). All constructs were expressed without fusion tags. The mutant parkin UbLD constructs were verified by DNA sequencing (Robarts Sequencing Facility).

3.2.2 Expression and purification of parkin ARJP substituted proteins

ARJP substituted UbLD constructs were overexpressed and purified as described for the wildtype human parkin UbLD, described in Chapter 2. The integrity of all proteins were confirmed by electrospray ionization mass spectrometry (2).

3.2.3 Expression and purification of ubiquitin

Human ubiquitin was overexpressed in the pLysS *Escherichia coli* strain. The bacterial culture was grown as described for the parkin UbLD, with the exception that induction of expression with the addition of 1 mM IPTG at an A_{600} of 0.4-0.5. Both the overnight culture and the large growths of bacteria were grown in Luria-Bertani media and contained ampicillin (50 μg/ml) and chloramphenicol (34 μg/ml). Cell lysis was completed using flash freezing with liquid nitrogen and thawing, followed by sonication. The cell homogenate was then spun at 132380 g for 60 minutes, the supernatant was slowly brought to a pH of 3.5 and spun at 7378g. The supernatant was extensively

dialyzed with 25 mM Tris, 1 mM EDTA, and 150 mM NaCl at pH 8, loaded onto a G75 sizing column and eluted as described previously for parkin UbLD, Chapter 2.

3.2.4 ARJP substituted parkin UbLD binding assay with His-tagged ataxin-3 UIM123$^{194-361}$

All pure protein samples were extensively dialyzed in binding buffer (20 mM sodium phosphate, 10 mM imidazole, 300 mM NaCl, pH 8) prior to mixing the proteins. Purified His-tagged ataxin-3 UIM123$^{194-361}$ proteins were placed in an eppendorf tube on a rotating mixer and incubated with either parkin UbLD, ARJP substitutions of the parkin UbLD (K48A, A46P, R33Q, V15M), or ubiquitin, to give a final volume of 300 μL, at 4°C for one hour. Mixtures of 1:2 molar ratio His-tagged ataxin-3 construct:UbLD, (or ubiquitin) were used; concentrations were determined by the BIO-RAD protein assay. The principal behind this assay involves using the acidic Coomassie Brilliant Blue G-250 dye that changes color upon binding to protein, which can then be measured at an absorbance of 595 nm by a spectrophotometer. Beer's law is then applied to quantitate the protein concentrations. Following incubation of the protein mixture, a total volume of 300 μL was loaded on a Ni-NTA spin column (Qiagen) and incubated for 3 minutes at room temperature before being spun at 6 g. The column was washed twice with 600 μL of binding buffer and eluted with the same buffer, but with 250 mM imidazole. Eluted samples were separated by electrophoresis on a 16.5% tris-tricine polyacrylamide gel and stained with Coomassie brilliant blue dye.

3.2.5 NMR spectroscopy titration experiments

The ^{1}H-^{15}N Heteronuclear Single Quantum Coherence (HSQC) NMR experiments were performed with a 600 MHz Varian Inova spectrometer (BioNMR Facility, UWO). All protein samples were extensively dialyzed into 11 mM KH_2PO_4, 150 mM NaCl, 1 mM EDTA, 1 mM dithiothreitol, at pH 7 and 100 μM imidazole was added in the final NMR sample to serve as a pH indicator. All spectra were recorded at 25°C. Prism 4 and NMRViewJ version 8.0.rc4 were used to fit non-linear regression and global fitting for a 3:1 multivalent binding model, derived from following chemical shift perturbations upon titrating an unlabeled binding partner into the ^{15}N-labeled protein species. Details about the equation used for the multivalent binding fit is included in the Materials and Methods section of Chapter 2.

3.3 Results

ARJP-substituted UbLD proteins had similar yields of pure protein per litre of bacterial growth compared to wildtype (WT) UbLD (approximately 10 mg), with the exception of $UbLD^{A46P}$ which has approximately half the $UbLD^{WT}$ yield (~5 mg). The purification protocol used for WT UbLD was also successful for purifying the ARJP-substituted proteins, $UbLD^{V15M}$, $UbLD^{R33Q}$, $UbLD^{A46P}$ and $UbLD^{K48A}$. This suggests that the size and shape of all the UbLD proteins are alike and soluble, with the exception of $UbLD^{A46P}$, which may be prone to degradation, shown previously, or in the insoluble fraction (2). Following purification, affinity binding assays and NMR titration experiments were utilized to investigate whether structurally intact ARJP-substituted UbLD proteins were able to sustain the interaction with the UIM region of ataxin-3.

3.3.1 K48A and V15M ARJP substitutions in the UbLD retain their domain structure

^{1}H-^{15}N HSQC experiments were used to determine whether any local or global changes in structure occur, upon the ARJP substitutions $UbLD^{V15M}$ and $UbLD^{K48A}$. Comparisons of the spectra between the $UbLD^{K48A}$ and the $UbLD^{WT}$ showed no drastic differences in spectral dispersion, as >80% of the resonances overlaid with the WT UbLD resonance positions (Figure 3.1). The ^{1}H-^{15}N HSQC spectra of the $UbLD^{V15M}$ had less overlap with the WT UbLD. Approximately 60% of the resonances overlaid with their locations on the original WT UbLD ^{1}H-^{15}N HSQC, and the broad spectral dispersion in the proton dimension was maintained (Figure 3.1). When comparing the $UbLD^{K48A}$ ^{1}H-^{15}N HSQC spectrum with the WT UbLD spectrum, there were approximately 5 peaks that show a greater difference in resonance position compared to others including Leu^{26}, Gln^{64}, Leu^{61}, Trp^{74}, and Arg^{75}. These residues do not reside in the same region of the UbLD. Leu^{61} is the closest in space with the Lys^{48} position. The remaining residues are located much farther in 3D space to the Lys^{48} position. For example, Gln^{64} is located at the N-terminus of the β5 strand, Trp^{74} and Arg^{75} are both located on the flexible C-terminal tail and Leu^{26} is on the α2 helix and has its side chain pointing towards the inside of the beta grasp fold. The resonances that change upon substitution of V15M are different than those seen in the K48A substituted UbLD. For example Leu^{61} changes its resonance for both ARJP substitutions but the resonance was more upfield in the $UbLD^{K48A}$ spectrum, meanwhile the Leu^{61} peak in $UbLD^{V15M}$ shifted more downfield (Figure 3.1). Despite all the resonances that are altered upon a single amino acid substitution, the peaks still remain well dispersed in the proton-dimension, and overlay

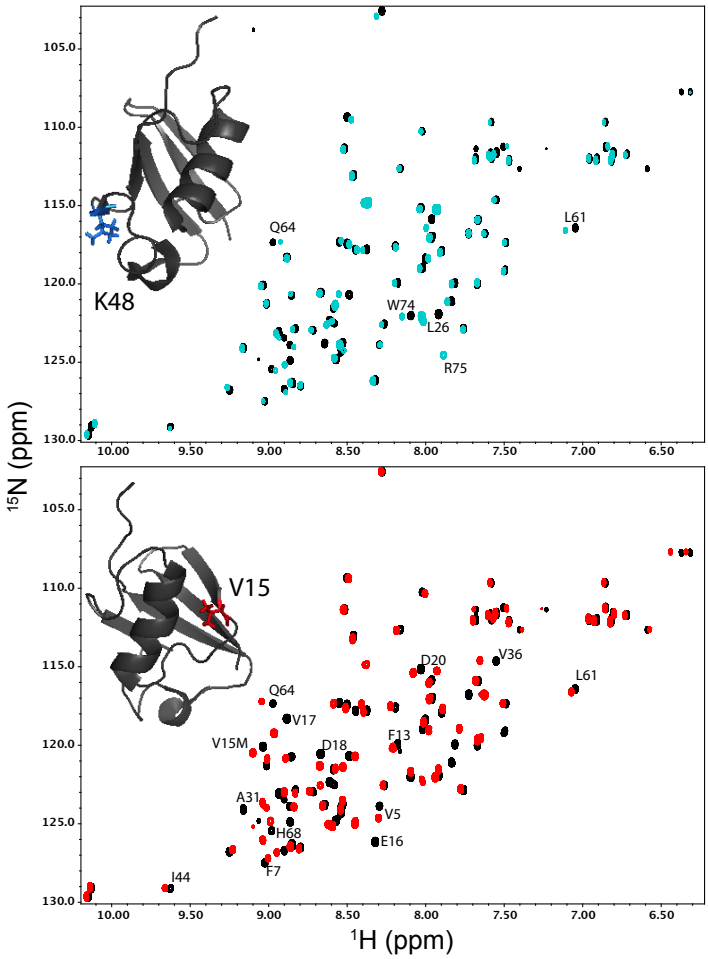

Figure 3.1. ^{1}H-^{15}N HSQC spectra of wildtype (black) UbLD overlaid with ARJP substituted UbLD^{K48A} (blue) and UbLD^{V15M} (red). The spectra were collected on a Varian INOVA 600 MHz NMR spectrometer with samples in a buffer containing 10 mM KH_2PO_4, 1 mM EDTA, 1 mM DTT pH 7.0 at 25°C (pH indicator, Imidazole). The concentration of ^{15}N labeled parkin wildtype UbLD and ARJP substituted UbLD^{K48A} samples were 100 µM, while the UbLD^{V15M} sample was 150 µM. The ribbon diagram of the UbLD highlights the position of the substitution depicted with the original side chain colored blue (K48) and red (V15).

well with the WT spectrum. Overall, the chemical shift changes are small (<0.1ppm in the proton dimension, and <2.0ppm in the nitrogen dimension) (Figure 3.1). This suggests that the general domain fold was intact and similar to the $UbLD^{WT}$, and only local changes occurred after the introduction of the V15M and K48A substitutions.

3.3.2 Structurally intact ARJP substituted UbLD proteins can interact with ataxin-3 $UIM123^{194-361}$

An affinity-binding assay was used to assess whether ARJP substitutions within the UbLD can interact with ataxin-3 $UIM123^{194-361}$. The ataxin-3 $UIM123^{194-361}$ construct contains a His-tag and was incubated with one of the UbLD proteins. After washing the nickel column with the pre-loaded incubated protein samples, gel electrophoresis was used to detect the presence the ARJP-mutant UbLD proteins from the eluted samples (Figure 3.2). $UbLD^{A46P}$ and the $UbLD^{WT}$ were used as negative and positive controls in the binding assay. The first three lanes in the gel show the Ni-NTA spin column elution of His-tagged ataxin-3 $UIM123^{194-361}$, UbLD, and Ub proteins alone. The elution fraction of the mixtures of His-tagged ataxin-3 $UIM123^{194-361}$ with Ub, UbLD, $UbLD^{V15M}$, $UbLD^{R33Q}$, $UbLD^{A46P}$ and $UbLD^{K48A}$ are shown (Figure 3.2). The intensity of the WT UbLD elution band was similar in intensity with $UbLD^{V15M}$, $UbLD^{R33Q}$, and $UbLD^{K48A}$ for the mixtures with His-tagged ataxin-3 $UIM123^{194-361}$. Loading amounts were the same amongst the WT UbLD and UbLD variants (Figure 3.2). The elution of the $UbLD^{A46P}$ and Ub band are fainter, indicating poorer binding. The His-tagged ataxin-3 $UIM123^{194-361}$, indicated by a yellow arrow, has a similar protein band intensity at the same position in the polyacrylamide gel to one another, just above 25 kDa (Figure 3.2).

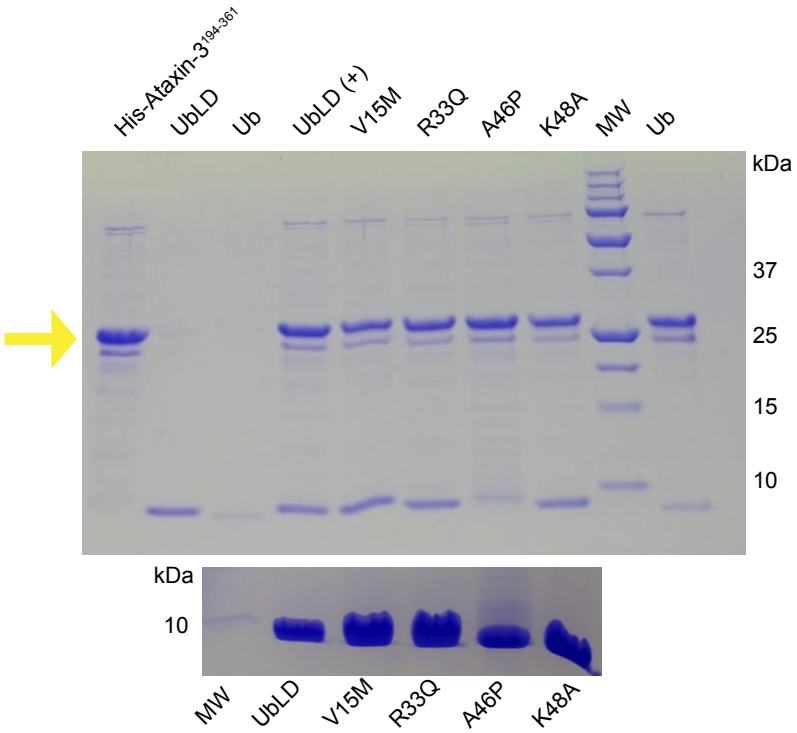

Figure 3.2. Affinity binding assay of the his-tagged ataxin-3 UIM123$^{194\text{-}361}$ and ARJP disease substitutions, UbLD^{V15M}, UbLD^{R33Q}, UbLD^{A46P}, UbLD^{K48A}, wildtype UbLD and ubiquitin. The top panel is an SDS-PAGE showing the elution of the Ni-NTA column for His-tagged ataxin-3 UIM123$^{194\text{-}361}$ and various UbLD species for an hour at room temperature. Mixtures of his-tagged ataxin-3 and UbLD, or ubiquitin in 1:2 molar ratios were used. Two washing steps were carried out prior to the elution step. The yellow arrow is indicating the his-tagged ataxin-3 UIMs protein band. The protein bands that are just below 10 kDa are the non-tagged eluted UbLD or Ub species. The bottom panel is an SDS-PAGE of the purified UbLD species from a 200 µM stock that was used in the binding assay. The (+), indicates the positive control in the binding assay.

The NMR titration experiments with ^{15}N-labeled UbLD^{K48A} and UbLD^{V15M} showed that specific residues experience different chemical shift changes upon titration with ataxin-3 UIM123$^{194-361}$. Residues Phe^{13}, Leu^{61}, Gln^{64} and Ile^{66} all experience changes in chemical shift in both similar magnitude and direction in both UbLD^{K48A} and UbLD^{V15M} proteins (Figures 3.3, 3.4). In the titration experiment involving UbLD^{V15M}, Lys^{48} showed the largest chemical shift change in response to ataxin-3 UIM titrations. The titration experiments involving ^{15}N UbLD^{K48A}, the resonance corresponding to Val^{15} also experiences a change in chemical shift (Figure 3.4). The V15M substitution resulted in the methionine resonance to experience very minimal chemical shift perturbations, originally shifting >0.5 ppm (Val^{15}) in the nitrogen dimension to <0.2 ppm (Met^{15}) (Figure 3.3). The resulting substituted Ala^{48} could not be identified on the HSQC spectra, as the backbone assignments for the UbLD^{K48A} had not been completed. These results suggest that both the Val^{15} and Lys^{48} positions are participating in the interaction with ataxin-3 UIM region and the substitution of these residues has the potential to compromise the interaction to ataxin-3.

3.3.3 K48A and V15M ARJP substituted UbLD proteins utilize the same binding surface on the UbLD to interact with the UIMs of ataxin-3

Multiple resonances from the ^{1}H-^{15}N HSQC spectra of UbLD^{K48A} and UbLD^{V15M} exhibit similar chemical shift perturbation behavior upon ataxin-3 additions. As mentioned above, residues Ile^{66}, Phe^{13}, Leu^{61}, and Gln^{64} all experience similar resonance movement in both titration experiments (Figures 3.3, 3.4, 3.5). These are also the

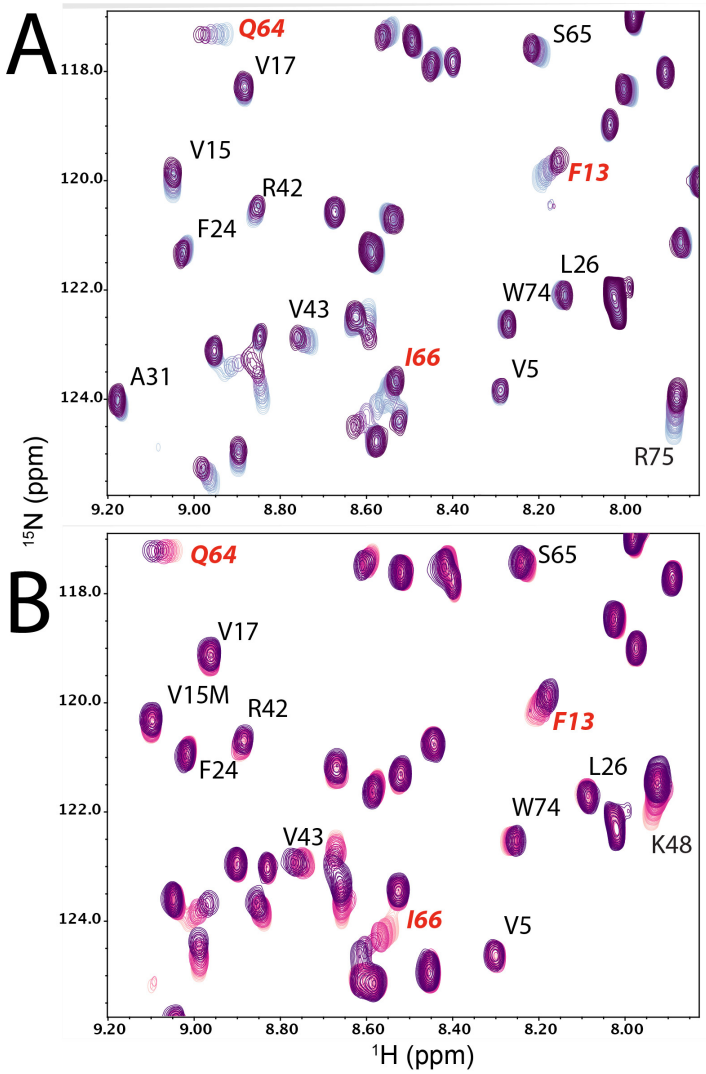

Figure 3.3 Select region of the ^{1}H-^{15}N HSQC spectra of ^{15}N-labeled parkin UbLD^{K48A} (A) and UbLD^{V15M} (B) overlaid following incremental additions of ataxin-3 UIM123$^{194-361}$. The starting concentration of ^{15}N labeled parkin UbLD^{K48A} was 100 µM and UbLD^{V15M} was 150 µM. The ARJP substituted UbLD were titrated with up to four (A), and five (B) equivalents of unlabeled ataxin-3 UIM123$^{194-361}$, respectively. Resonances that exhibit similar behavior (Phe^{13}, Ile^{66} and Gln^{64}) are highlighted (red) for both titration experiments. Peaks are shifting from light colored to dark colored.

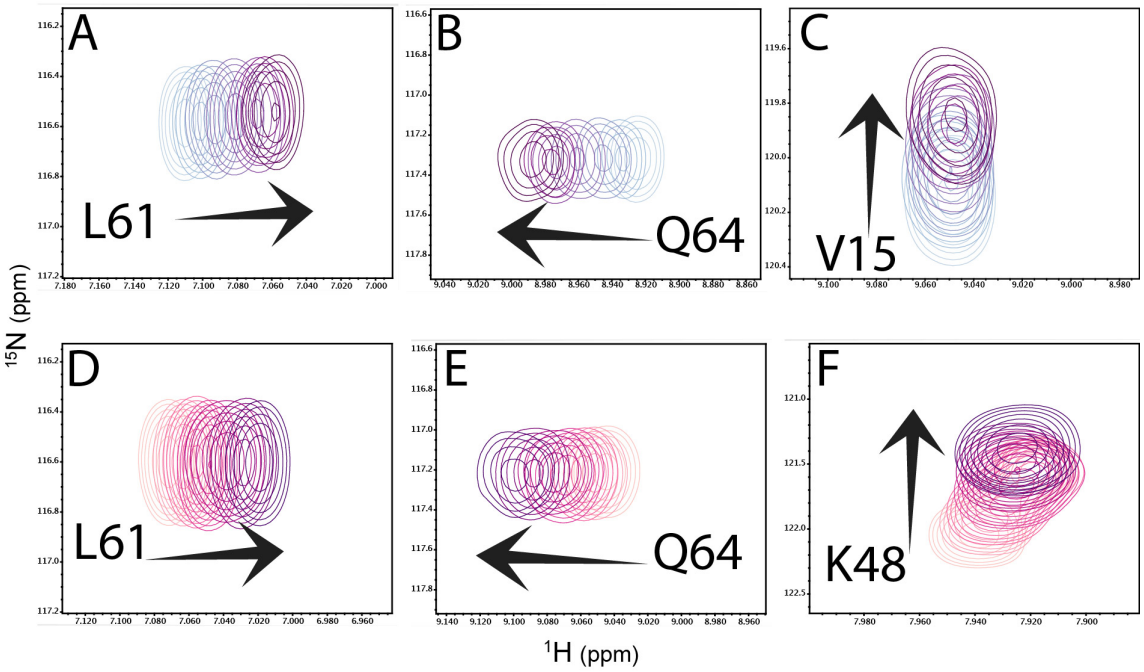

Figure 3.4 Regions of ^{1}H-^{15}N HSQC spectra of ^{15}N parkin UbLD^{K48A} (A, B, C) and UbLD^{V15M} (D, E, F) overlaid with HSQC spectra of incremental additions of ataxin-3 UIM123$^{194-361}$. NMR data was collected on a Varian INOVA 600 MHz NMR spectrometer with samples in a buffer containing 10 mM KH_2PO_4, 1 mM EDTA, 1 mM DTT pH 7.0 at 25°C (pH indicator, Imidazole). The starting concentration of ^{15}N labeled parkin UbLD^{K48A} was 100 µM and UbLD^{V15M} was 150 µM. The ARJP substituted UbLD was titrated with up to four (A, B, C), and five (D, E, F) equivalents of unlabeled ataxin-3 UIM123$^{194-361}$, respectively. This figure highlights the similar peak shifting behavior for amino acid residues Leu^{61} and Gln^{64} for both titration experiments. The V15 and K48 peak shifts are highlighted in the parkin UbLD^{K48A} and parkin UbLD^{V15M} spectra, respectively.

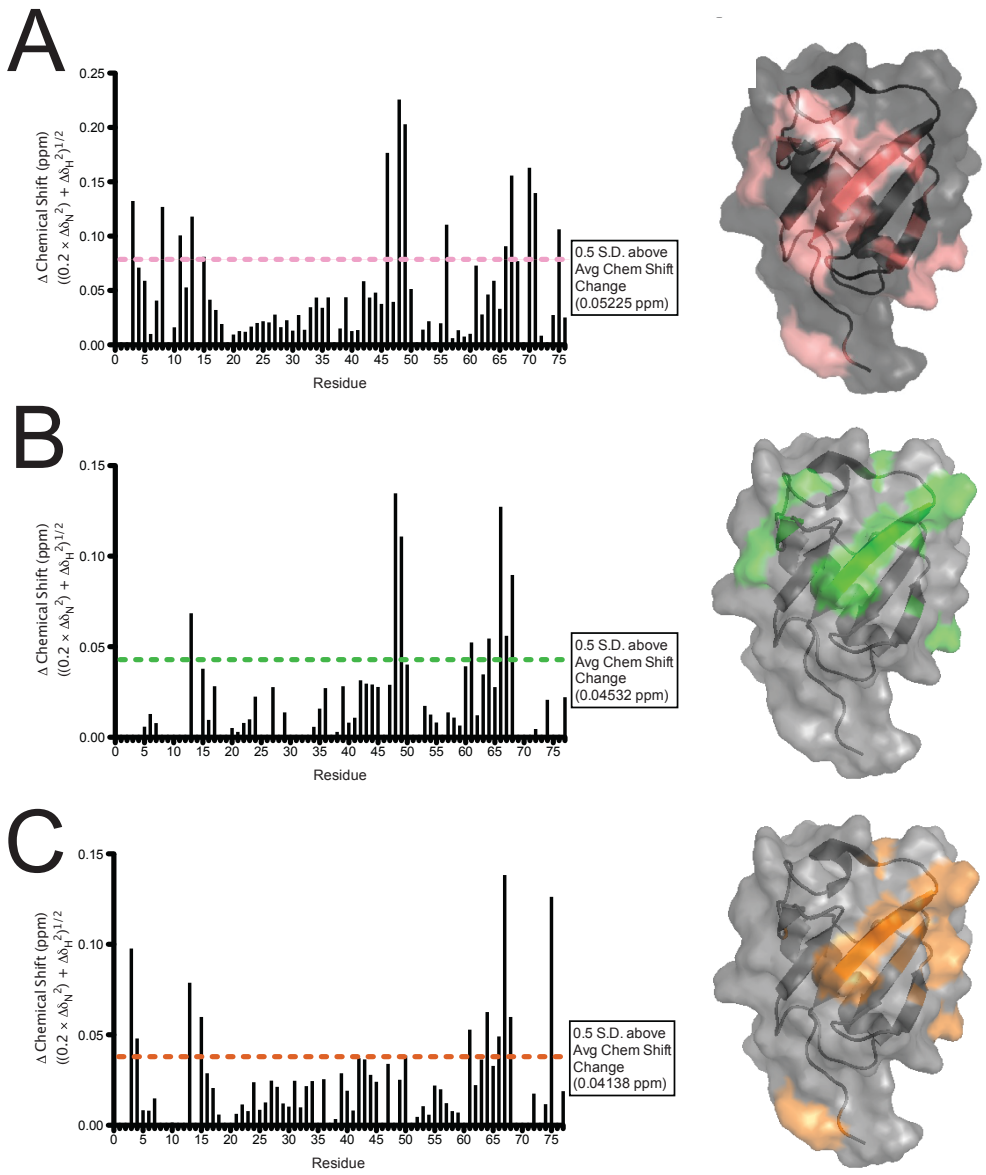

Figure 3.5 Chemical shift perturbation data and corresponding surface representation of the wildtype parkin UbLD (A), UbLD^{V15M} (B), and UbLD^{K48A} (C) upon ataxin-3 UIM123$^{194-361}$ binding. Chemical shift perturbation maps of the UbLD by measuring the absolute magnitude of peak shifting that occurs after addition of 6 eq.,5eq., and 4eq. of ataxin-3, respectively. The dotted lines indicate 0.5 S.D. above the average chemical shift perturbation value. The surface representations of where the three UIM containing region of ataxin-3 UIM123$^{194-361}$ confer their binding spot on the wildtype UbLD (A), UbLD^{V15M} (B), and UbLD^{K48A} (C). The residues that displayed more than 0.5 standard deviation above the average chemical shift were mapped on the surface of the UbLD, which is highlighted in pink (wildtype UbLD), green (UbLD^{V15M}) and orange (UbLD^{K48A}). The surface representations were created in the program PyMOL all using the PDB code 1IYF, structure of the wildtype human parkin UbLD.

resonances that experienced some of the greatest chemical shift perturbations upon titrations of ataxin-3 UIM123$^{194-361}$ (Figures 3.3, 3.4). The interaction surface is similar for ARJP substituted proteins UbLD^{V15M} and UbLD^{K48A} initially based on the observations that multiple similar residues display chemical shift changes for both NMR titration experiments. After further investigation, by using chemical shift perturbation data and mapping the residues on the UbLD for chemical shift changes greater than 0.5 S.D. above the average chemical shift, it is clear that the surface of the beta-grasp fold is utilized for ataxin-3 binding in both cases (Figure 3.5). The chemical shift perturbation data show that upon substitution of a particular residue, the nearby residues that once displayed a large absolute chemical shift difference upon addition of ataxin-3, greater than 0.5 S.D. above the average chemical shift (dotted line), now display a much smaller absolute change in chemical shift which is below the dotted line (Figure 3.5). An example of this is the K48A substitution, because in the original wildtype interaction, residues Lys^{48}, Glu^{49}, Ala^{46} all contribute to the binding surface for the UIM region of ataxin-3. However, once Lys^{48} is substituted to an alanine, those nearby residues do not experience a great chemical shift perturbation anymore (Figure 3.5C). The same occurs for the UbLD^{V15M} substitution. Nevertheless, even though these small differences occur, the UbLD^{V15M} and UbLD^{K48A} utilize a similar binding surface to interact with ataxin-3 UIM123$^{194-361}$ compared to each other and compared to the wildtype UbLD.

3.3.4 Structurally unaffected ARJP-substituted UbLD proteins interact with ataxin-3 with a similar binding affinity

The data from the NMR titration experiments (Figure 3.3) was used to calculate the affinities between the UbLD proteins, ($UbLD^{K48A}$ and $UbLD^{V15M}$) and the ataxin-3 $UIM123^{194\text{-}361}$. This analysis revealed that the affinities are very similar. Chemical shift changes for five residues, Phe^{13}, Val^{43}, Leu^{61}, Gln^{64} and Arg^{75}, from the $^{1}H\text{-}^{15}N$ HSQC of $UbLD^{K48A}$ spectra were plotted as a function of ataxin-3 $UIM123^{194\text{-}361}$ additions (Figure 3.6). The resonances followed for the $^{1}H\text{-}^{15}N$ HSQC of $UbLD^{V15M}$ belonged to residues, Phe^{13}, Leu^{61}, Gln^{64}, Ser^{65}, Val^{67}, and also plotted as a function of ataxin-3 $UIM123^{194\text{-}361}$ additions. The calculated dissociation constant for $UbLD^{K48A}$ was 658.9±48 μM and for $UbLD^{V15M}$ was 700.4±102 μM. These dissociation constants were calculated based on a global fit for a three-site multivalent binding model with equal binding affinities (Figure 3.6). These dissociation constants were very similar to that calculated for WT UbLD binding to ataxin-3, Chapter 2. These observations show the ARJP substitutions do not abolish the binding between the UbLD and ataxin-3.

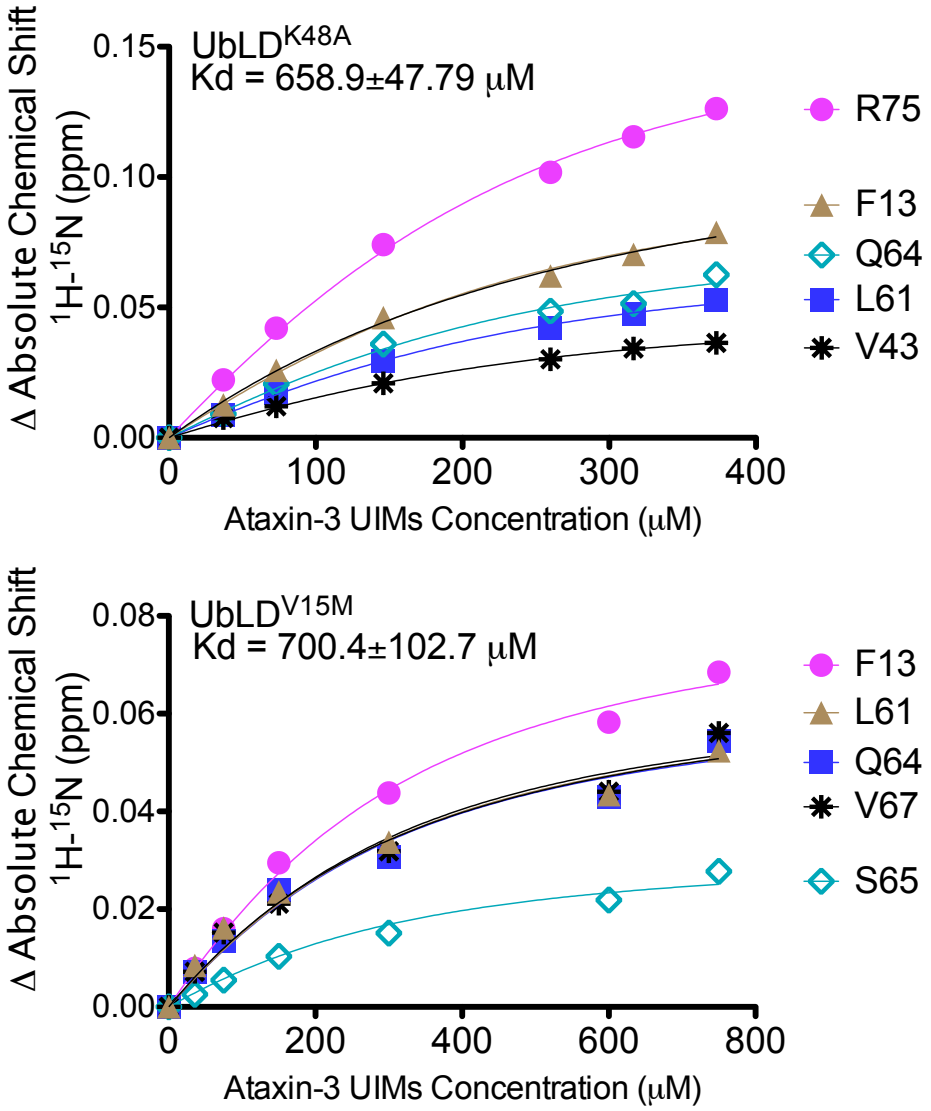

Figure 3.6 Binding curves of the absolute change in chemical shift of ^{15}N UbLD^{K48A} and UbLD^{V15M} with titrations of ataxin-3 UIM123$^{194-361}$. The absolute chemical shifts are taken into consideration, both the proton and nitrogen chemical shifts (in ppm). The K_D values are $K_{D,\ UbLDK48A}$ = 658.9±47.79 μM and $K_{D,\ UbLDV15M}$ = 700.4±102.7 μM and were based on a global fit for a three equivalent multisite binding model. The starting concentration of the ARJP substituted ^{15}N UbLD^{K48A} and UbLD^{V15M} were 100 μM and 150 μM, respectively.

3.4 Discussion

In this work the interactions between the ARJP substituted UbLD proteins and three UIM regions of ataxin-3 were investigated mostly by the ^{1}H-^{15}N HSQC spectra during titration experiments and the affinity-tag binding assays. Results show that the structurally intact ARJP substitutions retain the interaction with the ataxin-3 UIMs. As well, for the first time, dissociation constants were calculated for these interactions between the UbLD^{V15M}, UbLD^{K48A} and ataxin-3$^{194\text{-}361}$ and were found to have very similar to the K_D determined for the wildtype UbLD interaction. It should be noted that the pathogenic link to ARJP UbLD^{K48A} remains unclear although it has been reposted in the literature (7). Protein characterization studies continue to study UbLD^{K48A}, due to the importance of the residue for interactions. Although this mutation has been reported, it does not appear in Parkinson's disease databases (2, 7, http://www.molgen.ua.ac.be/PDmutDB).

3.4.1 ^{1}H-^{15}N HSQC experiments show that UbLD^{V15M} and UbLD^{K48A} are structurally intact

The dispersion of resonances in the proton dimension and the significant overlap of resonances in the ^{1}H-^{15}N HSQC spectra between ARJP substituted UbLD proteins and WT UbLD confirm that the protein domains remain well-folded with only local structural changes. The UbLD^{K48A} ^{1}H-^{15}N HSQC spectrum overlayed extremely well with that of the WT UbLD spectrum, indicating no gross structural changes had occurred (Figure 3.1). Approximately half of the resonances that were different from the WT UbLD

belonged to residues that were present in flexible regions, such as the C-terminal tail. There were a greater number of differences in resonance positions between the $UbLD^{V15M}$ ^{1}H-^{15}N HSQC spectrum compared to that of the WT UbLD, but this would be expected due to the location of the Val^{15} position in the UbLD structure (Figure 3.1). Unlike Lys^{48} position on the UbLD, which is solvent exposed, the Val^{15} position resides on the β2 strand pointing towards the α2 helix. This suggests that the substitution of Val^{15} could modify intramolecular Van der Waals and hydrophobic interactions that stabilize the fold of the protein such as that with Val^{29}, which is located on the α2 helix and points towards the Val^{15} side chain. The V15M substitution may be altering the existing hydrophobic stabilizing interaction and this loss may change the chemical environment for many residues that rely on this stabilization. Despite the greater number of resonances that differ between the $UbLD^{V15M}$ ^{1}H-^{15}N HSQC spectrum and the $UbLD^{WT}$ spectrum compared to the $UbLD^{K48A}$ ^{1}H-^{15}N HSQC spectrum and the $UbLD^{WT}$, the conclusion is that both $UbLD^{V15M}$ and $UbLD^{K48A}$ maintain the domain fold based on minimal changes in the proton dispersion in the spectra and thus, exposes the essential interacting residues in the hydrophobic patch to interact with the UIM region of ataxin-3.

In addition to the NMR experiments that were carried out, the structural integrity of the V15M, R33Q, and K48A ARJP substitutions within the UbLD have been previously studied by circular dichroism spectropolarimetry and NMR ^{1}H-^{15}N HSQC experiments (2). The results are consistent with our findings by NMR spectroscopy. These ARJP mutants maintain the five-strand β-grasp fold, typical of the UbLD and Ub molecule, while A46P was completely unfolded (2). The ^{1}H-^{15}N HSQC spectra of

$UbLD^{V15M}$ and $UbLD^{K48A}$ were identical to the spectra of previous work done to characterize these two proteins (Figure 3.1) (2).

3.4.2 The affinity binding assay shows that the interaction between the structurally unaffected disease-state UbLD proteins and UIMs of ataxin-3 are not disrupted

The affinity-binding assay was used as further confirmation and completeness of determining if an ARJP substituted UbLD was able to disrupt the interaction to ataxin-3 $UIM123^{194\text{-}361}$. The results showed that all proteins, WT UbLD, $UbLD^{V15M}$, $UbLD^{R33Q}$, and $UbLD^{K48A}$ were able to interact with the UIM region of ataxin-3 and with similar affinities (Figure 3.2). The $UbLD^{A46P}$ protein band appears more faint, suggesting that the interaction with ataxin-3 is much weaker than the WT UbLD, $UbLD^{V15M}$, $UbLD^{R33Q}$, and $UbLD^{K48A}$ (Figure 3.2). The ARJP substitution of a single amino acid, (V15M, K32T, R33Q, and P37L) has been previously shown to compromise the interaction between the UIM region of S5a (2). This led to the investigation of V15M, R33Q and K48A substitutions, on the basis that they are all structurally intact and also because of their close proximity to the binding interface of the UIM binding site on the UbLD. The $UbLD^{A46P}$ has been shown previously to be completely unfolded, by the loss of alpha helix and beta sheet signals in the CD spectra and by observing a collapse of peaks in the NMR HSQC experiments, which is an indication of protein unfolding (2). Thus, $UbLD^{A46P}$ was used as a negative control for the binding assay as the interaction surface where UIMs typically bind would be disrupted and should result in no binding. However, residual binding was detected for the $UbLD^{A46P}$ protein, possibly caused by nonspecific binding to the resin of the column used (Figure 3.2). Analysis of the affinity binding

assay alone provides a qualitative assessment that the structurally intact ARJP substituted UbLD proteins are able to bind to ataxin-3 with a similar affinity compared with $UbLD^{WT}$.

3.4.3 NMR titration interaction studies between $UbLD^{V15M}$, $UbLD^{K48A}$ and ataxin-3

The NMR titrations confirmed that the $UbLD^{V15M}$ and $UbLD^{K48A}$ utilize many identical residues to interact with ataxin-3 $UIM123^{194\text{-}361}$. The observation that Ile^{66}, Phe^{13}, Leu^{61}, and Gln^{64} participate in the interaction for both $UbLD^{V15M}$ and $UbLD^{K48A}$ was expected, because these are also the residues that display great chemical shifts in the NMR titrations of the wildtype interaction between the UbLD and UIMs as noted in Chapter 2. Even though both residues Lys^{48} and Val^{15} participate in the wildtype interaction, based on NMR titration experiments, the substitution of these residues does not disrupt the binding significantly. The dissociation constant for $UbLD^{K48A}$ and $UbLD^{V15M}$ were $K_{D,\ UbLD}{}^{K48A}$=658.9±47.79 μM and $K_{D,\ UbLD}{}^{V15M}$=700.4±102.7 μM for a three equivalent multisite binding model (Figure 3.5). These K_D values are not significantly different from the wildtype K_D which was 668.7±61.70 μM for a three equivalent multisite binding model (Chapter 2). An explanation for why these two particular structurally intact ARJP mutants did not drastically change the affinity of binding to the UIM region could be because both residues do not lie at the centre of the hydrophobic patch, which was found to be the 'heart' of the docking site for the ataxin-3 UIM region. Lys^{48} lies at the edge of the hydrophobic patch, on the β4 strand, while Val^{15} lies at the opposite edge of the hydrophobic patch with its side chain pointing away from the solvent exposed beta sheet. The proximity of these two ARJP substitutions were not

close to the center of the docking site for the UIMs and perhaps, are not important residues for the interaction with the UIM region of ataxin-3. In support of this, previous studies performed on ARJP substituted UbLD proteins and interactions with the UIM region of S5a showed that the structurally intact ARJP-substituted proteins which compromised the binding affinity to the S5a protein were residues that were interacting with a key residue, Phe^{13}, for the wildtype interaction between UbLD and UIM (2). Many of the ARJP-substituted UbLD proteins also had decreased stability, based on thermal unfolding experiments, which may have altered the interaction site for the S5a (2). Some of the ARJP-substituted UbLD proteins that resulted in decreased domain stability were also used in the study with ataxin-3, such as $UbLD^{V15M}$ and $UbLD^{R33Q}$, however, the decrease in stability does not effect the binding to ataxin-3. The structurally intact disease-state UbLD substitutions that were studied for interactions with ataxin-3 ($UbLD^{V15M}$, $UbLD^{R33Q}$, and $UbLD^{K48A}$), can all retain their interaction with ataxin-3. This suggests that these particular ARJP substitutions may have a larger impact on interactions to other proteins, such as S5a, or have an altered pathogenic pathway that does not involve ataxin-3.

3.4.4 Alternate pathogenic pathways for ARJP-substituted UbLD proteins

Many identified ARJP substitutions within the UbLD of parkin have been categorized in terms of how they could be contributing to pathogenic outcomes, such as completely unfolding the UbLD structure, disrupting important protein-protein interactions, or decreasing the stability of the domain structure and full-length parkin protein (2, 8, 9). There are also unidentified pathogenic outcomes for some ARJP

substitutions. Most recently, it has been proposed that the parkin UbLD has a role in autoinhibition of its catalytic ubiquitin ligase activity, more specifically in autoubiquitination (8). The N-terminal UbLD was found to interact with a ΔUbLD parkin$^{77-465}$ construct. The Lys^{48} position, which is completely conserved in ubiquitin and acts as the site of polyubiquitin chain building for degradation signaling, had been shown to be an essential residue to support the autoinhibited state of parkin (8). When the Lys^{48} was substituted with a non-charged residue alanine, as opposed to maintaining the same charge with a residue like arginine, the autoinhibition was compromised and it resulted in an increased autoubiquitination of parkin. This suggests that the electrostatic nature of the Lys^{48} is essential to the intramolecular autoinhibited state of parkin, and that the substitution of K48A could cause an increased turnover of parkin through the proteasomal degradation pathway (8). Walden's group also tested the UbLD^{A46P} and found that this ARJP substituted protein does disrupt the autoinhibition of parkin, suggesting that the UbLD structure must be intact to be able to expose the residues most important for interacting with a ΔUbLD parkin$^{77-465}$ construct (8).

3.5 References

1. Kitada, T., Asakawa, S., Hattori, N., Matsumine, H., Yamamura, Y., Minoshima, S., Yokochi, M., Mizuno, Y., and Shimizu, N. (1998). Mutations in the parkin gene cause autosomal recessive juvenile parkinsonism. Nature *392,* 605-608.
2. Safadi, S.S., Barber, K.R., and Shaw, G.S. (2011). Impact of autosomal recessive juvenile Parkinson's disease mutations on the structure and interactions of the parkin ubiquitin-like domain. Biochemistry *50,* 2603-2610.

3. Durcan, T.M., Kontogiannea, M., Thorarinsdottir, T., Fallon, L., Williams, A.J., Djarmati, A., Fantaneanu, T., Paulson, H.L., and Fon, E.A. (2011). The Machado-Joseph disease-associated mutant form of ataxin-3 regulates parkin ubiquitination and stability. Hum. Mol. Genet. *20,* 141-154.
4. Munoz E, Pastor P, Marti MJ, Oliva R, Tolosa E. 2000. A new mutation in the parkin gene in a patient with atypical autosomal recessive juvenile parkinsonism. Neurosci Lett 289:66–68.
5. Hertz JM, Ostergaard K, Juncker I, Pedersen S, Romstad A, Moller LB, Guttler F, Dupont E. 2006. Low frequency of Parkin, Tyrosine Hydroxylase, and GTP Cyclohydrolase I gene mutations in a Danish population of early-onset Parkinson's Disease. Eur J Neurol 13:385–390.
6. Xu Y, Liu Z, Wang Y, Tao E, Chen G, Chen B. 2002. [A new point mutation on exon 2 of parkin gene in Parkinson's disease]. Zhonghua Yi Xue Yi Chuan Xue Za Zhi 19:409–411.
7. Dev, K.K., van der Putten, H., Sommer, B., and Rovelli, G. (2003). Part I: parkin-associated proteins and Parkinson's disease. Neuropharmacology *45,* 1-13.
8. Chaugule, V.K., Burchell, L., Barber, K.R., Sidhu, A., Leslie, S.J., Shaw, G.S., and Walden, H. (2011). Autoregulation of Parkin activity through its ubiquitin-like domain. EMBO J. *30,* 2853-2867.
9. Henn, I.H., Gostner, J.M., Lackner, P., Tatzelt, J., and Winklhofer, K.F. (2005). Pathogenic mutations inactivate parkin by distinct mechanisms. J. Neurochem. *92,* 114-122

Chapter 4

SUMMARY AND PERSPECTIVES

4.1 Introduction

The ubiquitin signaling pathway (USP) involves hundreds of enzymes and is utilized in multiple regulatory pathways, such as proteasomal degradation, endocytosis and DNA repair. Many protein misfolding neurodegenerative diseases have been linked to the USP, which has drawn attention to the investigation of the structure and function of enzymes involved in this multifaceted pathway. Conjugation of a Ub molecule or a poly-Ub chain onto a target protein is a tightly regulated process and it is also reversible. An early-onset form of Parkinson's disease (PD) has been linked with parkin, an E3 Ub ligase, which participates in the last step of conjugating the Ub moiety onto a specific target protein. Machado Joseph disease (MJD) is the most common dominantly inherited ataxia and has been linked with a poly-glutamine expansion in the ataxin-3 DUB enzyme, which has a role in detaching Ub moieties. Both MJD and PD are progressive diseases and patients of these diseases can present with a wide variety of clinical symptoms. Interestingly, the clinical presentations in MJD and PD can overlap, as it has been reported that MJD patients have parkinsonism like behaviour (1).

4.2 Previous Work

There is potential for neuropathological overlap between the two disease states, PD and MJD, since parkin and ataxin-3 are multi-domain proteins with an assemblage of ubiquitin-signaling relevant domains. Observations of overlapping clinical symptoms for

patients with Machado Joseph Disease (MJD) and patients with PD, such as tremors and muscle rigidity, supports the hypothesis (1). In addition, similar areas of the brain are negatively affected in MJD and PD, such as the substantia nigra; however, there are many areas of the brain that are divergently affected in the two disease states (3). Some of the patients with MJD that display parkinsonism characteristics, respond well to levodopa treatment (4). These two proteins have already been identified to be functionally interactive by their interplay between ubiquitylating and deubiquitinating one another to regulate the function of both proteins (2,5). All of the clinical observations and experimental evidence emphasizes the importance of the interaction between parkin and ataxin-3. Further investigation needs to be focused on how the disease-relevant mutations, on either parkin or ataxin-3, affect the neurobiology in affected areas in the brain.

In 2010, parkin was reported to directly interact with ataxin-3, however details regarding the residues involved in the binding site, binding mechanism and affinity of binding were not elucidated (2). By performing multiple affinity binding assays, the group was able to narrow down the binding region to the C-terminal UIM region of ataxin-3 and the N-terminal UbLD of parkin (2). In Dr. Fon's group, they found that GST-tagged parkin lacking the UbLD could still bind to full-length ataxin-3, which suggests that there is another interaction site. Further investigation led to the discovery that is was an interaction between the ataxin-3 N-terminal Josephin domain with the IBR-RING2 of parkin (2). In this work, the focus was only on the UbLD and UIM constructs, but if this interaction is complicated by another site of binding, further investigation is needed to fully appreciate the biological binding mechanism between ataxin-3 and

parkin. It would be interesting to determine the binding affinity of this interaction through NMR titration experiments, however, the Josephin domain and IBR-RING2 would form a much larger complex than the UIM region and UbLD. The large complex will slow the tumbling time in the protein sample and the peaks may be difficult to resolve due to the broadening of peaks. It is important to study the second potential interaction site because it could be the site of disease pathogenesis for either ARJP or MJD.

4.3 Interactions between the parkin UbLD and UIM region of ataxin-3

Thorough analysis of eight different sets of NMR titration experiments, using multiple ataxin-3 UIM region constructs of various lengths and sequences and the parkin UbLD, were carried out to provide the first reports of the site (on parkin) for the interaction, strength of the interaction and proposal of a mechanism of binding between parkin and ataxin-3. The UIM region of ataxin-3, spanning residues 194-361 (including all three UIM sites), were found to bind to the beta-grasp fold on the UbLD of parkin. This binding region on the UbLD is called the hydrophobic patch, which includes residues Ala^{46}, Ile^{66}, and Val^{67} as well as a few basic residues, such as Lys^{48}. The beta-grasp surface on the parkin UbLD is also the binding site for two other UIM-containing proteins, S5a and Eps15, though there are variations in the size of the binding surface because of the difference in how many UIM sites are utilized in the interaction (8). The binding surface area where the UIM region of ataxin-3 binds to the UbLD, in comparison to previous studies, can be predicted to bind one to two UIM sites but is not large enough to simultaneously interact with all three UIM sites. Interestingly, the NMR titrations

involving C-terminal deletions of the ataxin-3 UIM region suggested that when all three UIM sites are intact, the binding affinity is the tightest. The evidence for this was displayed by determining the K_Ds by fitting the binding curves to the macroscopic or simple 1:1 binding model; the K_Ds were 230 μM, 430 μM, and >2 mM for ataxin-3 regions 194-361 (3 UIM sites), 194-261 (2 UIM sites), and 194-244 (1 UIM), respectively. This led to the proposal that a multivalent binding mechanism could be utilized by all three UIM binding regions of ataxin-3 upon interacting with parkin. Multivalent binding involves rapid kinetic substrate binding, of typically a tandem string of binding moieties; in this case the ataxin-3 UIM sites were proposed to be interchanging amongst one another in an intramolecular fashion at a rapid rate. Interestingly, this type of multivalent binding mechanism has been characterized for another UIM-containing protein involved in DNA repair, called Rap80, and its interaction with poly-ubiquitin chains (9).

4.4 ARJP substitutions on the UbLD and the effect on its interaction with ataxin-3

Three structurally unaffected ARJP substituted UbLD proteins, chosen based on residue positions that were within or proximal to the binding surface for ataxin-3, were analyzed for their effect on the interaction with ataxin-3 $UIM123^{194\text{-}361}$. Out of 20 possible ARJP substitutions within the parkin UbLD, the ones that were the focus of this study were $UbLD^{V15M}$, $UbLD^{R33Q}$, and $UbLD^{K48A}$ (5). All three ARJP substituted proteins were able to retain their interaction with the UIM region of ataxin-3, based on an affinity-tag binding assay. A detailed analysis was carried out for $UbLD^{V15M}$ and $UbLD^{K48A}$, by

^{1}H-^{15}N HSQC titration experiments, for determination of the binding site on the UbLD and the binding affinity. Results showed that although the binding site was not identical for ataxin-3 binding to $UbLD^{V15M}$ and $UbLD^{K48A}$, there were many identical residues that shifted upon additions of ataxin-3. The binding site on the $UbLD^{K48A}$ and $UbLD^{V15M}$, where the UIM region of ataxin-3 binds, was found to be on the solvent exposed surface of the beta-grasp fold, which is where the wildtype binding site is located. The K_D values for the interaction between the $UbLD^{V15M}$ and $UbLD^{K48A}$ to ataxin-$3^{194-361}$ were similar to that of the wildtype UbLD interaction, all of them within the 650-750 μM range for a multivalent binding fit. Therefore, the ARJP-substituted UbLD proteins used in this study are all able to interact with ataxin-3 $UIM123^{194-361}$, and likely uses a similar mechanism to recruit ataxin-3 $UIM123^{194-361}$.

4.5 Conclusions

The work presented here has contributed to the understanding of how an E3 ubiquitin ligase, parkin, recognizes a DUB enzyme, ataxin-3. Parkin was previously reported to directly interact with ataxin-3 by affinity binding assays but details regarding the binding affinity, recognition surface and mechanism of binding were not characterized until now (2). This work provides the first detailed understanding of where and how the three UIM regions in ataxin-3 make a weak interaction ($K_{D,macroscopic}$=230μM) with the parkin UbLD, and is proposed to use a multivalent binding mechanism to do so. Choosing only the structurally unaffected ARJP substituted UbLD proteins, based on previous structural characterization, provides the first analysis of the disease state UbLD proteins and their effect on the binding affinity and UbLD

binding surface upon addition of ataxin-3. These analyses showed that the interaction between the $UbLD^{V15M}$, $UbLD^{R33Q}$, $UbLD^{K48A}$ and ataxin-3 is retained and that the V15M and K48A substitutions do not completely alter the site of interaction on the UbLD.

The interaction between these two proteins is very interesting because they possess opposing functions of either attaching or detaching a Ub moiety from specific substrates or one another (2). The interactions between other DUB enzymes and E3 ligases have been reported, which has triggered interest in studying the biological importance and interplay between these protein pairings (2, 6). There is also evidence to suggest that there is regulatory interplay for the catalytic activity of parkin and ataxin-3, which provides another piece of evidence to explain why their interaction is biologically important (2, 4, 7). The USP is a complex system consisting of hundreds of enzymes and even more target proteins, which all need to be orchestrated for proper maintenance of intracellular protein level homeostasis. Due to the complexity of the USP, there are still many protein networks that need to be understood in order to address the neurodegenerative USP-linked disease states, such as ARJP and MJD.

4.6 References

1. Klein, C., Schneider, S.A., and Lang, A.E. (2009). Hereditary parkinsonism: Parkinson disease look-alikes--an algorithm for clinicians to "PARK" genes and beyond. Mov. Disord. *24,* 2042-2058.
2. Durcan, T.M., Kontogiannea, M., Thorarinsdottir, T., Fallon, L., Williams, A.J., Djarmati, A., Fantaneanu, T., Paulson, H.L., and Fon, E.A. (2011). The Machado-Joseph disease-associated mutant form of ataxin-3 regulates parkin ubiquitination

and stability. Hum. Mol. Genet. *20,* 141-154.

3. Yamada, M., Sato, T., Tsuji, S., and Takahashi, H. (2008). CAG repeat disorder models and human neuropathology: similarities and differences. Acta Neuropathol. *115,* 71-86.
4. Durcan, T.M., and Fon, E.A. (2011). Mutant ataxin-3 promotes the autophagic degradation of parkin. Autophagy *7,* 233-234.
5. Safadi, S.S., Barber, K.R., and Shaw, G.S. (2011). Impact of autosomal recessive juvenile Parkinson's disease mutations on the structure and interactions of the parkin ubiquitin-like domain. Biochemistry *50,* 2603-2610.
6. Kon, N., Kobayashi, Y., Li, M., Brooks, C.L., Ludwig, T., and Gu, W. (2010). Inactivation of HAUSP in vivo modulates p53 function. Oncogene *29,* 1270-1279.
7. Durcan, T.M., Kontogiannea, M., Bedard, N., Wing, S.S., and Fon, E.A. (2012). Ataxin-3 deubiquitination is coupled to Parkin ubiquitination via E2 ubiquitin-conjugating enzyme. J. Biol. Chem. *287,* 531-541.
8. Safadi, S.S., and Shaw, G.S. (2010). Differential interaction of the E3 ligase parkin with the proteasomal subunit S5a and the endocytic protein Eps15. J. Biol. Chem. *285,* 1424-1434.
9. Markin, C.J., Xiao, W., and Spyracopoulos, L. (2010). Mechanism for recognition of polyubiquitin chains: balancing affinity through interplay between multivalent binding and dynamics. J. Am. Chem. Soc. *132,* 11247-11258.

Curriculum Vitae

Jane J. Bai

Department of Biochemistry Faculty of Medicine and Dentistry

EDUCATION

M.Sc. Candidate **2010-Present**
Department of Biochemistry
Western University

Bachelor of Medical Sciences **2006-2010**
Honors Specialization in Medical Sciences
Western University

Ontario Secondary School Diploma **2002-2006**
A. B. Lucas Secondary School, London, Ontario

SCHOLARSHIPS AND AWARDS

UWO Dean's Honor List. **2006-2007, 2009-2012**

UWO Academic Achievement Award **2006-2007, 2009-2012**

- Achievement of >80% academic average while participating in a varsity sport

UWO Western Research Graduate Scholarship **2010-2012**

UWO Entrance Scholarship **2006**

Principal's Award for Student Leadership **2002**

CONFERENCES AND POSTER PRESENTATIONS

MOOT XXIV NMR Symposium, Toronto, Ontario October 22-23, 2011

Margaret P. Moffat Graduate Research Day 2011

Biochemistry Department Poster Day 2011

RESEARCH EXPERIENCE

M.Sc. Candidate **2010-Present**
Dr. Gary Shaw's Laboratory
- Current Year: 2

Western University **2010**
Dr. Gary Shaw's Laboratory
- Summer Research Student

COMMITTEES

Strong Bones, Strong Minds, Strong Muscles Committee **2011- Present**
Graduate Student Initiative- Fundraising towards Alzheimer Society of Canada

- In this role I attended the monthly committee meetings, and helped organize and promote charity events in support of the Alzheimer Society of Canada.

TEACHING EXPERIENCE

Graduate Teaching Assistant

Biochemistry (Biochemistry 2280A) **2011**
Course Enrollment: 1300 *Total number of hours per term: 70*

Clinical Biochemistry Lab (Biochemistry 3387G) **2011**
Course Enrollment: 18 *Total number of hours per term: 70*

Protein Design, Analysis and Structure (Biochemistry 4440A) **2010**
Course Enrollment: 25 *Total number of hours per term: 70*

VOLUNTEER EXPERIENCE/EXTRA CURRICULAR ACTIVITIES

Runner's Feed Running Group	2012-Present
Assistant Badminton Coach – A.B. Lucas S.S.	2007-Present
Western University Badminton Varsity Athlete	2006 - 2012
Recreation Assistant - McCormick Home (Alzheimer Outreach Program	2007 - 2011
Volunteer at Fowler Kennedy Sports Medicine Clinic	2011
Scotiabank Toronto Waterfront Marathon	2010
Scotiabank Toronto Waterfront Half Marathon	2009